# MODELING OF CRYOGEN LEAKAGE THROUGH COMPOSITE LAMINATES

A Thesis

by

NAGA VENKATA SATYA PRAVIN KUMAR PEDDIRAJU

Submitted to the Office of Graduate Studies of
Texas A&M University
in partial fulfillment of the requirements for the degree of

MASTER OF SCIENCE

December 2004

Major Subject: Aerospace Engineering

MODELING OF CRYOGEN LEAKAGE THROUGH

COMPOSITE LAMINATES

A Thesis

by

NAGA VENKATA SATYA PRAVIN KUMAR PEDDIRAJU

Submitted to Texas A&M University
in partial fulfillment of the requirements
for the degree of

MASTER OF SCIENCE

Approved as to style and content by:

| | |
|---|---|
| Dimitris C. Lagoudas | John D. Whitcomb |
| (Co-Chair of Committee) | (Co-Chair of Committee) |
| | |
| Roger Morgan | Walter E. Haisler |
| (Member of Committee) | (Interim Head of Department) |

December 2004

Major Subject: Aerospace Engineering

ABSTRACT

Modeling of Cryogen Leakage Through

Composite Laminates. (December 2004)

Naga Venkata Satya Pravin Kumar Peddiraju,

B.Tech, Indian Institute of Technology-Chennai

Co–Chairs of Advisory Committee: Dr. Dimitris C. Lagoudas
Dr. John D. Whitcomb

Cryogenic composites find critical application in the manufacture of fuel tanks for reusable launch vehicles due to significant reduction in overall structural weight of the tank. These fuel tanks contain pressurized cryogen such as hydrogen at cryogenic temperatures. Exposure to varying temperatures and mechanical loads resulting from flight cycle, containment of pressurized cryogen causes thermo-mechanical loading of the composite. The thermo-mechanical loading cycles combined with anisotropy of the composite and mismatch in the thermal and mechanical properties of fibers and matrix lead to transverse matrix cracks (TMC) in each ply. TMC in adjacent plies intersect in localized regions at ply interfaces called crack junctions, which open up due to delamination on application of thermo-mechanical load. TMC and crack junctions usually form a network of leakage paths that assists leakage of cryogen through the composite. In this study, the volumetric flow rate of cryogen leaking through a damaged cross-ply composite with five plies is determined by estimating the effective conductance of the leakage paths. For a given damage state and applied load, crack junction and TMC openings are obtained by finite element analysis. A computational fluid dynamics model is first used to estimate the effective conductance of a leakage

path to hydrogen leakage and then a simplified analytical model is used to compute the effective conductance from individual conductances of each crack junction and TMC through a series-parallel combination. A single phase flow model is considered for the numerical analysis of hydrogen flow through TMC and crack junctions. The simulations are carried out using a commercial computational fluid dynamics software, FLUENT. Parametric studies are carried out to investigate the dependence of leak rate of hydrogen on the irregularities of the TMC geometry and TMC, crack junction openings. The simplified model predictions of the effective conductance for the five ply composite show good comparison with numerical simulations.

To my beloved parents,

Smt. Kalyani Peddiraju and Shri. Radha Krishna Peddiraju

## ACKNOWLEDGMENTS

I would like to thank Dr. Dimitris C. Lagoudas for his guidance and support throughout the study. I would also like to thank Dr. John D. Whitcomb and Dr. Roger Morgan for serving on my committee. I would like to thank the Marshall Space and Flight Center for providing the experimental data and Dr. Vernon Bechell from the Air Force Research Laboratory for providing the optical inspection data. I would like to thank Dr. Jae Noh for helping me with the project.

I would like to thank my parents, Smt. Kalyani Peddiraju and Shri. Radha Krishna Peddiraju, for their constant support through out my life. I would like to thank my brother, Anil Kumar Peddiraju, and all my friends who have supported me through out my time of study.

TABLE OF CONTENTS

LIST OF TABLES

LIST OF FIGURES

FIGURE                                                                                        Page

CHAPTER I

INTRODUCTION

A.  Motivation

In the manufacture of structural components, composites find significant application due to their high strength to weight ratio property. In single stage reusable launch vehicles (RLV), the fuel tanks carrying cryogenic fuel like liquid hydrogen are usually made of metals. The launch cost of RLV can be minimized if the overall structural weight of the tank is reduced by a significant amount without any reduction in the strength of the structure. Usage of composite materials instead of metals reduces the structural weight of the tank by approximately 35% [1]. Usually, plies of different orientation are stacked together to enhance the strength of the structure under multi-axial loading. Thus, composite materials are preferred to metals in the manufacture of the fuel tanks of RLV.

The composite fuel tanks contain pressurized cryogen at very low temperatures such as 20.3°K for liquid hydrogen. During a typical flight cycle, the outside temperature of the tank can reach up to 560°K [2]. Thermal stresses develop inside the composite on exposure to such varying temperatures due to the anisotropic nature of composite and difference in thermal expansion coefficients of fiber and matrix. In addition to thermal stresses, mechanical stresses also develop as a result of pressure loads due to containment of cryogen, aerodynamic loading and boost acceleration during flight. Due to the thermo-mechanical loading, transverse matrix cracks (TMC) develop in each ply of the composite that run along the direction of fibers. Due to

_____

This thesis follows the style of International Journal of Fatigue.

difference in orientation, TMC in adjacent plies intersect at localized regions of ply interfaces called crack junctions. On application of load, these crack junctions open up due to delamination. A network of opened up TMC and crack junctions is defined as a leakage path. Several such leakage paths may exist in the composite contributing to cryogen leakage. Thus, modeling of cryogen flow through such leakage paths is essential in estimating the amount of cryogen leakage. Analysis for estimation of amount of cryogen leakage through composite laminates involves several key steps (Fig. 1) such as : 1. Structural analysis of the composite; 2. Construction of damage network (leakage path); and 3. Analysis of cryogen flow through the leakage paths. In the absence of connectivity between TMC in adjacent plies, cryogen leakage takes place by diffusion through matrix present between unconnected TMC in the composite. Diffusion is a slow transport process compared to actual flow through network of connected TMC. Hence, absence of connectivity between TMC in adjacent plies can reduce the amount of cryogen leakage by orders of magnitude. Accuracy in estimating the amount of cryogen leakage depends on all of the above mentioned factors, which must be carefully compared with experimental observations.

1. Structural analysis of tank

3. Cryogen flow analysis

Outlet

Inlet

2. Construction of damage network
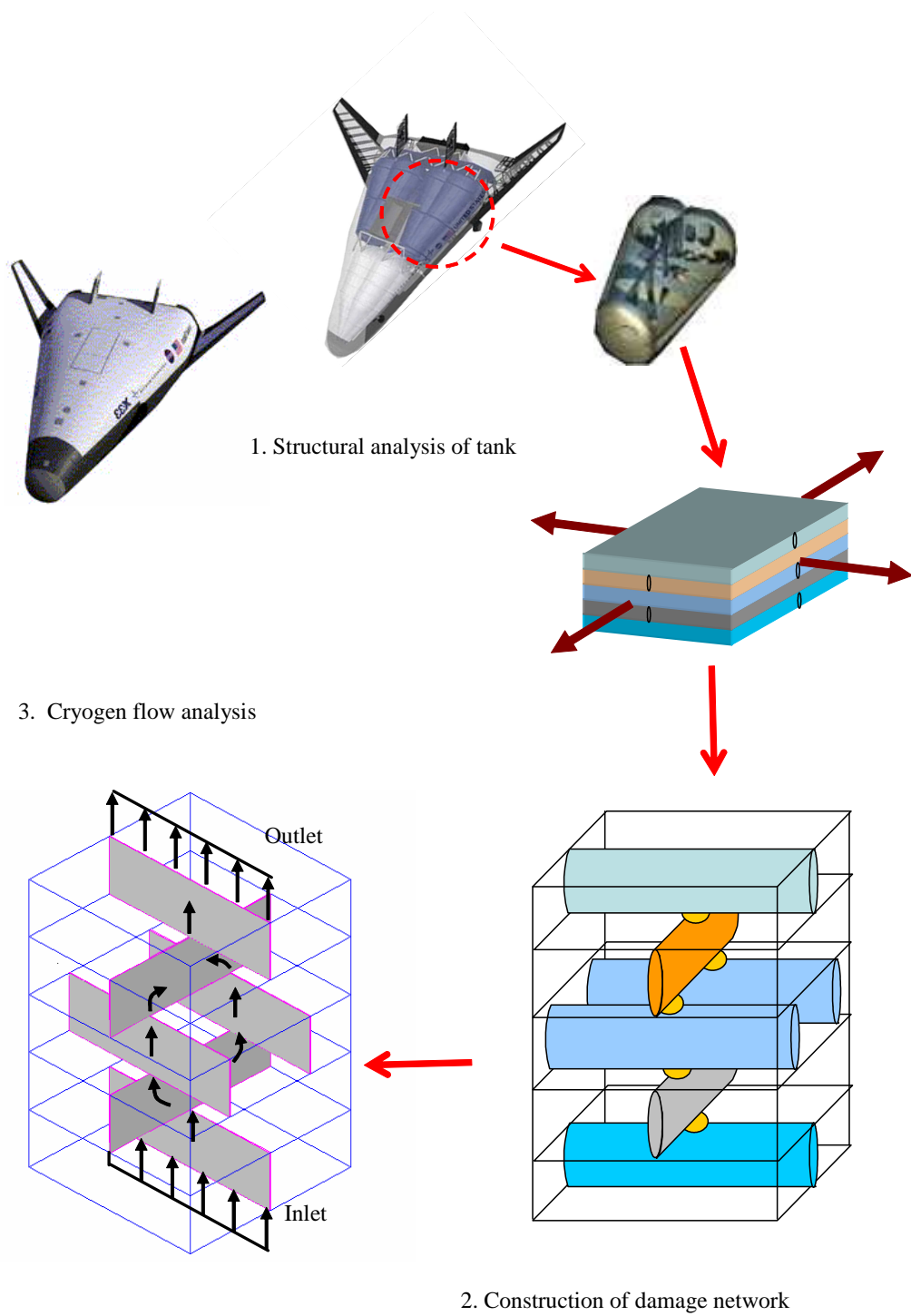
Fig. 1. Leakage of cryogen through interconnected damage in a cryogenic composite

B.   Literature review

In the fuel tanks of RLV, cryogen is usually stored in liquid phase at cryogenic temperatures. Since the outside temperatures can reach a maximum of about 560°K, cryogen will be in gaseous phase as it leaks out to the surface of the composite. Hence, the actual leakage process might be a double phase (liquid/gas) flow through the thickness of the composite. However, experiments are usually conducted with gaseous cryogen.

Morimoto *et al,* [3] conducted experiments on model tanks made of IM600/#133 composite material with high strength carbon fiber and toughened epoxy resin material under internal pressure at cryogenic temperature. Three tanks were prepared out of which two were made with eight-ply unidirectional quasi-isotropic lay-ups with different patterns and the third one was made with cloth lay-up. Different experiments such as gaseous helium leakage under pressure at room temperature, damage onset evaluation at cryogenic temperature and gaseous helium leakage under pressure at cryogenic temperature were carried out. Onset of microcracking was detected using helium flow measurement and acoustic emission techniques. Strain field resulting from the pressurization was measured using 3-line type strain guages. No significant leakage was detected in the tank during these tests.

Ishikawa *et al,* [4] investigated the pressurization of similar model tanks as described in the above paragraph at liquid nitrogen temperature along with identification of leak paths. They considered two tanks of different orientations made of IM600/#133 material. These tanks were pressurized with gaseous helium at cryogenic temperature (liquid nitrogen). Gaseous helium pressure was increased and increment in the hoop strain in the tanks was recorded. Leak paths in the two tanks were

identified from gaseous helium pressure variation with hoop strain data, which was supported by gaseous helium pressure rise in the vacuum chamber where the tanks were contained. The positions of leak paths were identified by sniffer method and snoop leak check. The strain levels at which leak paths were formed were identified for both tanks.

It is often convenient to perform leakage experiments on coupon specimens compared to model tanks discussed in previous paragraphs. Rivers *et al,* [5] researched on development of test apparatus and test methods for measurement of hydrogen and helium leakage through complex composite structures that could be loaded mechanically at cryogenic temperature. Composite specimens from the fuel tank of X-33 reusable launch vehicle, made of IM7/977-2 material were used for liquid hydrogen and helium leak rate estimation. The authors found that at certain thermo-mechanical loading conditions, hydrogen leak rates through the specimens were found to be larger than the acceptable leak rates mentioned in the work.

Robinson *et al,* [6] conducted studies for the establishment of optimum cryo tank design based on factors such as material, tank wall construction, cryo insulation, adhesives, liner materials and tank tooling/manufacturing approach. They considered that composite material selection is dependent on factors like permeation/micro-cracking resistance, mechanical performance at cryogenic and elevated temperatures, and ease of processing. Several composite samples with different materials were tested for permeability. An uni-axial loading method was developed to estimate the permeability of samples subjected to cyclic mechanical loading. No increase in permeability was found during the uni-axial test. Another method was developed to estimate the permeability under biaxial load. The biaxial loading was approximated by sequential

uni-axial loadings. Permeability measurements were made at two different cryogenic temperatures and at an elevated temperature. From these experiments, the permeation rate was found to increase with decrease in the temperature. Another method was employed where the samples were subjected to biaxial loading by using circular shaped specimens as a closure on high pressure cryostat. Several specimens such as IM7/977-2, IM7/3900-3, IM7/5250-4, IM7/8551-7 were considered for the biaxial testing. Permeation rates and micro strain data of these samples was recorded and for most of the samples, the permeability values were found to be less than the allowable values.

Gates *et al,* [7] conducted experiments on IM7/977-2 specimen to determine the correlation between damage state and permeability of composites subjected to mechanical and thermal loads. Test apparatus was developed to perform uni-axial mechanical cyclic loading at room and cryogenic temperatures. Due to the uni-axial testing, no leakage along the through thickness direction was observed. In plane permeability was measured due to the off-axis leakage paths existing in the composite. Crack density and permeability variation with applied mechanical load was reported. The results of the experiments suggested an increase in the permeability at cryogenic temperature compared to room temperature.

Bechel *et al,* [8] experimentally tested two composite specimens, IM7/5250-4 and IM7/977-3, which were subjected to thermal cyclic loads between liquid nitrogen and elevated temperatures. The number of thermal cycles was varied for each specimen till extensive damage was recorded in both samples. Due to the applied thermo cyclic loading, all plies in IM7/5250-4 were damaged and all plies except one were damaged in IM7/977-3. A test apparatus was built to measure the through thickness

permeability at room temperature and at no mechanical load. The permeability measurements indicated zero leakage in both the specimens suggesting that the actual measurements were less than the minimum recordable values of the apparatus.

In the absence of leakage paths, cryogen transport takes place by diffusion. The amount of cryogen leakage by diffusion can be estimated by measuring the permeation rate or coefficient of permeability. Evans *et al,* [9] examined coefficient of permeability for gases such as hydrogen *etc.,* through epoxy based resins. Diffusion was assumed to be the mode of gas transfer through the resin. Disdier *et al* [10] investigated the permeation of helium through different glass/epoxy composite specimens. They studied the effect of thermal, mechanical cyclic loading on permeation rate. The effect of glass fiber volume fraction on permeation rate was also investigated. It was found that the permeability values are affected by the volume fraction of fibers in the composite. Humpenoder [11], measured the permeation rates of helium, hydrogen and methane through different materials such as fiber reinforced plastics, thermoplastics and thermosetting plastics at temperatures varying from cryogenic to room temperature. It was found that in the absence of micro cracks in the composite at cryogenic temperature, the permeation rate was very small. Disdier *et al,* [12] investigated temperature dependence of permeability by measuring leak rates in a composite specimen at temperatures ranging from cryogenic to room temperature. Nishijima *et al,* [13] found that the permeation rate dependence on temperature could be expressed by an Arhenius type equation.

Usually, experiments can be performed mainly for specific designs and service conditions. Modeling of cryogen flow through the network of TMC and crack junctions will facilitate in designing the cryogenic composites subjected to various service con-

ditions for optimum performance. Kumazawa *et al*, [14] experimentally observed leak rates of gaseous helium through carbon fiber reinforced plastics under mechanical biaxial loading at room temperature. The researchers also proposed a semi-analytical method to predict the leak rate based on the TMC opening values in each ply. Certain parameters in the model were obtained experimentally which varied for different specimens considered for the leak test. The authors experimentally found that the leak rates due to diffusion are orders of magnitude smaller than the leak rates in the presence of well connected damage. They also investigated the variation of helium leak rate with applied load and load ratios. A good comparison of leak rates was observed between the semi-analytical predictions and experimental observations. With the help of the semi-analytical model predictions, it was found that the leak rates at cryogenic temperatures were higher compared to the leak rates at room temperature.

Roy *et al* [15] derived a mathematical expression for permeability estimation, based on Darcy's law for isothermal, viscous flow of gases. Dependence of gas density on pressure was incorporated in the derivation of permeability expression. The expression incorporates dependence of cryogen mass flow rate on parameters such as crack density and crack opening in each ply of the composite. Studies on variation of permeability with crack density of one of the plies, applied load, delamination length at different crack densities were investigated. In the first case, permeability was found to increase with increase in the crack density and the increment was found to decrease gradually. In the second case, permeability was found to increase in a parabolic fashion as the applied mechanical load is increased. In the third case, permeability was found to increase with increase in the delamination length and the increment was found to decrease with increase in the delamination length. However, the model requires estimation of some of its parameters through experiments. Hence, prediction

of permeability of a composite is contingent upon the availability of experimental data. Analytical or numerical modeling of cryogen leakage with minimal dependence on experiments is usually desired. This is possible only if the actual cryogen flow process through the micro cracks is clearly understood.

Researchers extensively studied fluid flow through fractures in rocks which can be applicable to cryogen flow through micro-crack network. Usually, for incompressible flow through fractures the governing equations for fluid flow are conservation of mass and momentum equations at steady state, which are supplemented by necessary boundary conditions. For an incompressible Newtonian fluid, these equations reduce to continuity and Navier-Stokes equations. Mozorenko *et al* [16] and Zimmerman *et al* [17] studied incompressible Newtonian fluid flow through rock fractures in their works. They assumed that the crack openings are small and the leakage is a slow transport process such that the fluid exhibits creeping behavior as it flows through the fractures. In such cases, the Reynolds number of the flow is sufficiently small (Re<1) to have negligible inertial effects and the Navier-Stokes equations further reduce to Stokes equations. A linear relation exists between the volumetric flow rate of the fluid and the pressure drop across the fracture. The authors also made systematic comparisons between the predictions of Stokes and Reynolds equations, that were employed in analyzing fluid flow. Often, the leakage paths can be visualized as a complex network of channels for fluid flow [18]. At higher Reynolds number (Re> 13), the linear relationship between the volumetric flow rate and the pressure drop breaks down due to the influence of inertial effects on the fluid flow. In straight channels, the non-linear behavior is widely observed when the flow becomes turbulent, but in the case of a complex network of channels the non-linear behavior is observed even when the flow is laminar. In such cases, the fluid volumetric flow rate and pressure drop

can be expressed in the form of a power law [19], which is employed in the current study.

As mentioned earlier, many experiments focus on gaseous cryogen leakage through composites. Hence, in the present research, gaseous hydrogen leakage through cryogenic composites is studied. The characteristic of hydrogen flow is found to depend on the operating temperature, which influences the flow properties of the cryogen. In the present work, hydrogen leakage through a micro crack damaged composite with five plies is analyzed numerically at two different temperatures namely cryogenic temperature of 33.1°K and room temperature of 300°K. Variation of hydrogen leak rate with crack density of one of the plies is investigated at the two temperatures. A Simplified model is developed that estimates the effective conductance of the composite from crack junction conductance and TMC resistance values.

CHAPTER II

MODELING OF CRYOGEN LEAKAGE

A.   Methodology for cryogen leakage analysis

The methodology for effective leakage estimation involves key steps such as damage inspection, ply level stress determination, TMC and crack junction opening estimation along with damage network construction followed by leakage prediction. Crack densities in each ply of a damaged composite are estimated through non-destructive techniques such as ultrasonic and X-ray inspections. However, in coupon specimens, ply level damage can be estimated through the edge optical inspection technique. For a given thermo-mechanical loading, ply level stresses are determined through finite element analysis or analytical procedures depending on the complexity of the problem. Estimated ply level stresses and crack density information are then utilized to predict the TMC and crack junction openings. Prediction of openings requires understanding of TMC and delaminations at TMC tips and crack junction areas in terms of crack density and ply level stresses. To construct the damage network, one needs to know the location of all TMC junctions, which is an extremely tedious and time-consuming task. In this case, some assumptions are required to make the analysis tractable. In this study, it is assumed that TMC run through the entire width of the ply and that TMC are evenly distributed in individual plies. It is also assumed that a delamination exists at every intersection of TMC. With these assumptions, the number of crack junctions can be determined from the number of TMC in individual plies. Knowing crack densities of individual plies, average TMC spacing values can be determined. As discussed in the work of Noh *et al* [20], the TMC openings depend on the applied thermo-mechanical loads, material properties of lamina, ply thickness, TMC spacing,

and ply-level stress. TMC openings along with delamination size can be obtained once these parameters are determined. network.

Once the openings of TMC and crack junction are calculated, the damage network needs to be constructed to analyze cryogen flow. Figure 2 illustrates three possible cases of TMC arrangement in three adjacent plies of a cross ply composite. In these arrangements, TMC are evenly distributed in each ply. In the first arrangement, crack densities of $i^{th}$ and $i+2^{th}$ plies is the same and TMC are evenly distributed in each ply. Due to this, the crack junctions in $i^{th}$ and $i+1^{th}$ ply-interfaces are aligned (*i.e,* no offset is present). In the second arrangement, crack densities of $i^{th}$ and $i+2^{th}$ plies is the same, but there is a relative shift in arrangement of TMC in $i+2^{th}$ ply relative to $i^{th}$ ply. Due to the relative shift, the crack junctions in $i^{th}$ and $i+1^{th}$ ply interfaces are offset by a distance. In the third arrangement, crack densities of $i^{th}$ and $i+2^{th}$ plies is different. The relative shift in arrangement of TMC between $i^{th}$ and $i+2^{th}$ plies, as described earlier is zero. However, there is an offset between crack junctions in $i^{th}$ and $i+1^{th}$ ply-interfaces due to difference in crack densities of these plies. Thus, an offset between crack junctions might exist either due to relative shift in the TMC arrangement or due to difference in crack densities of alternate plies. In presence of TMC resistance, off-set between crack junctions in adjacent ply-interfaces affects the flow rate through damage network. Thus the leak rate for the aligned crack junctions case is expected to be larger compared to the case where the crack junctions are offset by a distance. For simple models, it may be possible to determine all distances of crack junctions but it is impractical in reality. In the current study, due to the assumption that TMC are evenly distributed in individual plies with no relative shift in arrangement of TMC in alternate plies, the distances of crack junctions can be approximated as illustrated in Fig. 3. The $i^{th}$ and $i+2^{th}$ plies in the figure have

Aligned crack junctions

Ply $i+2$

Ply $i+1$

Ply $i$

a) Alternate plies of same crack density with crack junctions in adjacent ply-interfaces aligned.

Offset crack junctions

Crack junction

TMC

b) Alternate plies of same crack density with crack junctions in adjacent ply-interfaces offset.

Ply $i+2$

Ply $i+1$

Ply $i$

Offset crack junctions

Ply $i+2$

Ply $i+1$

Ply $i$

Ply-interface $i+1$

Ply-interface $i$

c) Alternate plies of different crack density with crack junctions in adjacent ply-interfaces offset.

Fig. 2. Different RVEs for cross-ply laminates with interconnected TMC
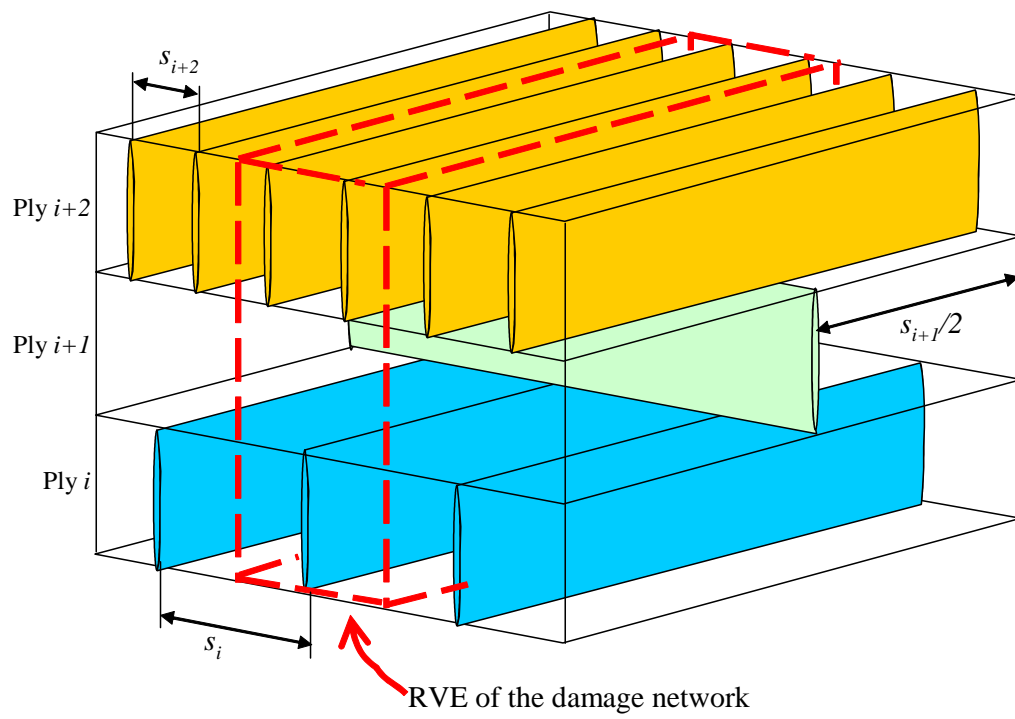
Fig. 3. Damage network in a cross-ply composite

different crack spacing $s_i$ and $s_{i+2}$, respectively. Using periodicity of TMC, only the boxed region needs to be analyzed. The distances between crack junctions in the region can be determined using $s_i$ and $s_{i+2}$. As mentioned, the calculation of distance depends on the relative location of TMC in $i+2^{th}$ ply with respect to TMC in $i^{th}$ ply. The relative location is important especially for plies with low crack density (large TMC spacing). The prediction of leak rate based on the aligned crack junction makes an upper bound and the prediction based on offset crack junctions makes a lower bound.

After modeling the damage network from the procedure described above, the amount of cryogen leakage is estimated by analyzing cryogen flow through the leakage paths of the damage network. An example of such a realistic case is shown in Fig. 4. Figure 4a illustrates an X-ray image of an eight ply cryogenic composite. The lay-up of the sample was $[0/45/90/-45]_s$. Micrograph of one of the edges of the specimen is also illustrated. The picture was taken through a metallographic microscope. Damage was induced into the composite due to pressurization during leak test. Crack density information is obtained through the above mentioned techniques. From the crack density information, damage network is constructed assuming that TMC in each ply are equally spaced (Fig. 4b). Based on the estimated TMC and crack junction openings, a three-dimensional model of leakage path is constructed as illustrated in Fig. 4d. A boundary value problem is formulated and cryogen flow through leakage paths is analyzed numerically. In the present study, a commercial computational fluid dynamics software, FLUENT is used to analyze cryogen flow through leakage paths. The amount of cryogen leakage is estimated by determining the effective conductance of the leakage path to the cryogen flow. In the presence of high aspect ratio TMC and large number of plies, it is computationally difficult to model the three-dimensional

a) X-ray of an unloaded IM6/950-1, graphite- epoxy specimen with $[90/45/0/-45]_s$ lay-up.

b) Schematic of damage network

c) 2-D Schematic of a leakage path.

**Cryogen Outlet**

**Cryogen Inlet**

d) 3-D Schematic of leakage path.
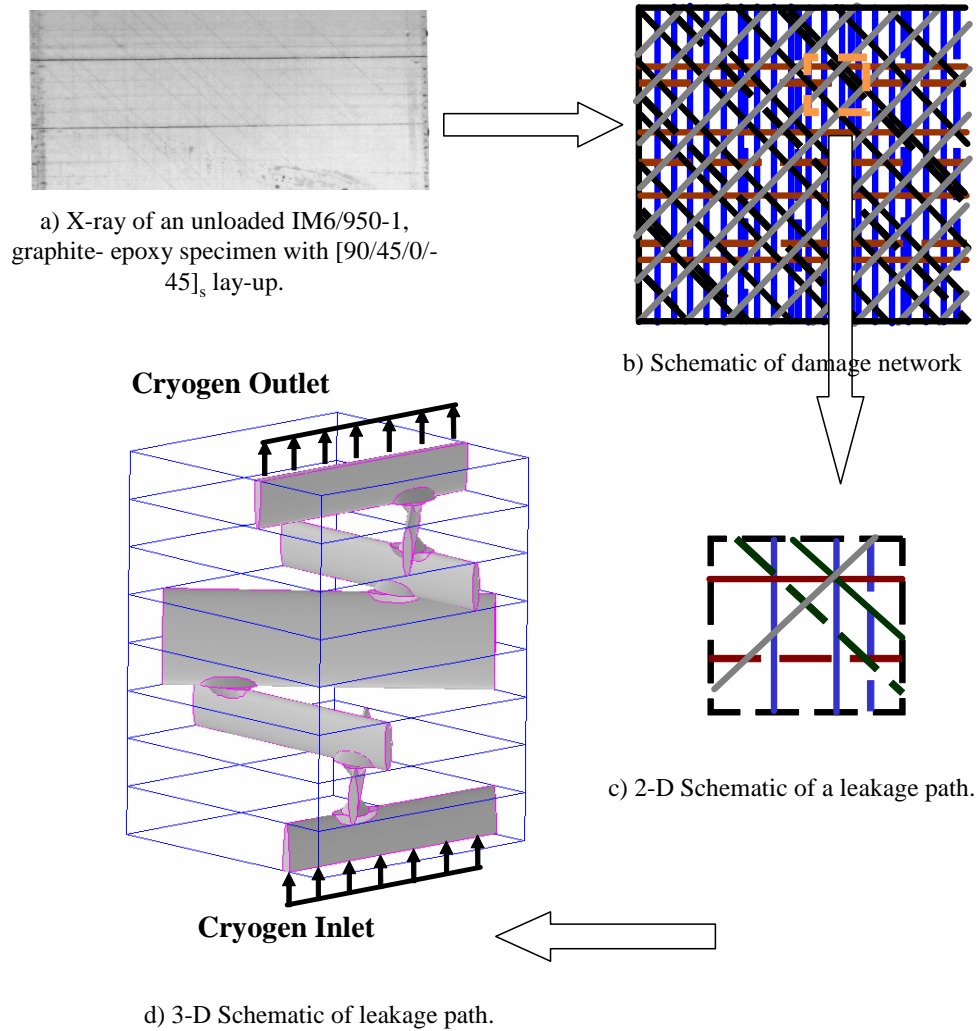
Fig. 4. Methodology for cryogen leakage estimation

leakage paths and analyze cryogen flow through it. In such cases, estimation of effective conductance through analytical procedures is advantageous. In the current work, a simple analytical method called Simplified model is presented to estimate the effective conductance. This method estimates the effective conductance from crack junction conductance and TMC resistance, arising from offset of crack junctions in adjacent ply-interfaces. The crack junction conductance and TMC resistance are estimated through numerical simulations.

The present work considers key steps involved in the construction of a leakage path in a damaged composite followed by estimation of effective conductance through numerical simulations. A cross-ply composite with five plies is considered. Gaseous hydrogen leakage through the leakage paths is investigated at two different temperatures namely cryogenic and room temperatures. The boundary value problem employed in simulating hydrogen flow through leakage paths of the composite are discussed in detail in the next section. Parametric studies are carried out to investigate the effect of variation in crack density of one of the plies on the effective conductance of the composite. Details of the numerical simulations along with results are discussed in Chapter III. Difference in volumetric flow rates of gaseous hydrogen at cryogenic and room temperatures is also addressed. The Simplified model used in estimating the effective conductance is explained in detail in Chapter IV. An expression for effective conductance in terms of crack junction conductance and TMC resistance is derived for all of the cases considered in the five ply composite study. Chapter V mainly discusses the numerical simulations performed in estimating crack junction conductance and TMC resistance at the two temperatures. Effect of irregularities in TMC geometry on the volumetric flow rate of hydrogen are studied through two-dimensional parametric studies. The amount of cryogen leakage also depends on the

relative orientation of adjacent plies which alters the crack junction area. Variation of volumetric flow rate of hydrogen with relative orientation of adjacent plies in a two-ply composite is researched. The effect of crack junction area on volumetric flow rate of hydrogen through crack junction is investigated by considering different TMC opening combinations in adjacent plies thereby changing the crack junction area. For all cases considered, effective conductance of the five ply composite is estimated from the expressions derived using the Simplified model. These values are compared with the numerical simulation values to verify the accuracy of the model. Besides flow through leakage paths, hydrogen leakage by diffusion through matrix layer between unconnected TMC in a composite is also investigated. Two-dimensional parametric studies are conducted to examine the variation of volumetric flux of diffusing hydrogen through matrix with the thickness of matrix between unconnected TMC. The diffusion studies are discussed in the appendix.

B.   Cryogen flow through leakage paths

In the presence of well connected damage, cryogen flow through leakage paths as shown in Fig. 5 will be analyzed to estimate the amount of cryogen leakage. The figure illustrates the Representative Volume Element (RVE) of the cross-ply composite with five plies considered for the numerical study. It represents a simple case where the crack densities in each ply are equal. In such a case, there is one representative TMC in each ply in the RVE. The RVE is periodic in the $0°$ and $90°$ directions *i.e*, the composite can be represented by repeating the RVE in $0°$ and $90°$ directions respectively. Cryogen leakage through the RVE takes place due to pressure difference across the inner and outer surfaces of the composite, represented by $S_1$ and $S_2$ respectively. Due to the applied pressure difference across the composite, cryogen

Fig. 5. Schematic of RVE in a cross-ply composite with five plies and interconnected damage

flows from the $1^{st}$ ply to the $5^{th}$ ply through the network of TMCs and crack junctions as indicated in the figure. In the presence of cryogen flow through leakage paths, cryogen transport by diffusion through matrix is negligible and the matrix is considered impermeable to cryogen flow. Hence, cryogen has zero velocity along the surface of TMC. Due to periodicity of RVE, velocity and pressure of cryogen are considered periodic along the surface of intersection between the TMC and the lateral walls of RVE. Due to exposure of the composite to large temperature variations, it is necessary to investigate cryogen leakage at different temperatures. As mentioned earlier, gaseous hydrogen flow through leakage paths is analyzed at cryogenic and room temperatures. The gaseous cryogen flow through micro cracks can be - compressible/incompressible, molecular/viscous, laminar/turbulent. The characteristic of cryogen flow depends on parameters like Knudsen, Mach and Reynolds numbers.

Knudsen Number:    Knudsen Number is defined as the ratio of mean free path of gaseous cryogen to characteristic dimension of leakage path. It indicates the possibility of molecular flow of gaseous cryogen. The expression for Knudsen Number can be written as

$$Kn = \frac{\lambda}{\delta} \tag{2.1}$$

where $\delta$ is the characteristic dimension of the leakage path, $\lambda$ is the mean free path of gaseous cryogen given by the following expression

$$\lambda = \frac{RT}{\sqrt{2}\pi p d^2} \tag{2.2}$$

where $R$ is the universal gas constant, $T$ is the absolute temperature, $p$ is the pressure and $d$ is the molecular diameter of gaseous cryogen. In the present study, the TMC

opening is considered as the characteristic dimension, inlet pressure is taken to be the pressure in Equation (2.2) and the diameter of the hydrogen molecule is taken to be $4.08 \times 10^{-10}$m, obtained from Reference [21]. For the five ply case, the TMC opening is set equal to 1 percent ply-thickness and the ply-thickness is taken to be 141 $\mu m$, which is the thickness of a typical graphite-epoxy composite. Change in the opening of TMC with temperature is neglected in the present study. Hence, the TMC opening is equal to 1.41 $\mu m$ at cryogenic and room temperatures, as listed in Table I. In the present work, hydrogen flow is analyzed at pressure difference of $2.2 \times 10^5$ Pa across the composite. The mean free path computed at cryogenic and room temperatures along with the Knudsen numbers is listed in Table I. For Knudsen numbers greater than 10, pure molecular flow exists in the leakage paths. For Knudsen numbers less than 0.01, the gaseous cryogen flow is purely viscous and can be characterized by equations in continuum regime along with no slip boundary conditions [22]. For the present problem, from the Knudsen number values listed in Table I, it is concluded that the gaseous cryogen flow can be described by equations in continuum regime.

Table I. Knudsen number at cryogenic and room temperatures

|  | **Cryogenic Temperature** | **Room Temperature** |
| --- | --- | --- |
| Mean free path ($nm$) | 2.7 | 25.2 |
| TMC opening ($\mu m$) | 1.4 | 1.4 |
| Knudsen number | 0.001 | 0.01 |

<u>Mach Number</u>:    Mach Number is defined as the ratio of characteristic speed of cryogen in the leakage path to speed of sound in the cryogen medium. Mach Number defines the appearance of compressibility effects as gaseous cryogen flows through the

leakage paths. The expression for Mach Number can be written as

$$Ma = \frac{v}{v_s} \tag{2.3}$$

where $v$ is the characteristic speed of cryogen and $v_s$ is the speed of sound in cryogen. The speed of sound in gaseous cryogen medium is usually expressed by the following formula

$$v_s = \sqrt{\gamma R T} \tag{2.4}$$

where $\gamma$ is the ratio of specific heats $(c_p/c_v)$ of cryogen. In the current work, the magnitude of maximum velocity of cryogen is taken to be its characteristic speed. For the applied pressure difference values mentioned earlier, the maximum velocities are found near the crack junctions equal to 360 and 220 $m/s$ at cryogenic and room temperatures. The speed of sound in hydrogen, characteristic speed and the Mach numbers at the two temperatures is listed in Table II. Compressibility effects are usually insignificant if the flow is subsonic *i.e, $Ma < 0.1$*. Based on the Mach number values given in Table II, it can be concluded that compressibility effects can be neglected at room temperature where as they might be present at cryogenic temperature. However, for simplicity, these effects are neglected in the current study and hydrogen is assumed to be incompressible.

Table II. Mach number at cryogenic and room temperatures

|  | Cryogenic Temperature | Room Temperature |
|---|---|---|
| **Speed of sound** (m/s) | 423 | 1287 |
| **Characteristic Speed** (m/s) | 360 | 220 |
| **Mach number** | 0.85 | 0.17 |

Reynolds Number:   Reynolds number is the ratio of inertial forces to viscous forces in cryogen flow. In the present study local Reynolds number is considered which is defined as

$$Re = \frac{\rho v \delta}{\mu} \tag{2.5}$$

where $\delta$ is the cube root of volume of the three-dimensional element in the computational domain, $v$ is the magnitude of velocity at the centroid of the element, $\rho$ is the density, $\mu$ is the viscosity of cryogen. In the current work, the Reynolds numbers are sufficiently small that the flow is laminar. However at very low Reynolds numbers (*i.e, Re* $\leq 1$) [18] inertial forces are negligible and creeping behavior is usually observed due to dominant viscous forces in cryogen flow. However, at higher Reynolds numbers, inertial effects might become important.

Based on the Knudsen, Mach and Reynolds numbers discussed above for the present problem, the governing equations for cryogen flow through leakage paths are conservation of mass and momentum equations given by

$$\frac{\partial \left( \rho v_i \right)}{\partial x_i} = 0 \tag{2.6}$$

$$\frac{\partial \left( \rho v_i v_j \right)}{\partial x_j} = -\frac{\partial p}{\partial x_i} + \frac{\partial \tau_{ij}}{\partial x_j} + \rho g_i \tag{2.7}$$

where $v_i$, $x_i$, $\tau_{ij}$ and $g_i$ are the velocity, position, shear stress and gravitational force components. Gravity effects are neglected in the current analysis. Further, cryogen is assumed to be a Newtonian fluid. The constitutive equation for cryogen is thus given by

$$\tau_{ij} = \mu \left[ \frac{\partial v_i}{\partial x_j} + \frac{\partial v_j}{\partial x_i} \right] \tag{2.8}$$

In the above equations due to the incompressibility assumption, the density does not vary spatially *i.e*, $\rho$ is independent of $x_i$. Utilizing this fact in Equation (2.6), and sub-

stituting Equation (2.8) in Equation (2.7), the governing equations for incompressible Newtonian fluid (cryogen) reduce to Continuity and Navier-Stokes equations, given by

$$\frac{\partial v_i}{\partial x_i} = 0 \tag{2.9}$$

$$\rho \left( v_j \frac{\partial v_i}{\partial x_j} \right) = -\frac{\partial p}{\partial x_i} + \mu \left( \frac{\partial^2 v_i}{\partial x_j \partial x_j} \right) \tag{2.10}$$

The boundary conditions employed to solve the above mentioned boundary value problem are: pressure at the inner and outer surfaces of the composite (i.e., the inlet surface $S_1$ and the outlet surface $S_2$) and no slip (zero- velocity) along the cryogen-TMC interface, $S_3$. These boundary conditions are described below

$$p = P_1 \text{ on } S_1;\ p = P_2 \text{ on } S_2;\ v_i = 0 \text{ on } S_3 \tag{2.11}$$

where $P_1$, $P_2$ are the prescribed pressures at inlet and outlet of the leakage path. In addition to Equation (2.11), the velocity is assumed to be periodic along the lateral surfaces of the RVE that intersect the TMC ($S_4$). The above mentioned boundary value problem is solved for the velocity components and pressure of cryogen in the leakage path.

The amount of cryogen leakage through the leakage paths can be measured by estimating either mass or volumetric flow rates. Since cryogen is considered incompressible, the mass flow rate can be expressed as the product of volumetric flow rate and the density. Thus, mass flow rate and volumetric flow rates are interchangeable by a factor of density. In the present study, volumetric flow rate is used as the quantity to measure the amount of cryogen leakage, which can be computed from the following expression

$$Q = \int_S v_i N_i \tag{2.12}$$

where $Q$ is the volumetric flow rate, $S$ ($=S_1$ or $S_2$) is the top or bottom surface of the leakage path (Fig. 5) and $N_i$ is the component of unit normal to the surface $S$.

In the cryogen leakage problem, pressure difference across the composite is pre-scribed and volumetric flow rate is usually estimated. Hence, it is advantageous to express volumetric flow rate in terms of applied pressure difference. It is possible to express volumetric flow rate as a power law in the pressure difference as

$$Q = C_{eff} \left( \Delta P \right)^n \tag{2.13}$$

where $C_{eff}$ is the effective conductance, $\Delta P = P_1\text{-}P_2$ is the applied pressure difference across the leakage path and $n$ is an exponent. $C$ and $n$ depend on the properties of cryogen and the geometry of leakage path. Usually a non-linear behavior is observed ($n \neq 1$) when the flow is turbulent but in presence of network of channels, even in the laminar flow regime a power law can be used to describe the dependence of volumetric flow rate on applied pressure difference. However, at low Reynolds numbers (Re<1) a linear dependence of volumetric flow rate on applied pressure difference is observed due to absence of inertial forces in cryogen flow. Deviation from linearity is observed when Re>13 [18]. At these Reynolds numbers the inertial effects become important along with the viscous forces in cryogen flow. Thus, if $C$ and $n$ are known in Equation (2.13) for a leakage path, the volumetric flow rate can be estimated for any given pressure difference value.

In certain cases, the volumetric flow rate can also be expressed by linear Darcy's relation [18]

$$Q = \frac{K_{22}A}{\mu} \frac{\Delta P}{T} \tag{2.14}$$

where $K_{22}$ is a component of the permeability tensor, $K$, $A$ is the cross-sectional area and $T$ is the thickness of the composite. Since the fluid flow is only in the $x_2$-direction, the rest of the components of the permeability tensor are zero. A similar expression is available when $n = 1$ in Equation (2.13). Thus, the permeability can be expressed in terms of the conductance as

$$K_{22} = \frac{CT\mu}{A} \tag{2.15}$$

CHAPTER III

NUMERICAL MODELING OF CRYOGEN FLOW THROUGH LEAKAGE

PATHS IN A CROSS-PLY COMPOSITE

A.   Estimation of effective conductance of a composite to cryogen flow

In this chapter, the effective conductance of a cross-ply composite with five plies (introduced in chapter II) to gaseous hydrogen flow is estimated through numerical simulations. Crack densities in each ply are chosen such that a simple RVE could be constructed. The dimensions of RVE depend on the average TMC spacing of $1^{st}$, $2^{nd}$, $3^{rd}$, $4^{th}$ and $5^{th}$ plies indicated by $s_1$, $s_2$, $s_3$, $s_4$ and $s_5$ respectively. In the current study, the average TMC spacings $s_1$, $s_2$, $s_4$ and $s_5$ are each set equal to $s = 4h$, where $h$ is the ply-thickness. Crack density in the middle ply $i.e,$ $3^{rd}$ ply is varied thereby varying the average TMC spacing $s_3$. Due to change in $s_3$, the number of representative TMC in the $3^{rd}$ ply is altered along with the number of crack junctions at $2^{nd}$ and $3^{rd}$ ply-interfaces. Different cases are studied with $s_3 = s$, $s/2$, $s/3$ and $s/4$. All of the cases are distinguished by a parameter called normalized crack density in the middle ply $(\widetilde{\alpha_3})$, which is defined as the ratio of crack density in the third ply $(\alpha_3)$ to the crack density in the first ply $(\alpha_1)$. Note that the average TMC spacing is reciprocal of the crack density and thus, the normalized crack density in the middle ply can also be expressed as $\widetilde{\alpha_3} = s/s_3$. As mentioned earlier, gaseous hydrogen flow through the RVE of the five ply composite is studied at cryogenic temperature of 33.1 °K and room temperature of 300 °K. Flow properties of hydrogen at these temperatures are obtained from Reference [23] and listed in Table III. In the present study, the four cases with normalized crack density in the middle ply = 1, 2, 3 and 4 are investigated for the numerical estimation of effective conductance at the two

temperatures. Schematics of RVE for these four cases are illustrated in Figures 6, 7, 8 and 9 respectively.

Table III. Flow properties of gaseous hydrogen at cryogenic and room temperature

|  | Cryogenic Temperature | Room Temperature |
|---|---|---|
| **Density** (Kg/m$^3$) | 0.7644 | 0.08189 |
| **Viscosity** (Kg/m.s) | 1.763x10$^{-6}$ | 8.411x10$^{-6}$ |

The TMC in each ply are approximated as straight channels. Variation of the opening of TMC and crack junctions with various loading conditions is discussed in Reference [20] and in the current analysis, the opening of each TMC in each ply is set equal. Variation of the opening of TMC with the crack density is neglected and the TMC opening in all plies is set equal to 1 % ply-thickness $i.e$, $\delta = 0.01h$ as mentioned in Chapter II. Also, the variation of TMC opening with temperature is not considered. Due to delamination at ply-interfaces, the intersection of TMC in adjacent plies is assumed to be squares of side $0.01h$ (since TMC are approximated as straight channels and the opening of each TMC is $0.01h$). For the numerical simulations, the thickness of each ply is taken to be 141 $\mu m$, which is the typical ply thickness of a graphite epoxy cryogenic composite (IM6/950-1) tested for gaseous hydrogen leakage by NASA. Thus, the opening of each TMC is equal to 1.41 $\mu m$. The dimensions of RVE depend on the maximum TMC spacing in 0° and 90° direction. In the current study, for all the cases, the maximum TMC spacing in both directions is equal to $s = 4h$. Thus, the cross sectional dimensions of RVE, $l$ x $w$ are 564 x 564 $\mu m$. Boundary value problem (BVP) mentioned in Chapter II is solved in the domain of RVE for all the cases. Commercial Computational Fluid Dynamics

Fig. 6. Schematic of RVE of a cross-ply composite with five plies and normalized crack density in middle ply, $\widetilde{\alpha_3} = 1$ (w/s$_3$ = 1)

Fig. 7. Schematic of RVE of a cross-ply composite with five plies and normalized crack density in middle ply, $\widetilde{\alpha_3} = 2$ (w/s$_3$ = 2)
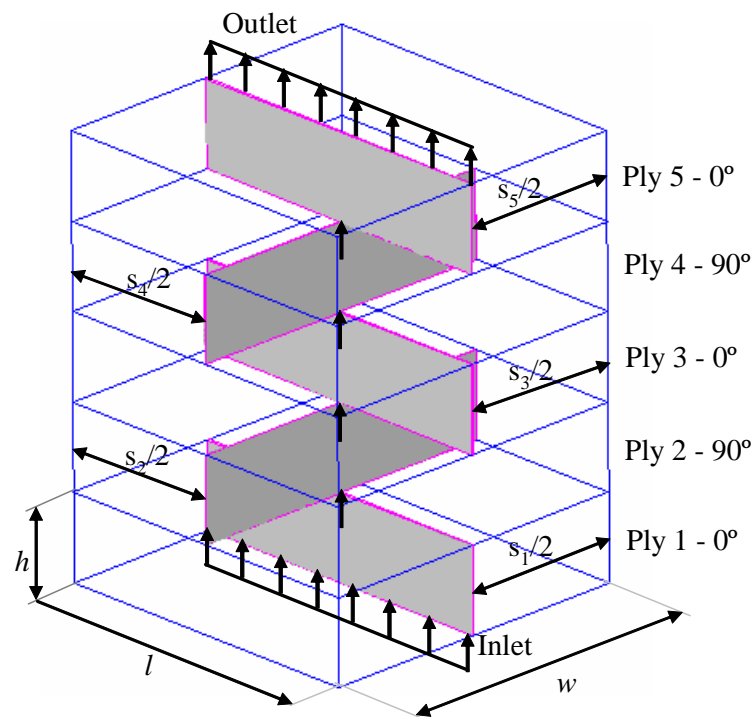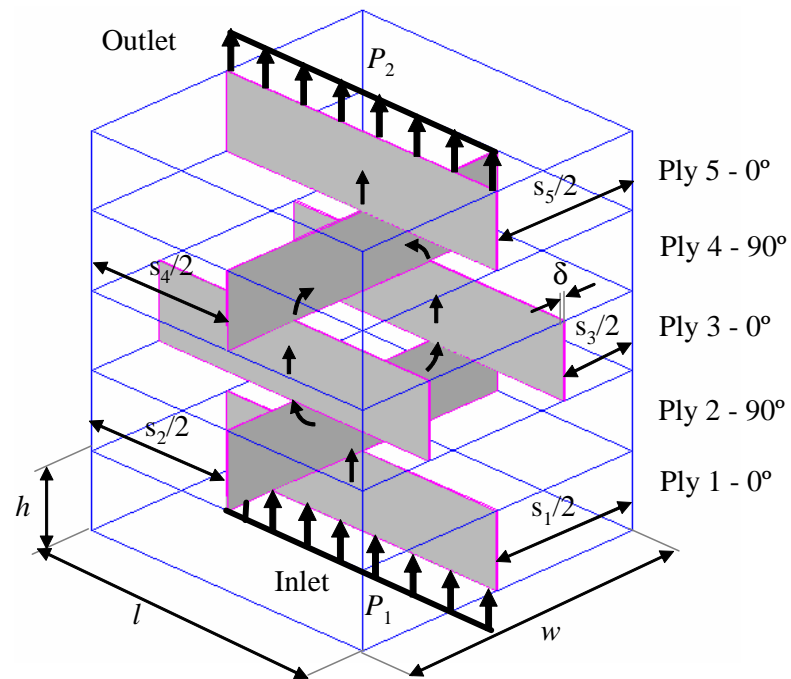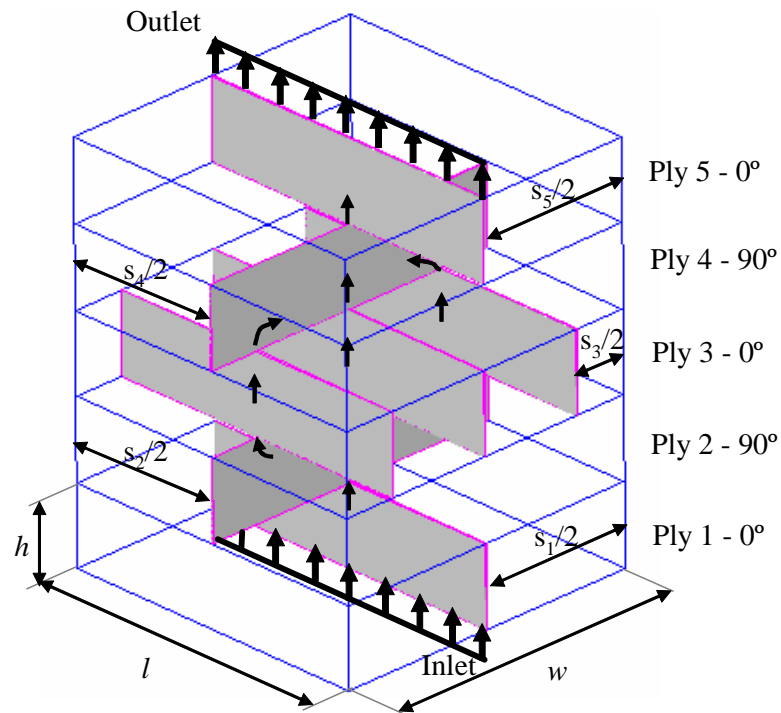
Fig. 8. Schematic of RVE of a cross-ply composite with five plies and normalized crack density in middle ply, $\widetilde{\alpha_3} = 3$ ($w/s_3 = 3$)
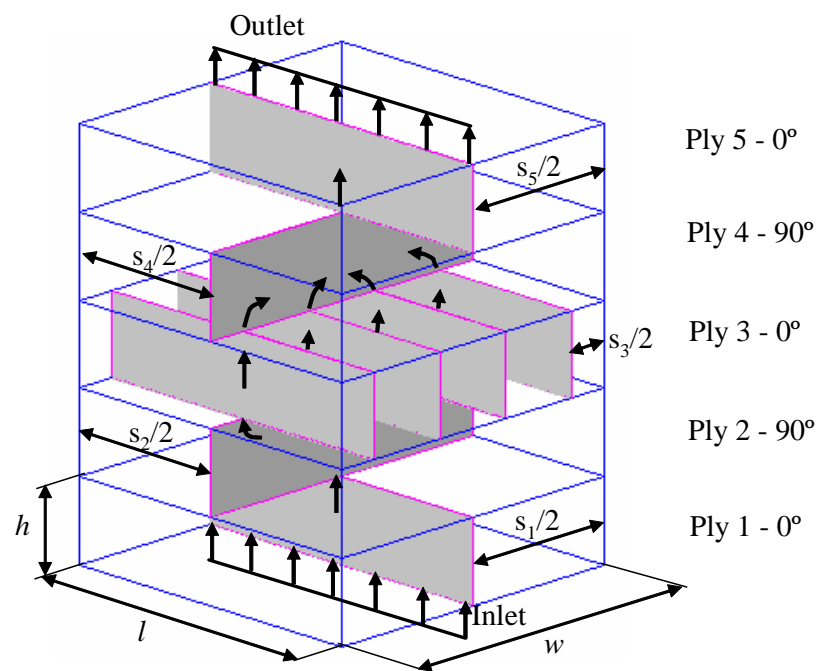
Fig. 9. Schematic of RVE of a cross-ply composite with five plies and normalized crack density in middle ply, $\widetilde{\alpha_3} = 4$ (w/s$_3$ = 4)

 Software, FLUENT is used to solve the BVP. A pressure difference of $\Delta P = P_1 - P_2$ = 2.2 x $10^5$ Pa is applied across the composite and the velocity, pressure distributions in the RVE are computed. The pressure gradient (ratio of pressure difference to the thickness of the composite) chosen for the current analysis is equivalent to the pressure gradient applied across the IM6/950-1 specimen, tested for gaseous hydrogen leakage at Marshall Space and Flight Center (MSFC). Hydrogen volumetric flow rate through the composite is determined using Equation (2.12). To obtain the variation of hydrogen volumetric flow rate with applied pressure difference, the volumetric flow rate is determined for three other values of pressure differentials. The other three pressure differentials are $\Delta P$ = 1.8 x $10^5$, 9.0 x $10^4$, 4.5 x $10^4$ Pa. For all four cases, the volumetric flow rate is determined at these pressure differentials. The effective conductance, $C_{eff}$, and the exponent $n$ in Equation (2.13) are then estimated by approximating the pressure differentials and volumetric flow rates using a power law equation.

 As mentioned in the previous paragraph, the boundary value problem is solved using a commercial Computational Fluid Dynamics software, FLUENT. FLUENT employs the Finite Volume Method to discretize the governing equations in the computational domain. Second-order upwind scheme is used in the discretization of momentum equation. With Second-order scheme, quantities at faces of a cell in the computational domain are obtained through Taylor series expansion of cell centered solution about the cell centroid. Similarly, second order scheme is used in the interpolation of pressure at cell faces. The SIMPLEC (SIMPLE-Consistent) algorithm is used for pressure-velocity coupling. The pressure and momentum under-relaxation factors are set to 0.2 and 0.5 respectively to aid convergence in the solution. The governing equations are linearized to implicit form. Segregated solver algorithm is used to

solve the reduced momentum and continuity equations sequentially. The discretized linear scalar equations in the computational domain are solved using Gauss-Seidel linear equation solver. The computations are performed using SGI Origin 3800 super computer. Each case is solved for 1000 iterations until the scaled residuals of continuity, $v_1$, $v_2$ and $v_3$ components of velocities are nearly constant, equal to $10^{-5}$ in magnitude. The equality of volumetric flow rate of hydrogen at inlet and outlet of the RVE is also checked. All the computations nearly took 3 hours of computational time to meet the above mentioned specifications on convergence.

The results of numerical simulations for the cases with normalized crack density in middle ply = 2 and 3 at cryogenic and room temperatures are discussed below.

1.    Normalized crack density in middle ply, $\widetilde{\alpha_3} = 2$

The schematic of RVE of the five ply composite is illustrated in Figure 7. The average TMC spacing in $1^{st}$, $2^{nd}$, $4^{th}$, and $5^{th}$ plies is $4h$ each; whereas, the average TMC spacing in the $3^{rd}$ ply is $2h$. Because of these TMC spacings, the number of representative TMC in the $3^{rd}$ ply in RVE is 2 and the number of representative TMC in remaining plies is 1 each. Schematic of the computational mesh is illustrated in Figure 10. Approximately 600,000 hexahedral elements are used to mesh the computational domain. The results of the numerical simulations at cryogenic and room temperatures are discussed below

Cryogenic Temperature:    For a pressure differential of 2.2 x $10^5$ Pa across the RVE, Fig. 11 illustrates the contour plot of the magnitude of velocity $v$ and Fig. 12 illustrates the contour plot of Reynolds number. These contour plots are two-dimensional plots along the mid-plane of the RVE. Since the two crack junctions at

$2^{nd}$ and $3^{rd}$ ply-interfaces are offset by the same distance relative to crack junctions at $1^{st}$ and $4^{th}$ ply-interfaces, the velocity values at these junctions are found equal. Also, the Reynolds number is maximum near the crack junctions, approximately equal to 90. The volumetric flow rate is computed at several pressure differentials and the variation is plotted in Figure 13. Using a curve fit, the relation between volumetric flow rate and applied pressure differential can be expressed by the following relation

$$Q = 3.28 \text{ x } 10^{-10}(\Delta P)^{0.66} \tag{3.1}$$

Comparing the equation with Equation (2.13), the effective conductance of the five ply composite is $3.28 \text{ x } 10^{-10} m^3/(\text{s.Pa}^{0.66})$ and the exponent $n$ is 0.66.

Room Temperature: At room temperature, the contour plot of magnitude of velocity $v$ and the Reynolds number are illustrated in Figures 14 and 15 respectively. In this case, the maximum hydrogen velocity is less than the value at cryogenic temperature. This is due to the decrease in the viscosity of hydrogen by a factor of 4.7 at cryogenic temperature. At low viscosity, the viscous resistance is less resulting in higher velocities. Similarly, the maximum Reynolds number at room temperature is less than that at cryogenic temperature. Variation of volumetric flow rate with applied pressure difference is illustrated in Fig. 16. Volumetric flow rate and the applied pressure differentials are related by the following equation

$$Q = 15.06 \text{ x } 10^{-11}(\Delta P) \tag{3.2}$$

Comparing the equation with Equation (2.13), the effective conductance of the five ply composite is $15.06 \text{ x } 10^{-11} m^3/(\text{s.Pa})$ and the exponent $n$ is 1.

Ply 3

0 °

Ply 2

90 °

Fig. 10. Two-dimensional schematic of computational mesh in $2^{nd}$ ply along the mid-plane of RVE for $\widetilde{\alpha_3} = 2$

Fig. 11. Two-dimensional contour plot of velocity magnitude $v$ along the mid-plane of RVE of the cross-ply composite with five plies and $\widetilde{\alpha_3} = 2$ at cryogenic temperature

Fig. 12. Two-dimensional contour plot of Reynolds number along the mid-plane of RVE of the cross-ply composite with five plies and $\widetilde{\alpha_3} = 2$ at cryogenic temperature

Fig. 13.  Variation of volumetric flow rate with applied pressure difference in cross-ply composite with five plies and $\widetilde{\alpha_3} = 2$ at cryogenic temperature

Fig. 14. Two-dimensional contour plot of velocity magnitude v along the mid-plane of RVE of the cross-ply composite with five plies and $\widetilde{\alpha_3} = 2$ at room temperature

Fig. 15. Two-dimensional contour plot of Reynolds number along the mid-plane of RVE of the cross-ply composite with five plies and $\widetilde{\alpha_3} = 2$ at room temperature

Fig. 16. Variation of volumetric flow rate with applied pressure difference in cross-ply composite with five plies and $\widetilde{\alpha_3} = 2$ at room temperature

2.   Normalized crack density in middle ply, $\widetilde{\alpha_3} = 3$

When the normalized crack density in the middle ply is 3, the schematic of RVE of the five ply composite is shown in Fig. 8. The average TMC spacing in the $3^{rd}$ ply is $1.33h$ where as the average TMC spacing in remaining plies is $4h$. The RVE contains three representative TMC in the third ply, and one representative TMC in each of the remaining plies. The computational mesh of the RVE is illustrated in Fig. 17. The domain is meshed with approximately 600,000 hexahedral elements. Results of the numerical simulations at cryogenic and room temperatures are discussed below

Cryogenic Temperature:   Figures 18 and 19 illustrate the two-dimensional contour plots of magnitude of velocity and the Reynolds number respectively$3^{rd}$. The velocities of hydrogen at the middle crack junction in $2^{nd}$ and $3^{rd}$ ply-interfaces is larger compared to the velocities at the outer most crack junctions. Also, velocities at outer most crack junctions in these ply-interfaces are found to be equal. This behavior is observed due to difference in the offset distance between middle crack junction, outermost crack junctions and crack junction in adjacent ply-interface. Variation of volumetric flow rate of hydrogen with applied pressure difference is illustrated in Fig. 20. The volumetric flow rate and applied pressure differentials are found to obey the following relation

$$Q = 3.59 \text{ x } 10^{-10}(\Delta P)^{0.66} \tag{3.3}$$

Comparing the equation with Equation (2.13), the effective conductance of the five ply composite is $3.59 \text{ x } 10^{-10} m^3/(s.Pa^{0.66})$ and the exponent $n$ is 0.66.

Room Temperature:   Contour plot of magnitude of velocity along the mid-plane of the RVE is shown in Fig. 21, and Fig. 22 illustrates the contour plot of the Reynolds number. Variation of volumetric flow rate of hydrogen with applied
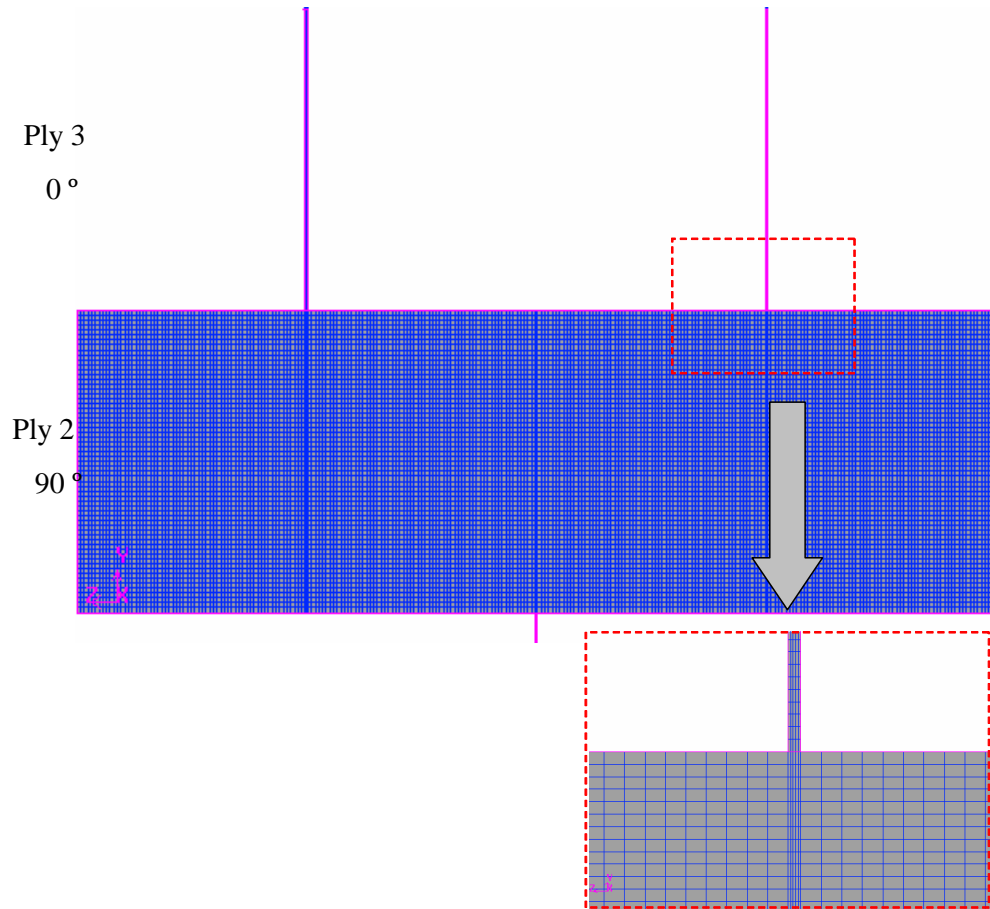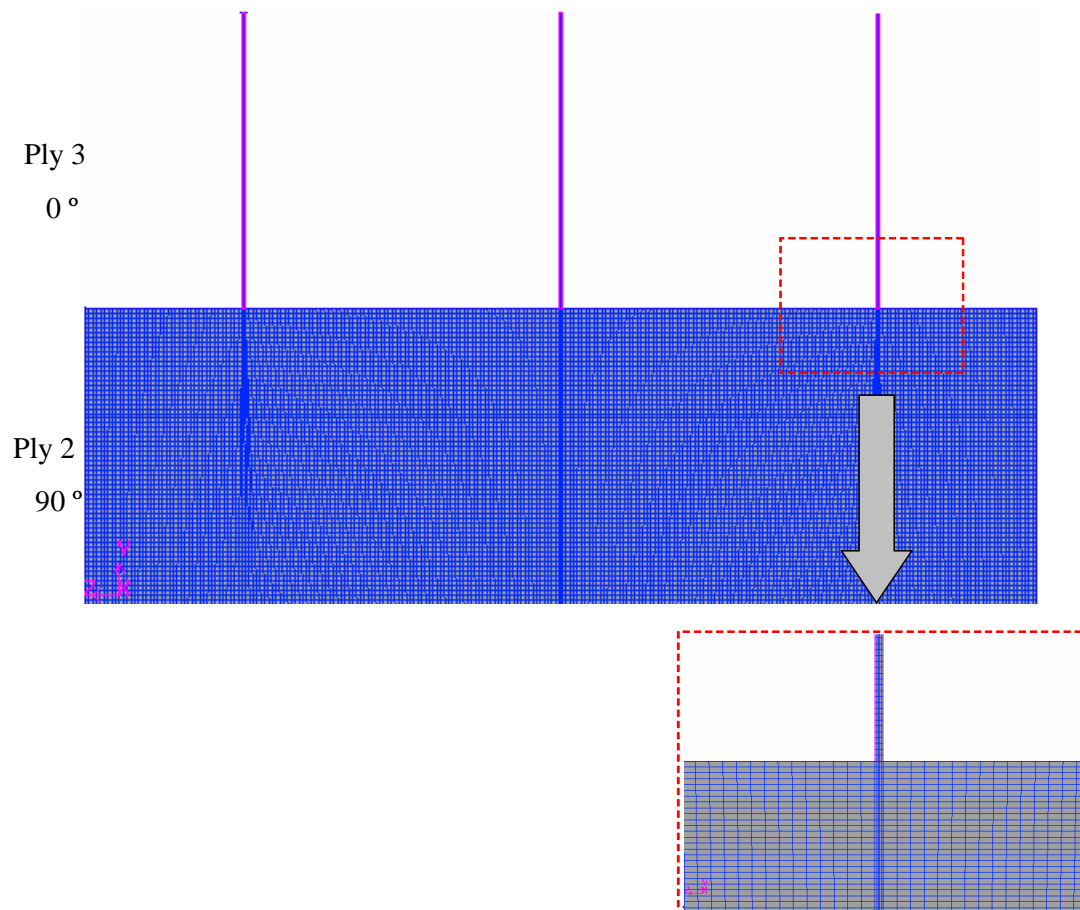
Fig. 17. Two-dimensional schematic of computational mesh in 2nd ply along the mid-plane of RVE for $\widetilde{\alpha_3} = 3$
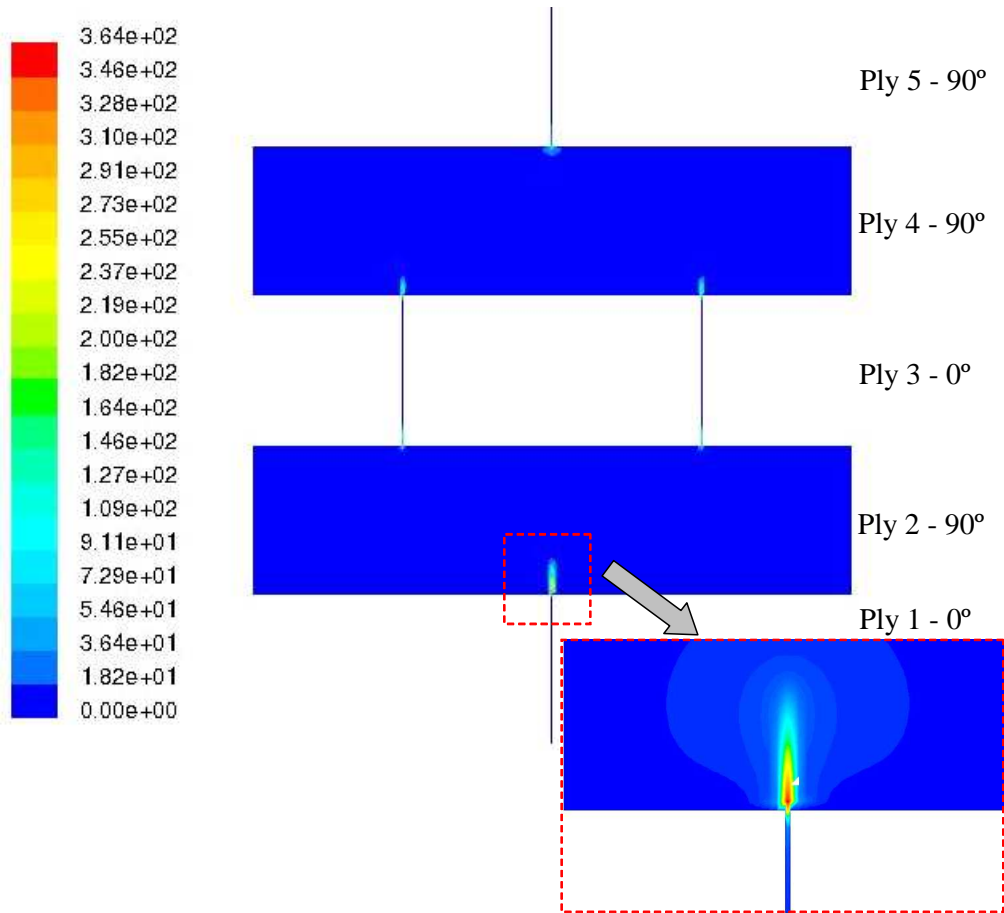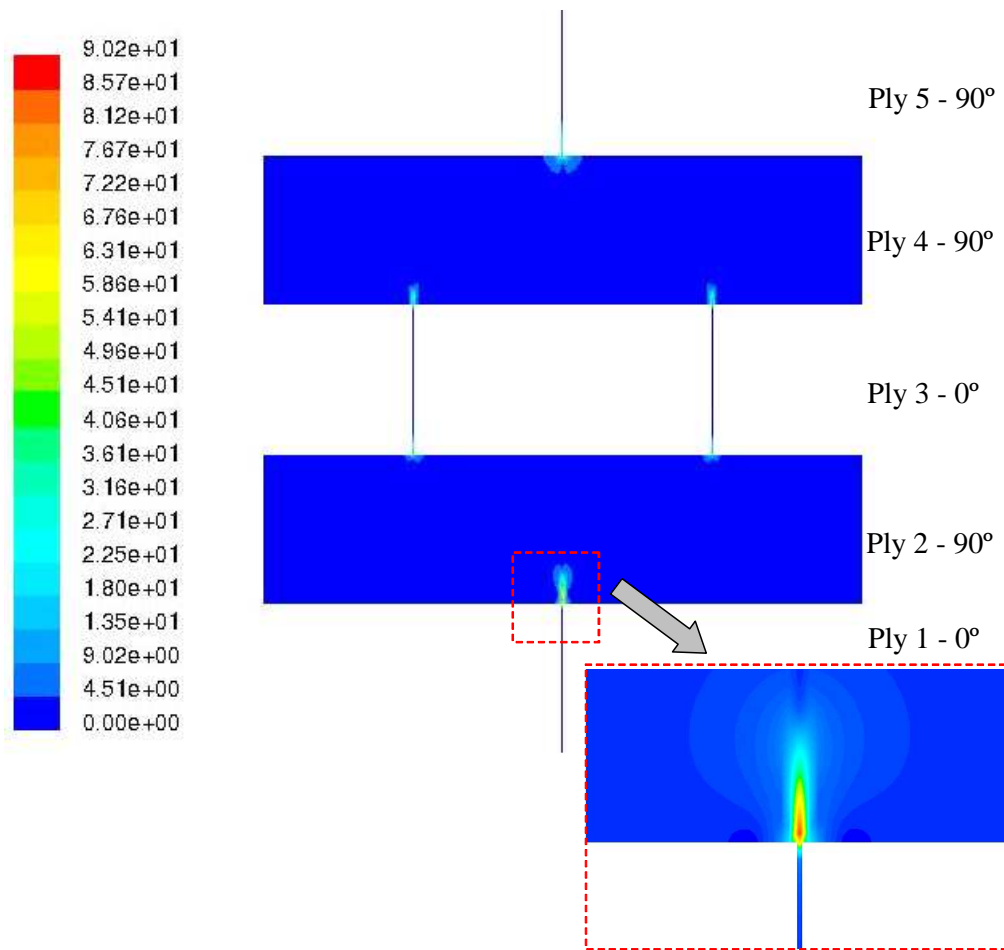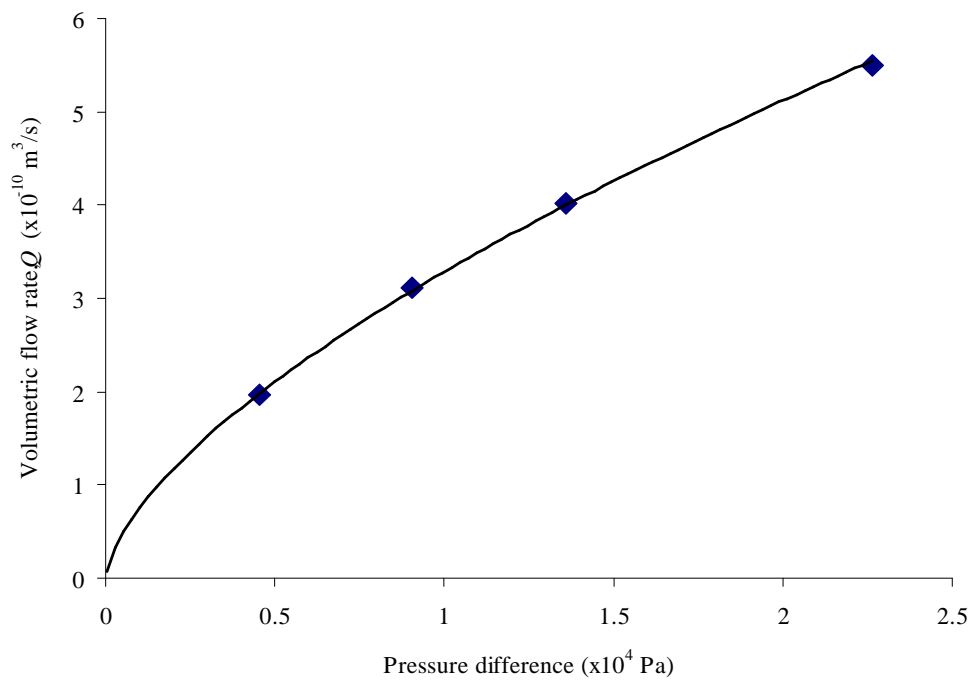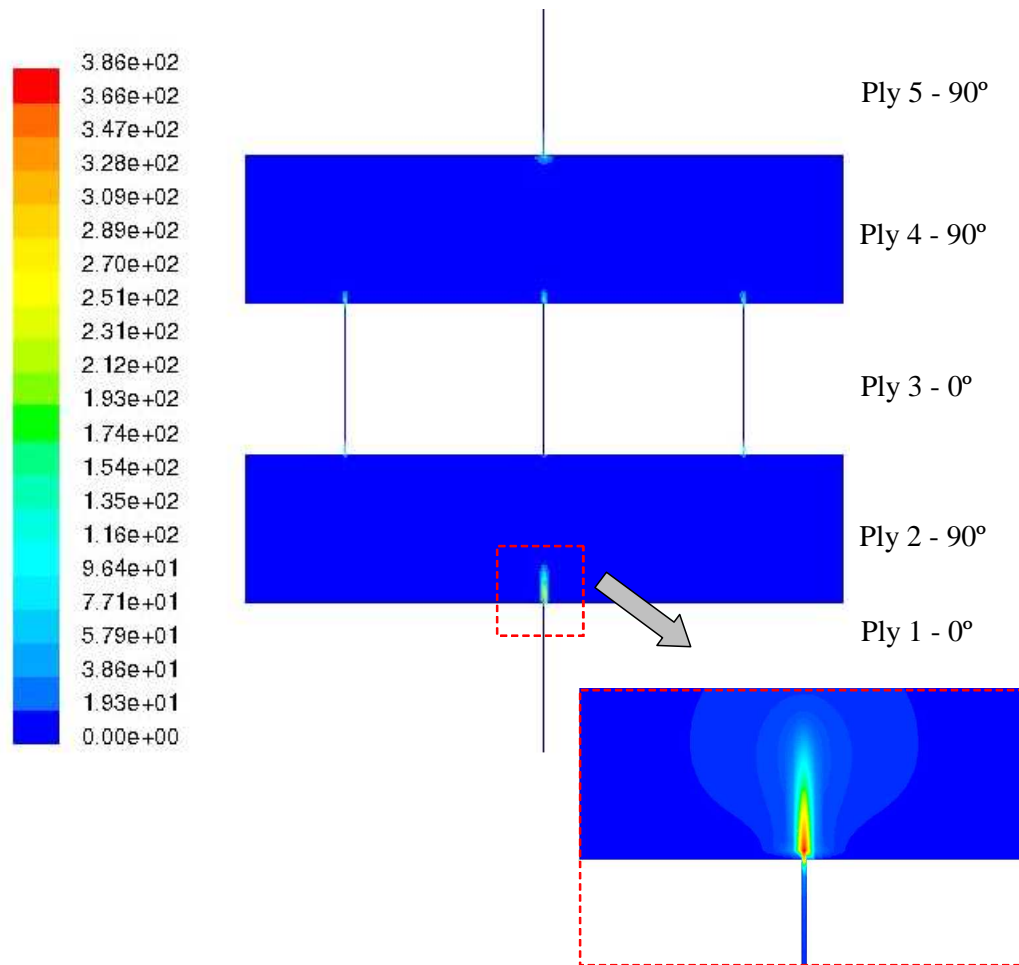
Fig. 18. Two-dimensional contour plot of velocity magnitude v along the mid-plane of RVE of the cross-ply composite with five plies and $\widetilde{\alpha_3} = 3$ at cryogenic temperature

Ply 5 - 90º

Ply 4 - 90º

Ply 3 - 0º

Ply 2 - 90º

Ply 1 - 0º
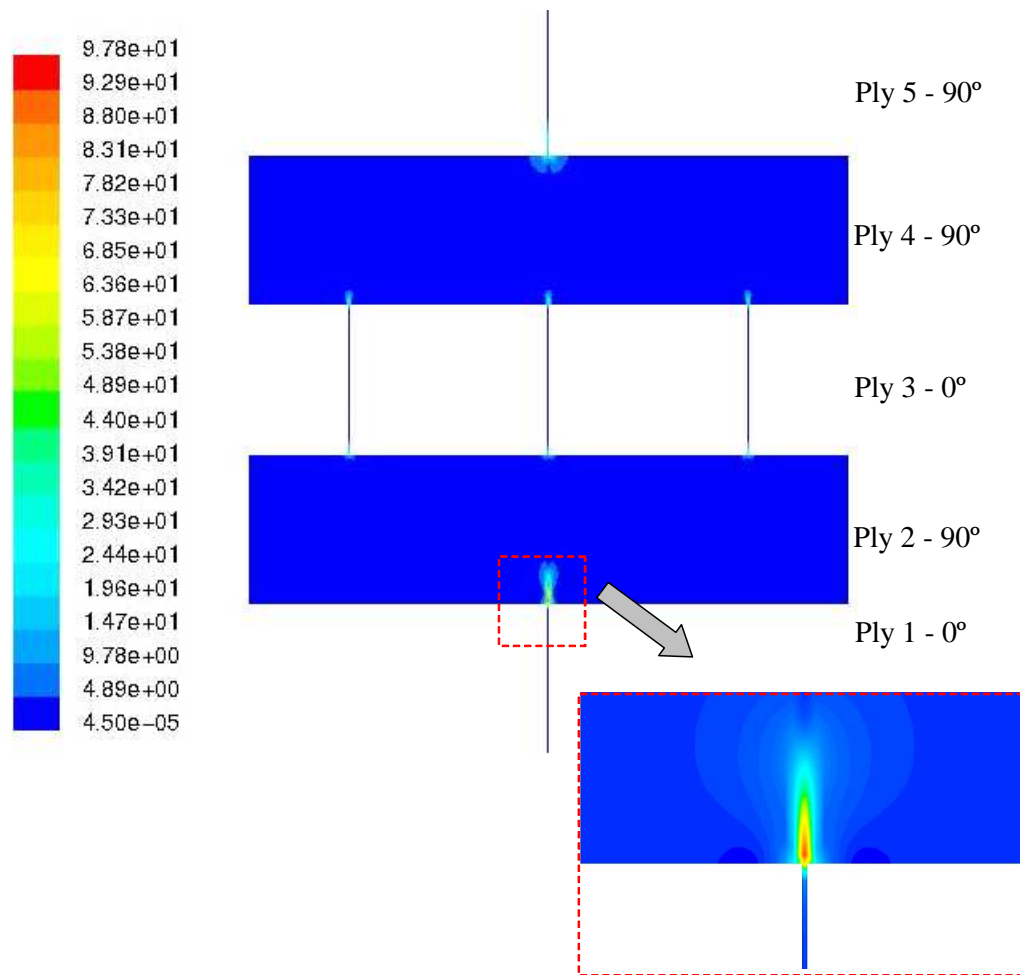
Fig. 19. Two-dimensional contour plot of Reynolds number along the mid-plane of RVE of the cross-ply composite with five plies and $\widetilde{\alpha_3} = 3$ at cryogenic temperature
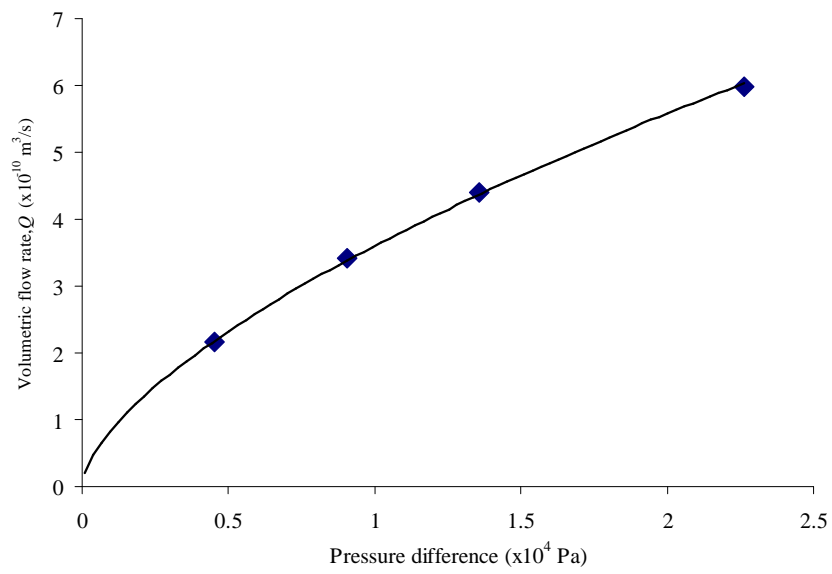
Fig. 20. Variation of volumetric flow rate with applied pressure difference in cross-ply composite with five plies and $\widetilde{\alpha_3} = 3$ at cryogenic temperature
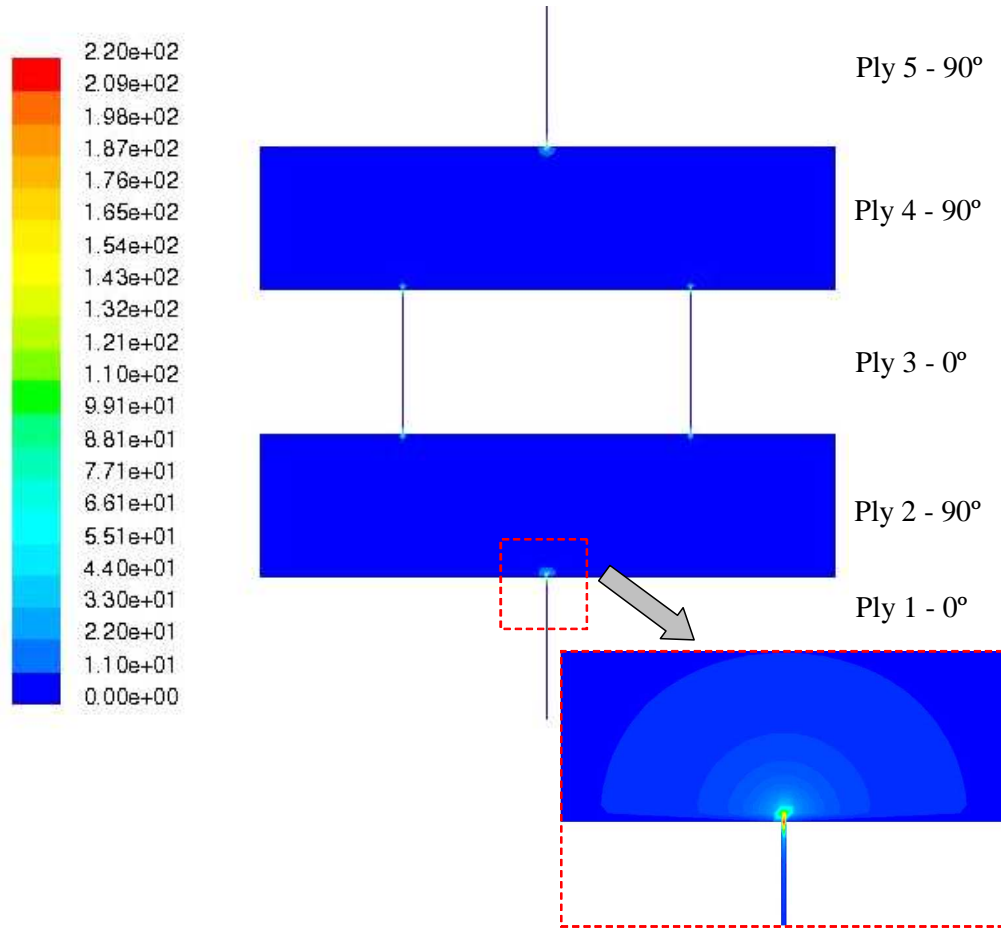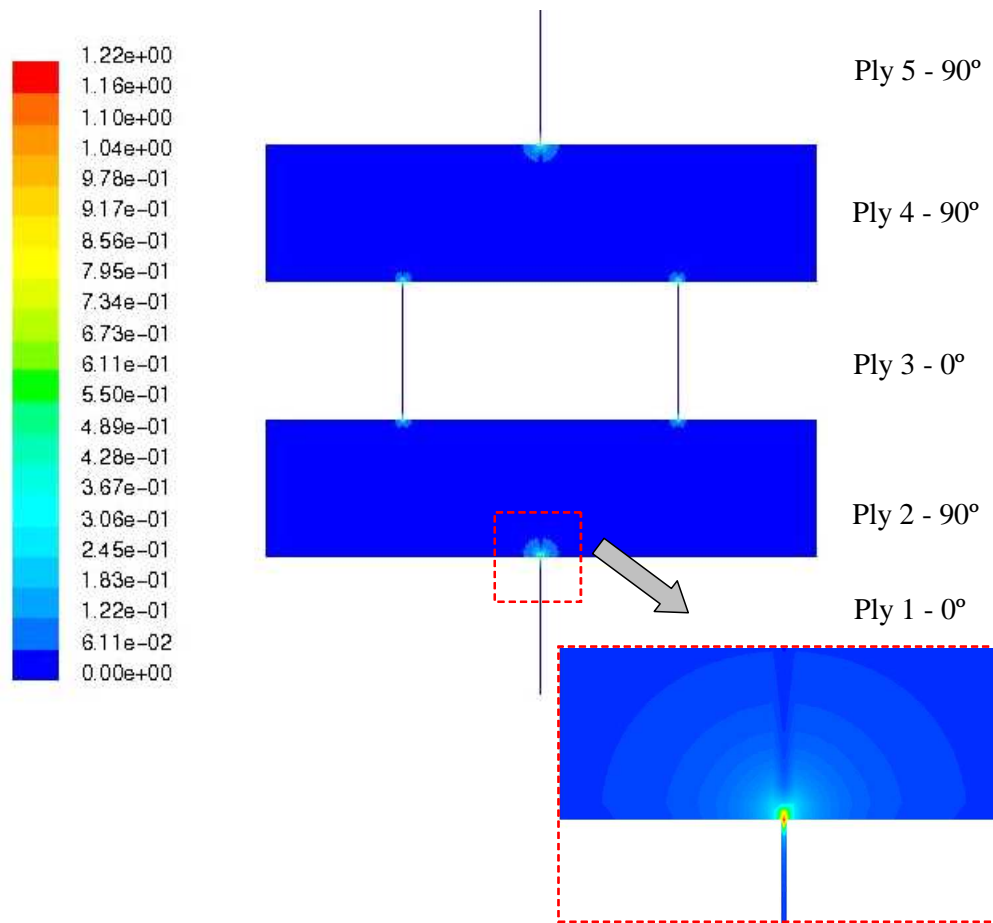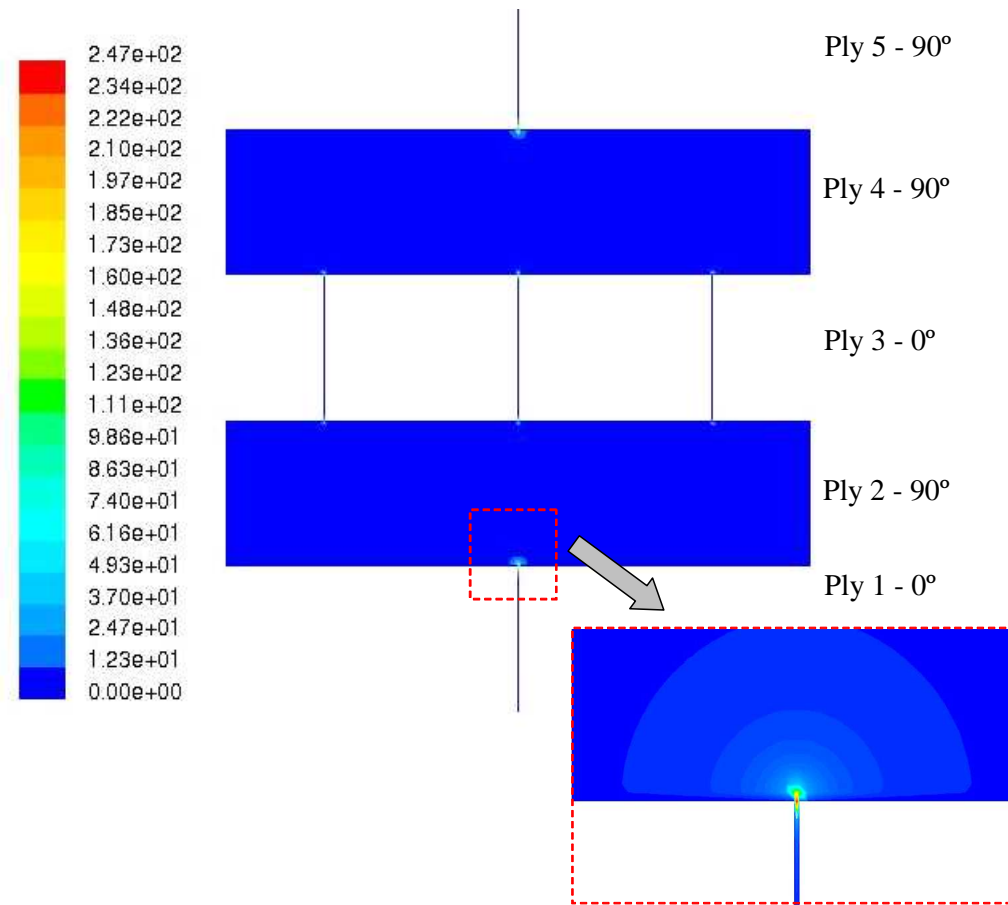
Fig. 21. Two-dimensional contour plot of velocity magnitude v along the mid-plane of RVE of the cross-ply composite with five plies and $\widetilde{\alpha_3} = 3$ at room temperature
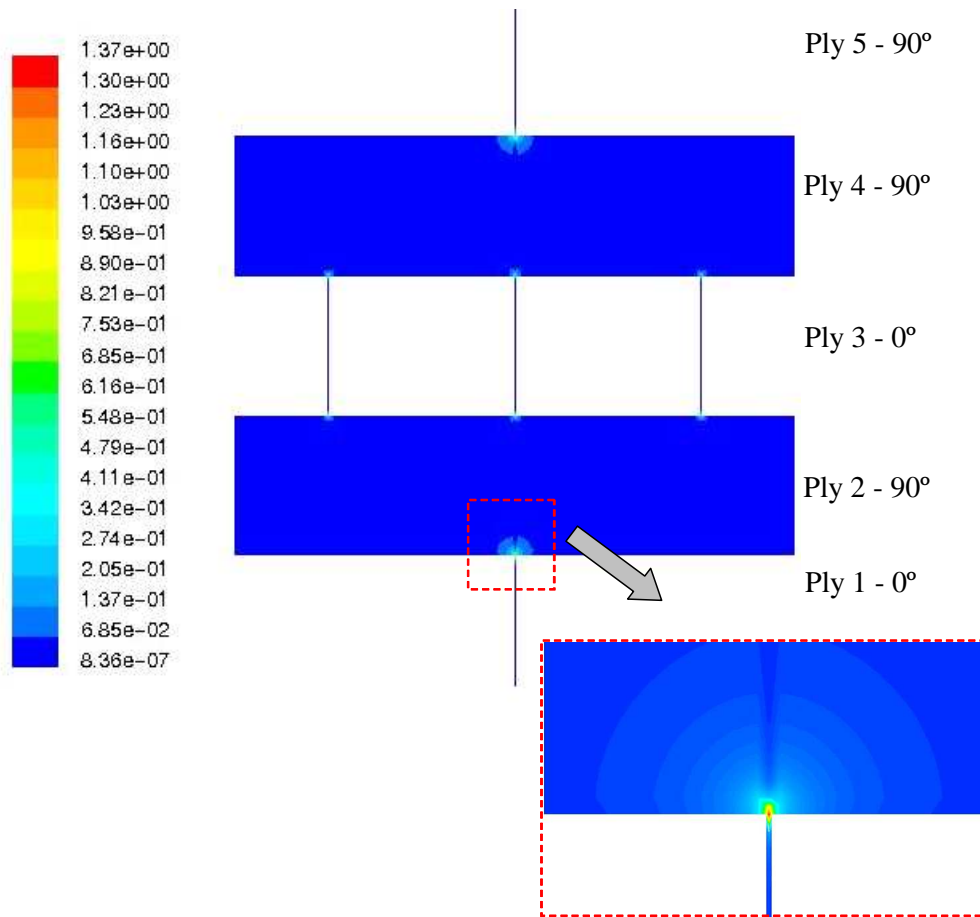
Fig. 22. Two-dimensional contour plot of Reynolds number along the mid-plane of RVE of the cross-ply composite with five plies and $\widetilde{\alpha_3} = 3$ at room temperature
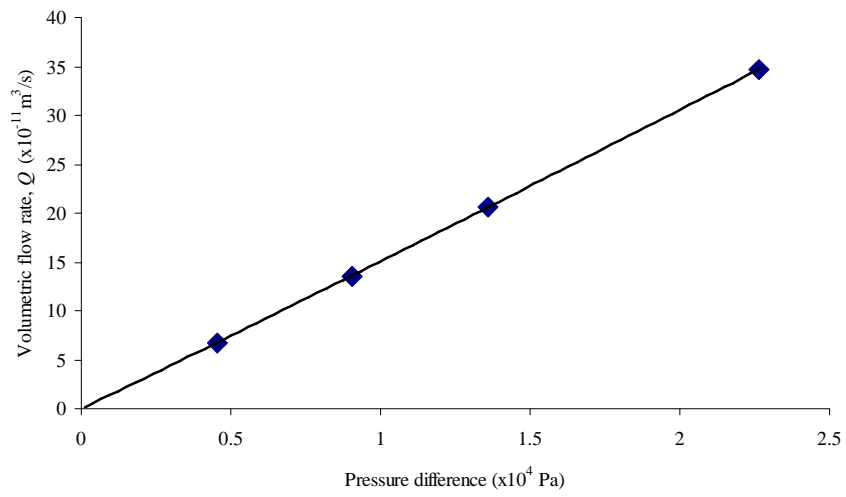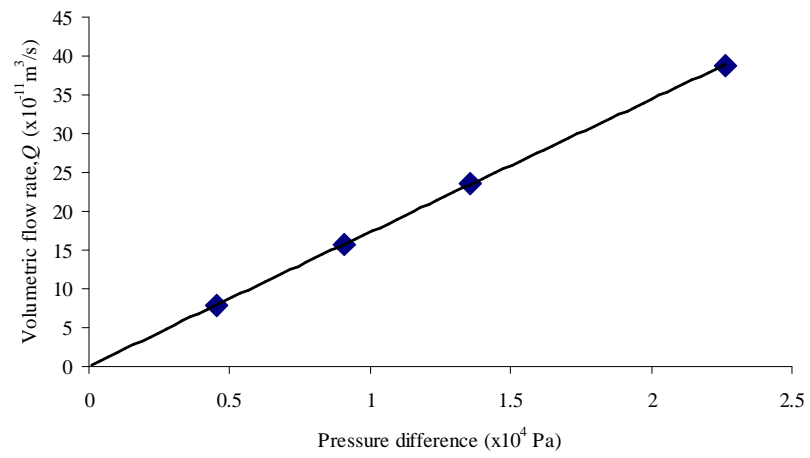
Fig. 23. Variation of volumetric flow rate with applied pressure difference in cross-ply composite with five plies and $\widetilde{\alpha_3} = 3$ at room temperature

pressure differential is illustrated in Fig. 23. Volumetric flow rate and the pressure differentials are related by the following equation

$$Q = 17.34 \text{ x } 10^{-10}(\Delta P) \tag{3.4}$$

Comparing the equation with Equation (2.13), the effective conductance of the five ply composite is 17.34 x $10^{-11} m^3/$(s.Pa) and the exponent $n$ is 1.

From the results of the numerical simulations for the four cases studied at cryogenic and room temperatures, it is found that the velocities of hydrogen are maximum near the crack junctions indicating that crack junctions act as main resistance blocks to hydrogen flow. Also, the Reynolds number is found to be maximum near the crack junctions due to high flow velocities. It is also found that the volumetric flow rate and applied pressure differential obey a non-linear relation at cryogenic temperature. The maximum Reynolds number is found to be approximately 90, at which the inertial forces in flow become comparable with the inertial forces. However, at room temperature a linear relation is observed between volumetric flow rate and the pressure differential. At this temperature, the Reynolds number is around 1, which results in negligible inertial forces compared to the viscous forces. Hence a creeping motion is observed and a linear relation is observed between the volumetric flow rate and applied pressure difference. The main difference in the flow characteristic at cryogenic and room temperatures is due to change in the flow properties discussed in the beginning of this chapter.

For all of the cases studied, the exponent $n$ is found to be independent of the normalized crack density in the middle ply but is affected by the operating temperature. This suggests that the exponent $n$ depends on the properties of hydrogen. Variation
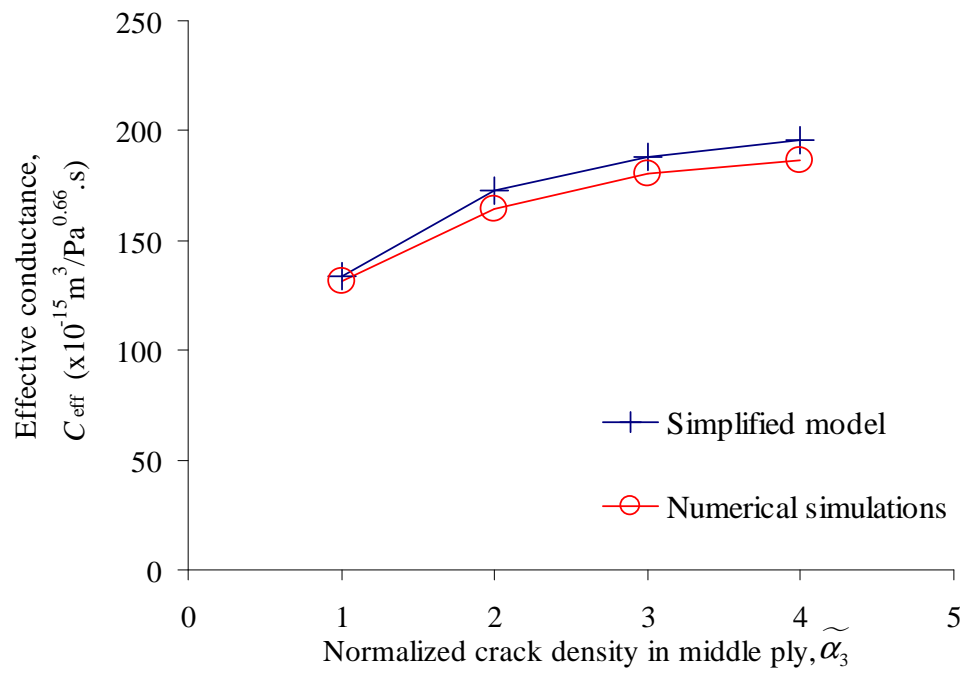
Fig. 24. Variation of effective conductance of cross-ply composite (with five plies) with normalized crack density in middle ply, $\widetilde{\alpha_3}$ at cryogenic temperature
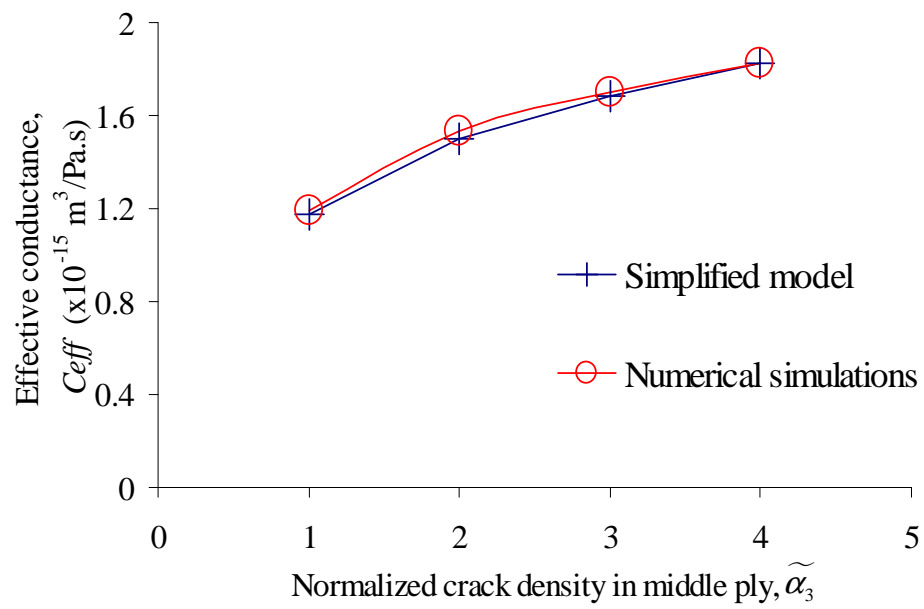
Fig. 25. Variation of effective conductance of cross-ply composite (with five plies) with normalized crack density in middle ply, $\widetilde{\alpha_3}$ at room temperature
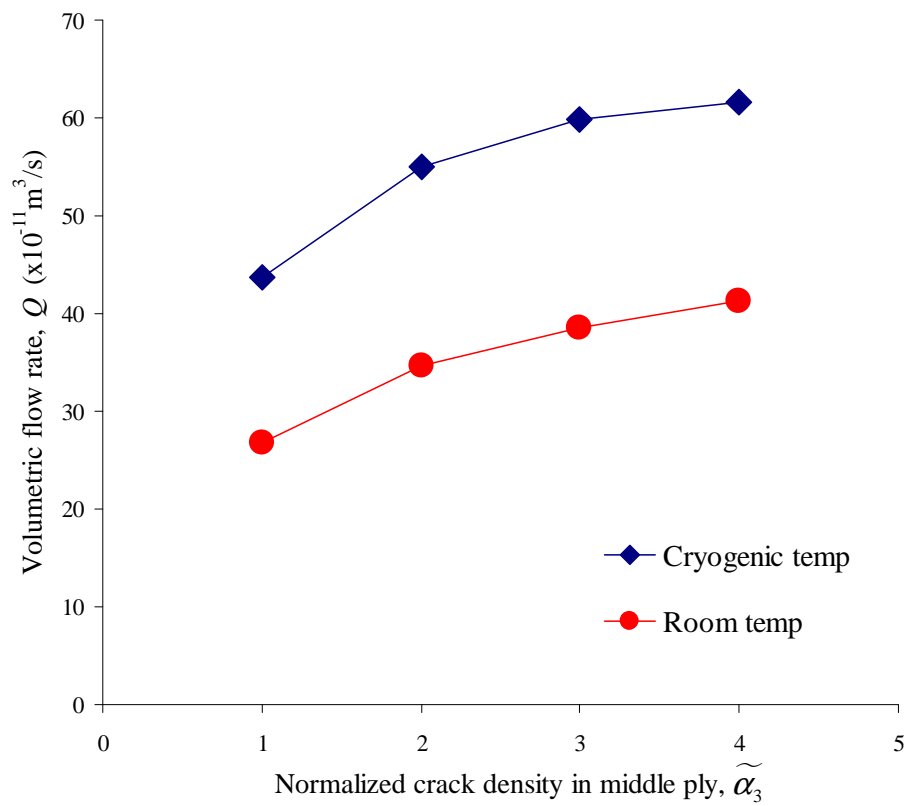
Fig. 26. Comparison of hydrogen volumetric flow rates through the cross-ply composite at cryogenic and room temperatures for different $\widetilde{\alpha_3}$

of effective conductance of the five ply composite with normalized crack density, at cryogenic and room temperatures is illustrated in Figures 24 and 25 respectively. The effective conductance is found to increase with increase in the normalized crack density in the middle ply. Increase in the crack density increases the number of crack junctions resulting in an overall increase in the leakage area for hydrogen. However, the increment in the effective conductance is found to decrease with increase in the normalized crack density.

At a pressure difference of 2.2 x $10^5$ Pa across the RVE, variation of hydrogen volumetric flow rate with normalized crack density at cryogenic and room temperatures is illustrated in Fig. 26. The volumetric flow rates are found to vary in the same way in which effective conductance varied with the normalized crack density. Also, the volumetric flow rates at cryogenic temperature are found to be approximately 50 % higher than the flow rates at room temperature. The reason could be because of the change in hydrogen properties at the two temperatures. As shown in Table I, the viscosity decreases by a factor of 4.7 as the temperature is decreased from room to cryogenic temperature. Hydrogen has less viscous resistance at cryogenic temperature, which results in higher volumetric flow rate through the RVE.

CHAPTER IV

SIMPLIFIED MODEL FOR EFFECTIVE CONDUCTANCE ESTIMATION

A.  Simplified model

In cryogenic composites with very low crack densities, the aspect ratio of TMC is
very high and it is computationally difficult to model representative TMC in each ply.
When the TMC network is large (due to presence of large number of plies), numeri-
cal analysis of cryogen flow through the complex network might be computationally
cumbersome. Under such circumstances, estimation of effective conductance of the
composite from crack junction conductance, TMC resistance (reciprocal of conduc-
tance) due to offset of crack junctions in adjacent ply-interfaces and the number of
crack junctions in each ply-interface is more effective. A simple analytical model is
presented in this chapter, where the effective conductance is determined from series-
parallel combination of crack junctions and TMC. The crack junction conductance
and TMC resistance are estimated through numerical simulations.

Consider an RVE of a cross-ply composite with $N$ plies. Figure 27 illustrates part
of the RVE that contains three plies. All the plies and ply-interfaces in the RVE
are in series combination *i.e,* the volumetric flow rate of cryogen leaking through the
RVE is equal to the volumetric flow rate through each ply and ply-interface. Overall
pressure drop across the RVE can be expressed as the sum of individual pressure
drops across each ply and ply-interface, given by

$$\Delta P_{RVE} = \sum_{i=1}^{N} \Delta P_i^P + \sum_{i=1}^{N-1} \Delta P_i^I \tag{4.1}$$

where $\Delta P_{RVE}$ is the overall pressure drop across the RVE, $\Delta P_i^I$ is the pressure drop
across the $i^{th}$ ply-interface due to resistance from crack junctions and $\Delta P_i^P$ is the
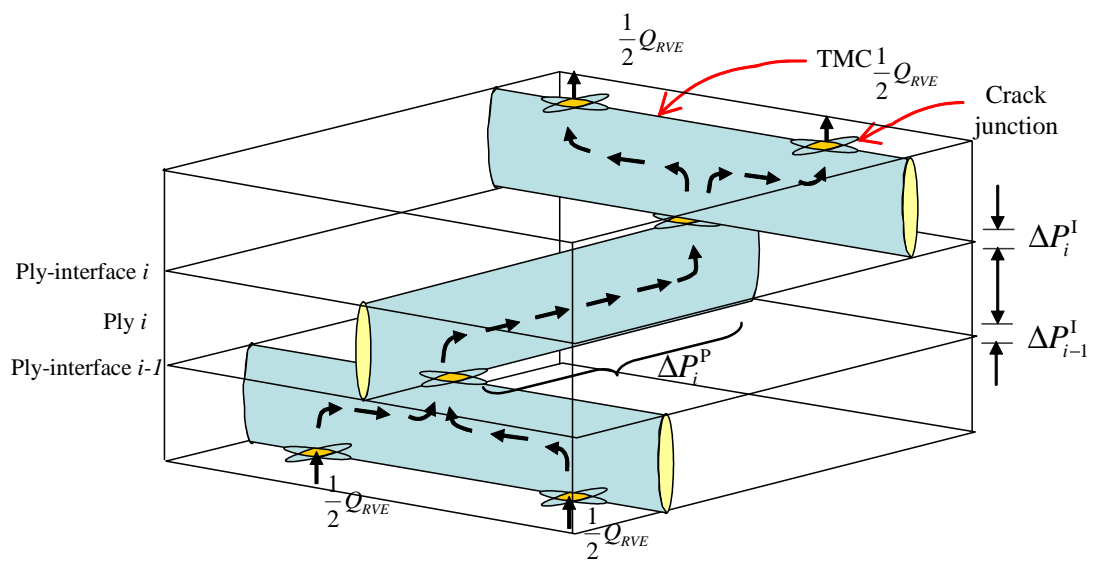
Fig. 27. Schematic of three plies in an RVE of a cross-ply laminate

pressure drop in $i^{th}$ ply due to resistance from TMC because of offset crack junctions in adjacent ply-interfaces (Fig. 27).

Using Equation (2.13), the overall pressure drop across the RVE can be expressed in terms of the volumetric flow rate through RVE as

$$\Delta P_{RVE} = \left(\frac{Q_{RVE}}{C_{eff}}\right)^{1/n} \tag{4.2}$$

where $Q_{RVE}$ is the cryogen volumetric f low rate through RVE and $C_{eff}$ is the effective conductance.

In a similar way with Equation (2.13), assuming that a similar formula is valid for the pressure drop across each ply-interface and ply, one can define the pressure drops across each ply-interface and ply as

$$\Delta P_i^I = \left(\frac{Q_{RVE}}{C_i^I}\right)^{1/n}, \ \Delta P_i^P = \left(\frac{Q_{RVE}}{C_i^P}\right)^{1/n} \tag{4.3}$$

where $C_i^I$ and $C_i^P$ are the overall conductance of $i^{th}$ ply-interface and $i^{th}$ ply respectively.

In the outermost plies, pressure drop due to offset between crack junctions is considered zero due to absence of crack junctions on one of the sides. By combining Equations (4.1), (4.2) and (4.3), the effective conductance can be expressed in terms of the overall conductance of the ply-interfaces and plies as

$$\left(\frac{1}{C_{eff}}\right)^{1/n} = \sum_{i=1}^{N-1} \left(\frac{1}{C_i^I}\right)^{1/n} + \sum_{i=2}^{N-1} \left(\frac{1}{C_i^P}\right)^{1/n} \tag{4.4}$$

The overall conductance of the ply-interfaces and plies are obtained by considering parallel combination of crack junctions in a ply-interface and TMC in a ply. Details of estimation of $C_i^I$ and $C_i^P$ are explained using an example in next section.

B.  Estimation of effective conductance of five ply composite

A cross-ply laminate with five plies and [0/90/0/90/0] lay-up, mentioned in Chapters II and III is considered for the effective conductance estimation using the Simplified model. Details about the TMC and crack junction arrangement in the composite are discussed below. An expression for the effective conductance of the five ply composite for the four cases *i.e,* normalized crack density in middle ply = 1, 2, 3, and 4 is derived in terms of the crack junction conductance and TMC resistance.

### 1. Normalized crack density in middle ply, $\widetilde{\alpha_3} = 1$

When the normalized crack density in middle ply is 1, the schematic of RVE of the five ply composite is as shown in Fig. 6. In this case, the crack density of all plies in the composite is the same. The RVE contains one representative TMC in each ply and one crack junction at each ply interface. All the crack junctions in the RVE are aligned and no offset exists between crack junctions in adjacent ply-interfaces. Since the openings of crack junctions at each ply-interface are equal, their conductance are also equal, each being equal to $C^J$.

As per Equation (4.3), the individual pressure drops across each ply-interface is expressed in terms of the conductance of the ply-interface and the cryogen volumetric flow rate through it as

$$\Delta P_1^I = \left(\frac{Q_{RVE}}{C_1^I}\right)^{1/n}, \ \Delta P_3^I = \left(\frac{Q_{RVE}}{C_3^I}\right)^{1/n},$$
$$\Delta P_2^I = \left(\frac{Q_{RVE}}{C_2^I}\right)^{1/n}, \ \Delta P_4^I = \left(\frac{Q_{RVE}}{C_4^I}\right)^{1/n} \tag{4.5}$$

where $C_1^I$, $C_2^I$, $C_3^I$ and $C_4^I$ are the overall conductance and $\Delta P_1^I$, $\Delta P_2^I$, $\Delta P_3^I$, and $\Delta P_4^I$ are the individual pressure drops across $1^{st}$, $2^{nd}$, $3^{rd}$, and $4^{th}$ ply-interfaces

respectively. Since there is one crack junction at each ply-interface, the cryogen volumetric flow rate through each crack junction is the same as the volumetric flow rate through the ply-interface, $Q_{RVE}$. The pressure drop across the crack junction is equal to the pressure drop across ply interface. This pressure drop can be expressed in terms of the conductance of the crack junction and the volumetric flow rate through crack junction as

$$\Delta P_1^I = \left(\frac{Q_{RVE}}{C^J}\right)^{1/n}, \quad \Delta P_2^I = \left(\frac{Q_{RVE}}{C^J}\right)^{1/n},$$
$$\Delta P_3^I = \left(\frac{Q_{RVE}}{C^J}\right)^{1/n}, \quad \Delta P_4^I = \left(\frac{Q_{RVE}}{C^J}\right)^{1/n} \tag{4.6}$$

From Equations (4.5) and (4.6), the overall conductance of $1^{st}$, $2^{nd}$, $3^{rd}$ and $4^{th}$ ply-interfaces is expressed in terms of conductance of crack junction as

$$C_1^I = C^J, C_3^I = C^J,$$
$$C_2^I = C^J, C_4^I = C^J \tag{4.7}$$

Since all the crack junctions in RVE are aligned, as cryogen flows from one crack junction to the other, no additional pressure drop is present in TMC due to offset between crack junctions. Thus, the overall ply resistances (inverse of the conductance) due to offset of crack junctions in $2^{nd}$, $3^{rd}$ and $4^{th}$ plies is zero. Hence, combining Equations (4.4), and (4.7), the effective conductance of the five ply composite is written as

$$\left(\frac{1}{C_{eff}}\right)^{1/n} = 4\left(\frac{1}{C^J}\right)^{1/n} \tag{4.8}$$

2.  Normalized crack density in middle ply, $\widetilde{\alpha_3} = 2$

When the normalized crack density in the middle ply is 2, the number of representative TMC in the third ply in RVE is two and one in the remaining plies. Schematic of the RVE of the five ply composite is illustrated in Fig. 7. The number of crack junctions at $1^{st}$, $2^{nd}$, $3^{rd}$ and $4^{th}$ ply-interfaces is 1, 2, 2, and 1 respectively. The two crack junctions at $2^{nd}$ and $3^{rd}$ ply-interfaces are offset by an equal distance relative to the crack junctions at $1^{st}$ and $4^{th}$ ply-interfaces respectively.

As the number of crack junctions at $1^{st}$ and $4^{th}$ ply-interfaces is one, the cryogen volumetric flow rate through the crack junction is equal to $Q_{RVE}$. At $2^{nd}$ and $3^{rd}$ ply-interfaces, for an equal pressure difference across the ply-interface and crack junctions, the cryogen volumetric flow rate through each crack junction is equal to $Q_{RVE}/2$. The pressure drop across these crack junctions is expressed in terms of their conductance and volumetric flow rate as

$$\Delta P_1^I = \left(\frac{Q_{RVE}}{C^J}\right)^{1/n}, \ \Delta P_2^I = \left(\frac{Q_{RVE}}{2C^J}\right)^{1/n},$$
$$\Delta P_3^I = \left(\frac{Q_{RVE}}{2C^J}\right)^{1/n}, \ \Delta P_4^I = \left(\frac{Q_{RVE}}{C^J}\right)^{1/n} \tag{4.9}$$

Pressure drop across the ply-interfaces in terms of the overall conductance of the ply-interface and the volumetric flow rate is given in Equation (4.5). By comparing Equations (4.5) and (4.9), the overall conductance of the ply-interfaces is expressed in terms of the conductance of crack junctions, given by

$$C_1^I = C^J, \ C_3^I = 2C^J,$$
$$C_2^I = 2C^J, \ C_4^I = C^J \tag{4.10}$$

TMC resistance is assumed to be directly proportional to the offset distance between crack junctions (which is proved through numerical simulations in the next chapter). Since the crack junctions at $2^{nd}$ and $3^{rd}$ ply-interfaces are offset by the same distance relative to the crack junctions at $1^{st}$ and $4^{th}$ ply-interfaces respectively, TMC resistance in $2^{nd}$ and $4^{th}$ plies due to offset of each of these crack junctions is set equal to $1/C^{T_1}$. For an equal pressure drop across the ply and TMC, total cryogen volumetric flow rate through the ply is the sum of individual flow rates through each TMC. In each TMC, the cryogen volumetric flow rate is the sum of flow rates through each set of offset crack junctions. Since there are two sets of offset crack junctions in $2^{nd}$ and $4^{th}$ plies, the volumetric flow rate through each set is equal to $Q_{RVE}/2$. The pressure drop across the TMC in $2^{nd}$ and $4^{th}$ plies is expressed in terms of the volumetric flow rate and TMC resistance as

$$\Delta P_2^P = \left(\frac{Q_{RVE}}{2C^{T_1}}\right)^{1/n}, \ \Delta P_4^P = \left(\frac{Q_{RVE}}{2C^{T_1}}\right)^{1/n} \tag{4.11}$$

The pressure drop across $2^{nd}$ and $4^{th}$ plies can also be expressed in terms of the overall resistance of the ply as per Equation (4.3)

$$\Delta P_2^P = \left(\frac{Q_{RVE}}{C_2^P}\right)^{1/n}, \ \Delta P_4^P = \left(\frac{Q_{RVE}}{C_4^P}\right)^{1/n} \tag{4.12}$$

where $1/C_2^P$ and $1/C_2^P$ are the overall resistance of $2^{nd}$ and $4^{th}$ plies. Comparing Equations (4.11) and (4.12), the overall resistance of $2^{nd}$ and $4^{th}$ plies is given by

$$\frac{1}{C_2^P} = \frac{1}{C_4^P} = \frac{1}{2C^{T_1}} \tag{4.13}$$

The crack junctions at $2^{nd}$ and $3^{rd}$ ply-interfaces are aligned and hence, no pressure drop is present as cryogen flows from one crack junction to the other and the overall resistance of $3^{rd}$ ply is thus equal to zero. The effective conductance of the five ply

composite is then obtained by combining Equations (4.4), (4.10), and (4.13).

$$\left(\frac{1}{C_{eff}}\right)^{1/n} = 2\left(\frac{1}{C^J}\right)^{1/n} + 2\left(\frac{1}{2C^J}\right)^{1/n} + 2\left(\frac{1}{2C^{T_1}}\right)^{1/n} \qquad (4.14)$$

3. Normalized crack density in middle ply, $\widetilde{\alpha_3} = 3$

The schematic of RVE when the normalized crack density in the middle ply $= 3$ is shown in Fig. 8. Here, the crack density in middle ply (i.e, $3^{rd}$ ply) is one third of the crack density in remaining plies. The number of representative TMC in $3^{rd}$ ply in RVE is 3, compared to one from each of the remaining plies. Hence, the number of crack junctions at $1^{st}$, $2^{nd}$, $3^{rd}$ and $4^{th}$ ply-interfaces is 1, 3, 3 and, 1 respectively. Middle crack junctions at $2^{nd}$ and $3^{rd}$ ply interfaces are aligned with crack junctions at $1^{st}$ and $4^{th}$ ply-interfaces, whereas the two outer most crack junctions at $2^{nd}$ and $3^{rd}$ ply-interfaces are offset by a distance with respect to the crack junctions at $1^{st}$ and $4^{th}$ ply-interfaces respectively.

As there is one crack junction at $1^{st}$ and $4^{th}$ ply-interfaces, the volumetric flow rate of cryogen through each of these crack junctions is equal to $Q_{RVE}$. Whereas $2^{nd}$ and $3^{rd}$ ply-interfaces have three crack junctions each. For an equal pressure drop across the ply-interface and crack junctions, the volumetric flow rate of cryogen through each crack junction is equal to $Q_{RVE}/3$. Pressure drop across each ply-interface is expressed in terms of the conductance of the crack junction as

$$\Delta P_1^I = \left(\frac{Q_{RVE}}{C^J}\right)^{1/n}, \ \Delta P_2^I = \left(\frac{Q_{RVE}}{3C^J}\right)^{1/n},$$
$$\Delta P_3^I = \left(\frac{Q_{RVE}}{3C^J}\right)^{1/n}, \ \Delta P_4^I = \left(\frac{Q_{RVE}}{C^J}\right)^{1/n} \qquad (4.15)$$

Comparing Equations (4.5) and (4.15), the overall conductance of the ply-interfaces is expressed in terms of the conductance of crack junction as

$$C_1^I = C^J, \ C_3^I = 3C^J,$$
$$C_2^I = 3C^J, \ C_4^I = C^J \tag{4.16}$$

As the cryogen flows from crack junction at $1^{st}$ ply-interface to the middle crack junction at $2^{nd}$ ply-interface, no additional pressure drop due to offset between crack junctions exists. The TMC resistance is zero between these crack junctions. On the other hand, as the cryogen flows from crack junction at $1^{st}$ ply-interface to outer most crack junctions in $2^{nd}$ ply-interface, an additional pressure drop exists due to offset between these crack junctions. These TMC resistances in $2^{nd}$ ply are assumed to be in parallel combination and the overall resistance of the ply can be expressed as the harmonic sum of individual TMC resistances. Hence, the overall resistance of $2^{nd}$ ply reduces to zero. Similarly, the overall resistance of $4^{th}$ ply also reduces to zero. The crack junctions at $2^{nd}$ and $3^{rd}$ ply-interfaces are aligned and the TMC resistance in $3^{rd}$ ply due to offset of crack junctions is zero. With these conclusions, the effective conductance of the five ply composite is obtained by combining Equations (4.4), and (4.16) as

$$\left(\frac{1}{C_{eff}}\right)^{1/n} = 2\left(\frac{1}{C^J}\right)^{1/n} + 2\left(\frac{1}{3C^J}\right)^{1/n} \tag{4.17}$$

4.  Normalized crack density in middle ply, $\widetilde{\alpha_3} = 4$

Schematic of RVE of the five ply composite when the normalized crack density in middle ply $= 4$ is shown in Fig. 9. In this case, the number of representative TMC in $3^{rd}$ ply in the RVE is 4 and in each of the remaining plies the number of representative TMC is 1. The number of crack junctions in $1^{st}$, $2^{nd}$, $3^{rd}$ and $4^{th}$ ply-interfaces are 1, 4,

4, and 1 respectively. Each of the four crack junctions at $2^{nd}$ and $3^{rd}$ ply-interfaces are offset by certain distance relative to the crack junctions at $1^{st}$ and $4^{th}$ ply-interfaces respectively. The inner crack junctions at $2^{nd}$ and $3^{rd}$ ply-interfaces are offset by equal distance from the crack junction at $1^{st}$ and $4^{th}$ ply-interface respectively. Both the outer crack junctions are offset by another equal distance, different from the offset distance of inner crack junctions.

$1^{st}$ and $4^{th}$ ply interfaces have one crack junction each. The cryogen volumetric flow rate through these crack junctions is equal to $Q_{RVE}$. $2^{nd}$ and $3^{rd}$ ply-interfaces have four crack junctions each. For an equal pressure drop across the ply-interface and the crack junctions, the cryogen volumetric flow rate through each crack junction is equal to $Q_{RVE}/4$. Pressure drop across the crack junction at the four ply-interfaces is expressed in terms of the conductance of the crack junction as

$$\Delta P_1^I = \left(\frac{Q_{RVE}}{C^J}\right)^{1/n}, \ \Delta P_2^I = \left(\frac{Q_{RVE}}{4C^J}\right)^{1/n},$$
$$\Delta P_3^I = \left(\frac{Q_{RVE}}{C^J}\right)^{1/n}, \ \Delta P_4^I = \left(\frac{Q_{RVE}}{4C^J}\right)^{1/n} \tag{4.18}$$

Pressure drop across the ply-interface in terms of the overall conductance of the ply-interface is given in Equation (4.5). Comparing Equations (4.5) and (4.18), the overall conductance of the ply-interfaces is given by

$$C_1^I = C^J, \ C_3^I = 4C^J,$$
$$C_2^I = 4C^J, \ C_4^I = C^J \tag{4.19}$$

TMC resistance in $2^{nd}$ ply due to offset between each of the inner crack junctions at $2^{nd}$ ply-interface and the crack junction at $1^{st}$ ply-interface is equal to $1/C^{T_2}$. As TMC resistance is directly proportional to the offset distance, TMC resistance in $3^{rd}$

ply due to offset between each of inner crack junctions at $3^{rd}$ ply-interface and crack junction at $4^{th}$ ply-interface is also equal to $1/C^{T_2}$. TMC resistance due to offset of each of the outer crack junctions relative to the crack junction at $1^{st}$ ply-interface is equal to $1/C^{T_3}$, which is the same as the TMC resistance in $3^{rd}$ ply due to offset between each of the outer crack junctions in $3^{rd}$ ply-interface and the crack junction at $4^{th}$ ply-interface. For an equal pressure drop across the ply and TMC, total cryogen volumetric flow rate through the ply is the sum of individual flow rates between each set of crack junctions in adjacent ply-interfaces. Let the cryogenic volumetric flow rate through the set of inner crack junction at $2^{nd}$ ply-interface and crack junction at $1^{st}$ ply-interface be $Q_1$ and the flow rate through the set of outer crack junction at $2^{nd}$ ply-interface and the crack junction at $1^{st}$ ply-interface be $Q_2$. The total volumetric flow rate through the $2^{nd}$ ply is then given by

$$2Q_1 + 2Q_2 = Q_{RVE} \tag{4.20}$$

These flow rates can be expressed in terms of the TMC resistances and pressure drops across the ply as per following equations

$$Q_{RVE} = C_2^P \left( \Delta P_2^P \right)^n,$$
$$Q_1 = C^{T_3} \left( \Delta P_2^P \right)^n,$$
$$Q_2 = C^{T_4} \left( \Delta P_2^P \right)^n \tag{4.21}$$

Comparing Equations (4.20) and (4.21), the overall resistance of $2^{nd}$ ply is written as

$$\frac{1}{C_2^P} = \frac{1}{2(C^{T_2} + C^{T_3})} \tag{4.22}$$

Similarly the overall resistance of $4^{th}$ ply is given by

$$\frac{1}{C_4^P} = \frac{1}{2(C^{T_2} + C^{T_3})} \tag{4.23}$$

The crack junctions at $2^{nd}$ and $3^{rd}$ ply-interfaces are aligned and no pressure drop due to offset between crack junctions is present. The overall resistance of $3^{rd}$ ply is thus equal to zero and the effective conductance of the RVE is obtained by combining Equations (4.4), (4.19), (4.22), and 4.23).

$$\left(\frac{1}{C_{eff}}\right)^{1/n} = 2\left(\frac{1}{C^J}\right)^{1/n} + 2\left(\frac{1}{4C^J}\right)^{1/n} + 2\left(\frac{1}{2\left(C^{T_2} + C^{T_3}\right)}\right)^{1/n} \tag{4.24}$$

Estimation of effective conductance of the RVE for these cases requires estimation of crack junction conductance, $C^J$ and the TMC resistances, $1/C^{T_1}$, $1/C^{T_2}$, and $1/C^{T_3}$. This is achieved through numerical simulations, discussed in detail in the next chapter. With the help of the Simplified model, the whole problem reduces to finding out the crack junction conductance and TMC resistance values. Usage of the Simplified model is necessary when the crack density in each ply of the composite is low. In such cases, the aspect ratio of TMC is high and computational modeling of the RVE becomes difficult. Also, the model provides flexibility in designing composites for cryogen leakage, avoiding enormous computational time.

CHAPTER V

COMPARISON OF SIMPLIFIED MODEL AND NUMERICAL SIMULATION
PREDICTION OF EFFECTIVE CONDUCTANCE

To estimate the effective conductance of the five ply composite using the Simplified model, crack junction conductance and TMC resistance are required. In this chapter these values are determined through numerical simulations carried out at cryogenic and room temperatures. The generalized expressions derived in the previous chapter are used to estimate the effective conductance of the five ply composite at these two temperatures. Further, the Simplified model predictions of effective conductance are compared with the numerical estimations at cryogenic and room temperatures.

A.   Crack junction conductance

Conductance of a crack junction to gaseous hydrogen flow is estimated numerically by simulating hydrogen flow through an RVE of a two-ply network, with [0/90] lay-up, shown in Fig. 28. The dimensions of the RVE $l$ x $w$ are chosen to be $4h$ x $4h$, *i.e,* 564 x 564 $\mu m$ and the thickness of each ply is set to $0.5h = 70.5$ $\mu m$. The opening of each representative TMC in the RVE, $\delta_1 = \delta_2 = 0.01h$. Boundary value problem mentioned in Chapter II is solved in the domain of RVE at cryogenic and room temperatures. Different pressure differentials are applied across the RVE with $\Delta P = 4.5$ x $10^4$, $2.7$ x $10^4$, $1.8$ x $10^4$, $9.05$ x $10^3$ Pa. Volumetric flow rates at these pressure differentials are determined using Equation (2.12). The pressure differentials are chosen such that the pressure gradients for the two-ply network and the five ply composite are equal. Results of the numerical simulations at the two temperatures are discussed below.

Cryogenic Temperature:    Figure 29 illustrates the contour plot of the magnitude of velocity $v$ in the RVE at cryogenic temperature. Similar to the five ply composite case, the velocities of hydrogen are found maximum near the crack junction. Figure 30 illustrates the contour plot of the Reynolds number in the RVE. The maximum Reynolds number is found to be 75 (Re>13, Reference [18]) near the crack junction. Hence , a non-linear relation is observed between the volumetric flow rate and the applied pressure differential as illustrated in Fig. 31. The volumetric flow rate as a function of the applied pressure differential is given by the following equation.

$$Q = 6.65 \text{ x } 10^{-10} \left(\Delta P\right)^{0.66} \tag{5.1}$$

Comparing the above equation with Equation (2.13), the effective conductance of the crack junction is 6.65 x $10^{-10} m^3/(\text{s.Pa}^{0.66})$ and the exponent $n$ is 0.66.

Room Temperature:    The contour plot of the velocity magnitude at room temperature is illustrated in Fig. 32. The velocities of hydrogen at room temperature are lower than the values at cryogenic temperature. This is due to higher viscosity of hydrogen at room temperature. Higher viscosity implies higher viscous resistance, which results in lower velocities. Contour plot of the Reynolds number in the RVE is illustrated in Fig. 33. The maximum Reynolds number is 0.75 (less than 1) resulting in a linear variation of volumetric flow rate with applied pressure differential as shown in Fig. 34. The volumetric flow rates and applied pressure differentials are found to obey the following relation

$$Q = 46.9 \text{ x } 10^{-11} \left(\Delta P\right) \tag{5.2}$$

The effective conductance of the crack junction at room temperature is equal to 4.76 x $10^{-11} m^3/(\text{s.Pa})$ and the exponent $n$ is 1.
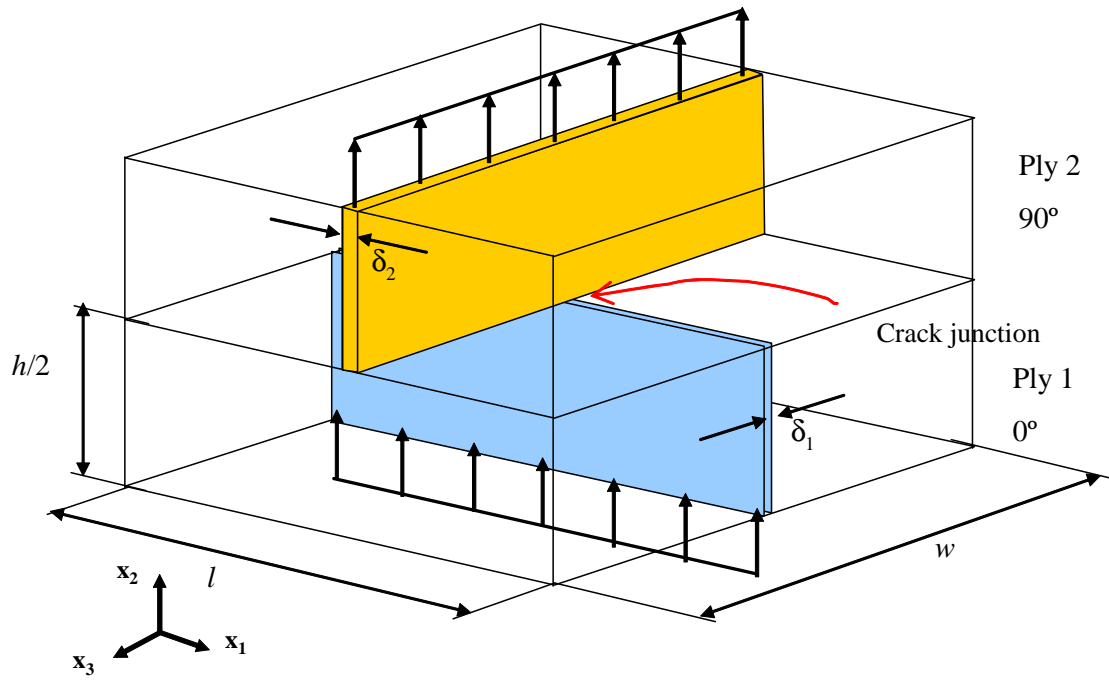
Fig. 28. Schematic of RVE of two-TMC network with [0/90] lay-up

Fig. 29. Two-dimensional contour plot of velocity magnitude v along the mid-plane of RVE for crack junction at cryogenic temperature

Fig. 30. Two-dimensional contour plot of Reynolds number along the mid-plane of RVE of for crack junction at cryogenic temperature

Fig. 31. Variation of volumetric flow rate of hydrogen with applied pressure difference
for the two-TMC network at cryogenic temperature
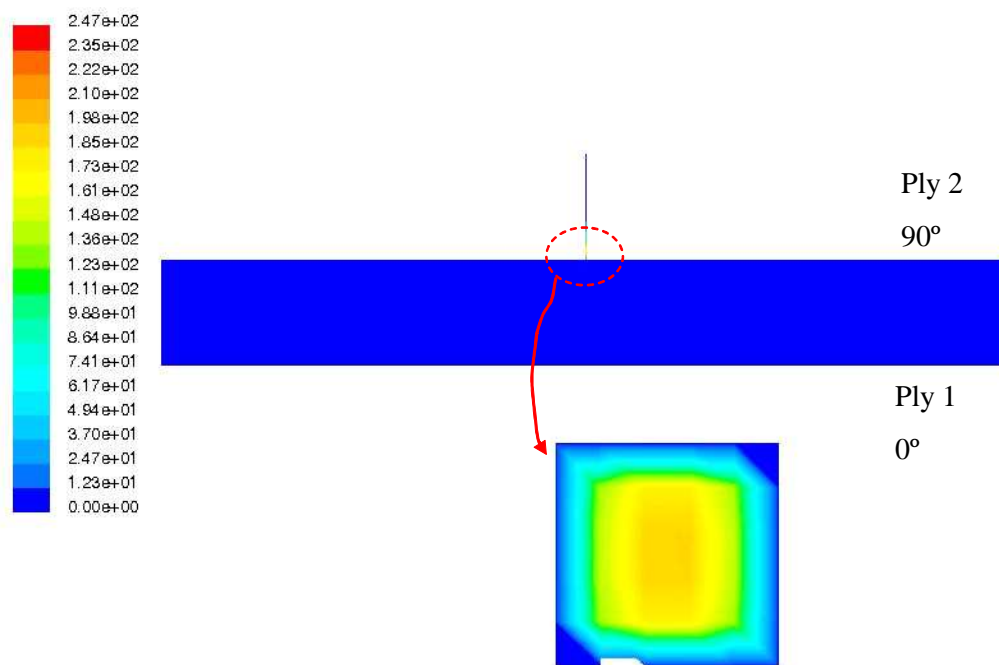
Fig. 32. Two-dimensional contour plot of velocity magnitude v along the mid-plane of RVE of for crack junction at room temperature
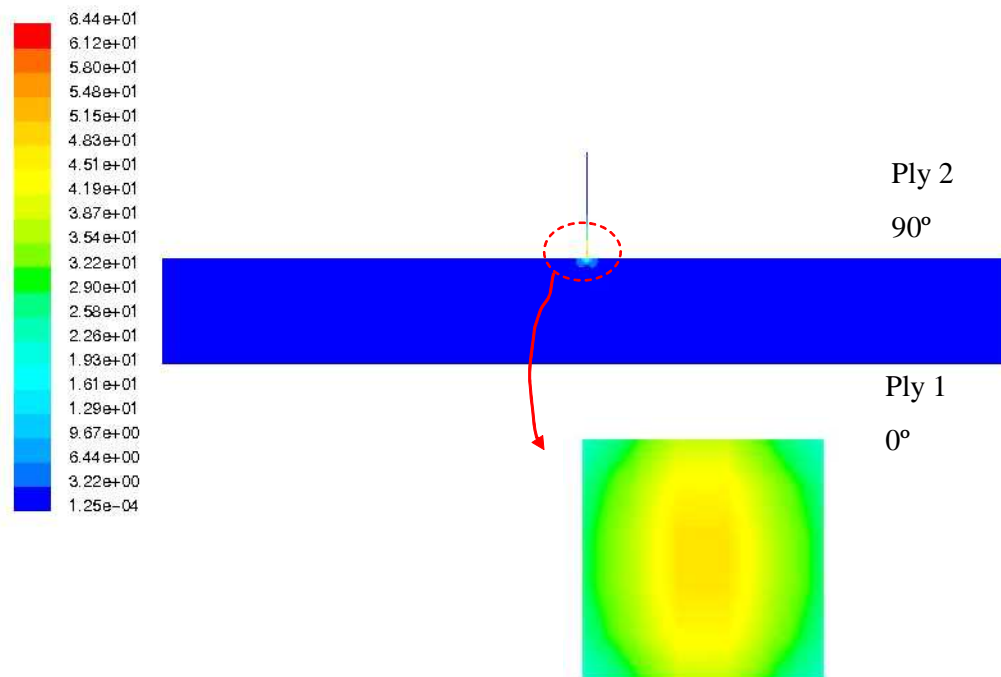
Fig. 33. Two-dimensional contour plot of Reynolds number along the mid-plane of RVE of for crack junction at room temperature
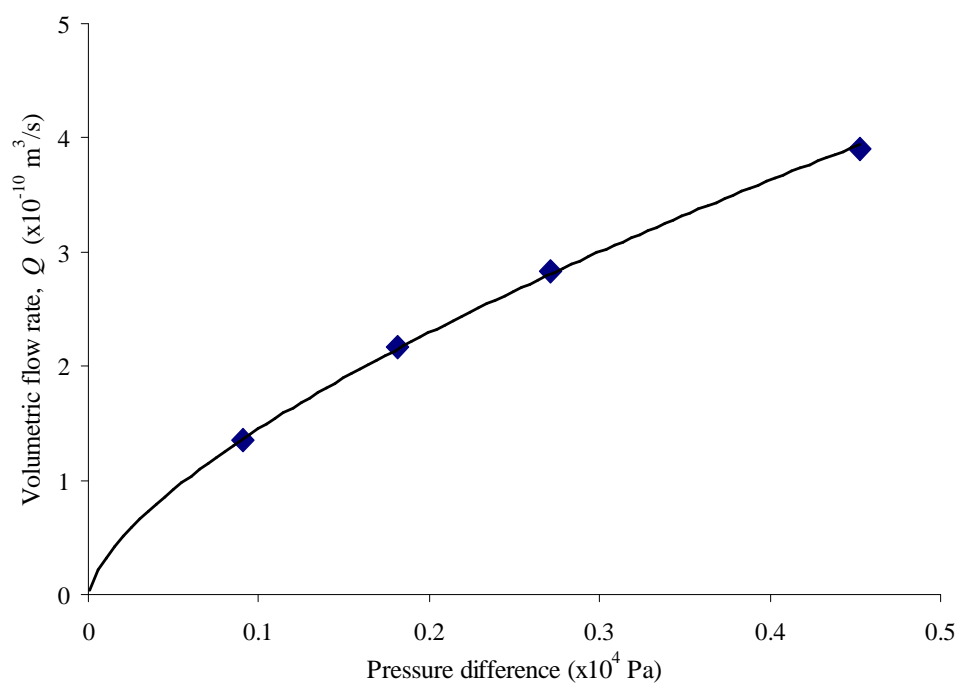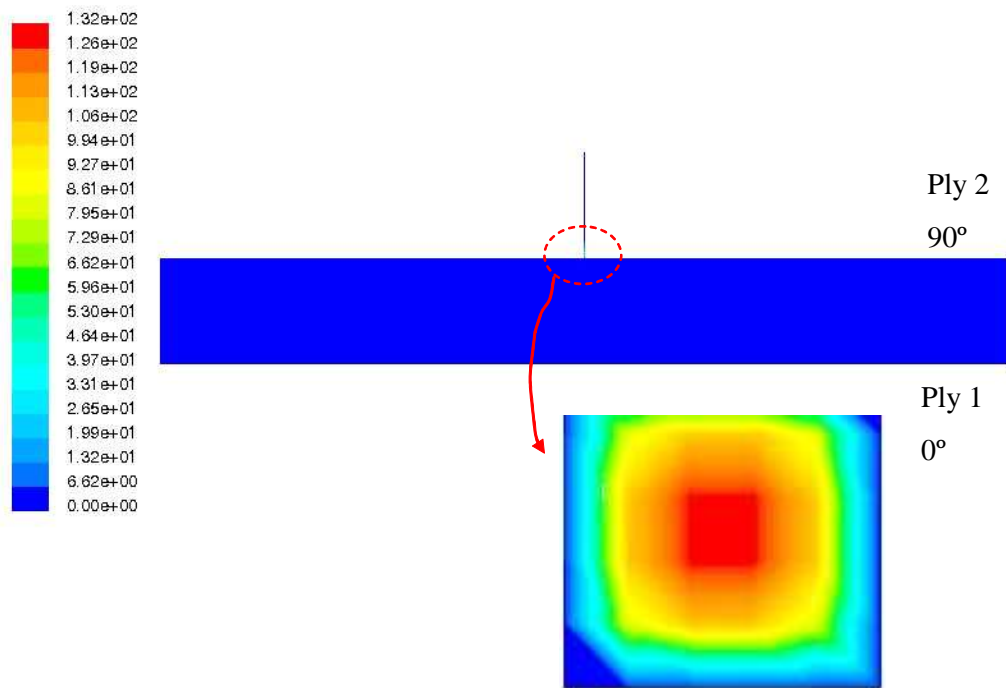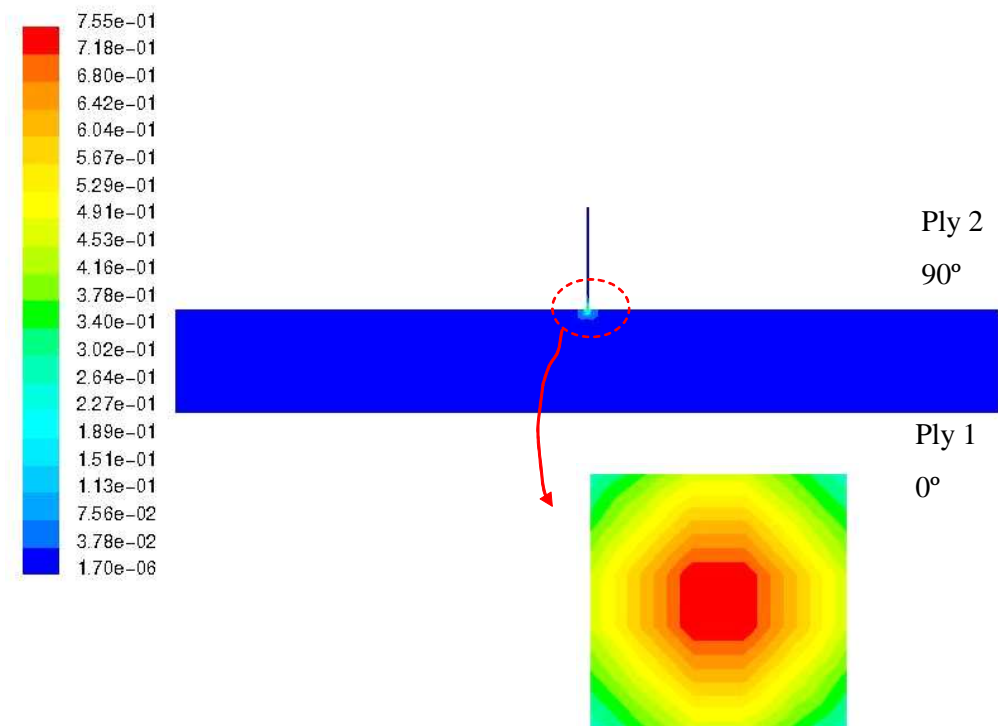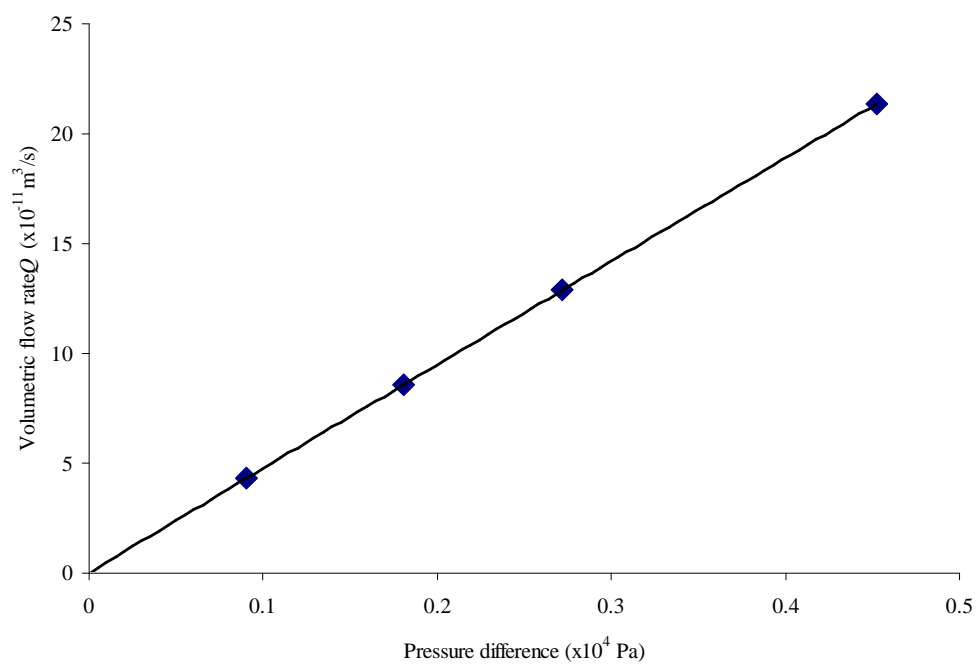
Fig. 34. Variation of volumetric flow rate of hydrogen with applied pressure difference
in two-TMC network at room temperature

Factors such as delamination size, TMC shape and the relative orientation of adjacent plies affect the conductance of a crack junction and thus the composite. The flow pattern through TMC and crack junctions depends on their geometry too. For example, in the straight channel approximation of TMC, sharp changes in geometry are experienced when the cryogen flows through TMC and crack junction, that might affect the flow pattern compared to flow through smooth geometry of TMC and crack junctions. Change in delamination size and relative orientation of adjacent plies change the area of crack junction and alter the cryogen leak rate. Parametric studies are conducted to investigate these effects on the leakage rate of hydrogen through TMC network.

Usually, TMC in a ply have an irregular geometry as shown in the micrographs of IM7/5250-4, a graphite epoxy specimen, with $[90/45/0/-45]_s$ in Fig. 35a. This specimen was tested for gaseous hydrogen leakage at MSFC. After the test, the specimen was subjected to different uni-axial loads ranging from 47 MPa to 101 MPa at Air Force Research Laboratory. Crack density and openings of representative TMC in 90-degree ply at different loads were measured through edge optical inspection. Figure 35b illustrates the micrograph of representative TMC in 90 degree ply at 101 MPa load. Several approximations can be made to the TMC geometry to reduce the computational effort in modeling the complex TMC geometry and analyzing cryogen flow through it. The effect of straight channel approximations to TMC with irregular geometry on the amount of cryogen leakage through a single ply is studied through two-dimensional parametric studies.

Due to the assumed periodicity, the dimensions of RVE are obtained from the crack density information. The width $w$ of the RVE (Fig. 35b) is equal to the

Ply 8 [90º]
Ply 7 [45º]
Ply 6 [0º]
Ply 5 [-45º]
Ply 4 [-45º]
Ply 3 [0º]
Ply 2 [45º]
Ply 1 [90º]

a) 100X resolution



45º

90º

Ply 2

B

$h$ Ply 1

A

$w$

RVE for TMC in 90º ply.

b) 400X resolution
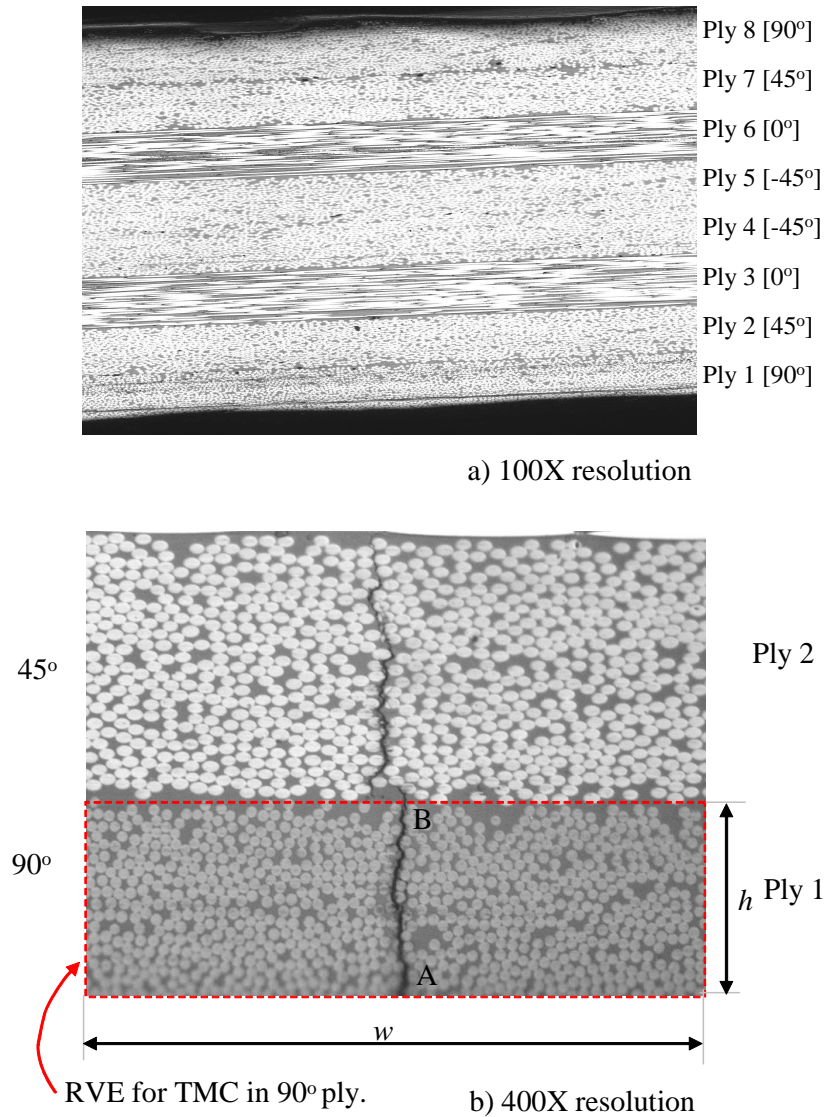
Fig. 35. Micrograph of TMC in IM7/5250-4 with $[90/45/0-45]_s$ at 101MPa load

Table IV. Crack density in different plies of IM7/5250-4

| **Ply orientation** (degrees) | **Crack density** (Cracks per mm) |
|:---:|:---:|
| 90 | 0.523 |
| 45 | 0.187 |
| 0 | 0.009 |
| -45 | 0.026 |

average TMC spacing in the ply. The crack density values in all plies of the composite at the end of applied mechanical load are given in Table IV. Based on this, the RVE dimensions are $h = 73\mu m$ and $w = 1909\mu m$. TMC opening for the actual TMC (TMC with irregular geometry) at the inlet A, outlet B and the average opening at different loads are given in Table V. The opening at the outlet B is measured 5 fiber diameters away from the ply-interface in order to minimize the interface delamination effects due to stress concentrations. Currently, there is no experimental data characterizing these effects and it is difficult to deduce them numerically. The average TMC opening is obtained by integrating the opening of the actual TMC along the height of the TMC divided by the TMC height. The ply under consideration is an outermost ply in the composite and the difference in the opening of the actual TMC in the ply at the inlet and outlet, is due to the redistribution of stress on the free surface of the composite. It should be noted that the actual TMC opening at 93 MPa applied load is approximately equal to that for 47 MPa load and is smaller than 62 and 78 MPa. This is probably caused by the formation of new cracks as the load is increased from 78 to 93 MPa.

Table V. TMC opening at different loads in 90° ply of IM7/5250-4 composite specimen

| Load (MPa) | Actual crack opening at outlet B ($\mu m$) | Actual crack opening at inlet A ($\mu m$) | Average crack opening ($\mu m$) |
|---|---|---|---|
| 47 | 1.06 | 2.79 | 1.71 |
| 62 | 1.18 | 1.73 | 1.80 |
| 78 | 1.38 | 3.63 | 2.13 |
| 93 | 1.10 | 2.54 | 1.94 |
| 101 | 1.34 | 4.26 | 2.58 |

The effect of the irregular geometry of the actual TMC on the volumetric flow rate is studied by different straight and tapered channel approximations. In the straight channel approximation, the width of the channel is taken to be the inlet opening at A, outlet opening at B, and the average opening of actual TMC. The tapered channel approximation at the inlet and outlet has width equal to the opening of the actual TMC at inlet and outlet respectively, connected by straight walls. For each load case the actual TMC geometry is obtained by digitizing the available micrographs.

The results from the numerical simulations for the volumetric flow rate through the 90-degree ply for the actual TMC geometry and for the different straight-walled approximations at different applied loads are given in Table VI. A typical velocity profile is illustrated in Fig. 36. The straight channel approximations have significant differences in the estimated volumetric flow rate values when compared to the one for the actual TMC. The use of a tapered channel allows for a more accurate estimation of the volumetric flow rate values compared to the corresponding straight channel
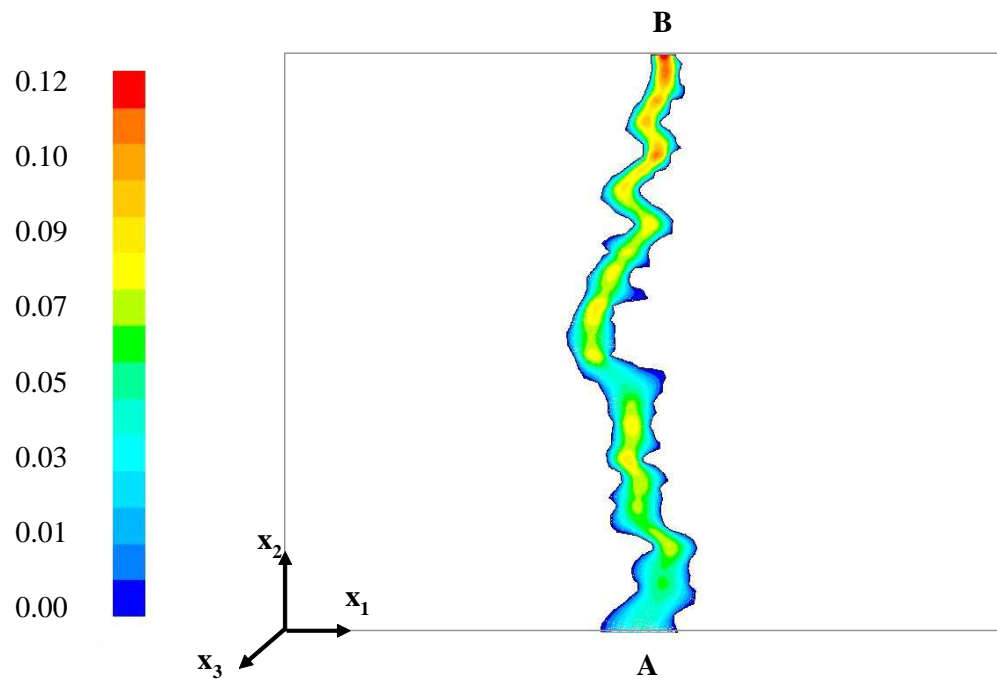
Fig. 36. Contour plot of fluid velocity $v_2$ (m/s) inside the representative crack in the 90-degree ply of IM7/5250-4 at 101 MPa load. (figure not drawn to scale: horizontal scale is exaggerated)

Table VI. Hydrogen volumetric flow rate in $10^{-10}$ m$^3$/s through 90° ply at different loads, for different TMC approximations

| Load (MPa) | Actual TMC | Tapered channel | Straight channel | | |
|:---:|:---:|:---:|:---:|:---:|:---:|
| | | | inlet opening | outlet opening | avg. opening |
| 47 | 5.3 | 11.2 | 56.3 | 2.9 | 12.4 |
| 62 | 9.4 | 7.1 | 13.0 | 4.1 | 14.8 |
| 78 | 11.8 | 25.5 | 124.0 | 6.5 | 24.9 |
| 93 | 10.0 | 11.2 | 42.1 | 2.9 | 18.4 |
| 101 | 24.9 | 30.2 | 200.0 | 5.9 | 43.9 |

approximations. The relative error in the estimated volumetric flow rate values for tapered channel is around 20 percent for 62, 93 and 101 MPa loads. At 47 and 78 MPa loads however the tapered channel approximation results in two-fold error in the volumetric flow rate.

The variation of volumetric flow rate of hydrogen through the 90-degree ply for actual TMC as a function of applied mechanical load is illustrated in Fig. 37. The flow rate value increases as the applied load is increased from 47 MPa to 78 MPa. The value then decreases as the load is increased to 93 MPa and finally the volumetric flow rate value increases when the load is further increased to 101 MPa. The decrease in the flow rate value at 93 MPa is expected because the flow rate depends on the TMC opening. The observed decrease in the TMC opening at this load is probably due to the formation of new cracks as the load increases from 78 to 93 MPa.

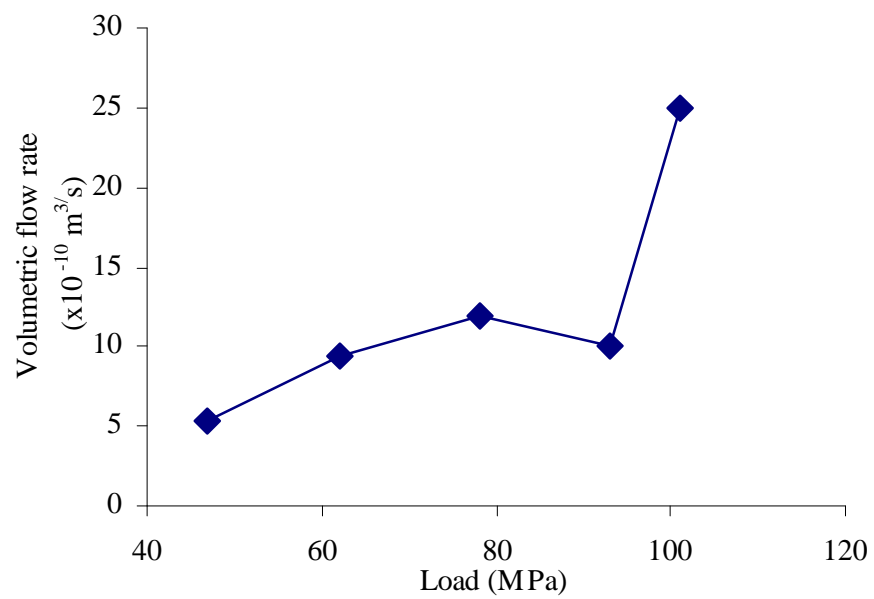Fig. 37. Variation of volumetric flow rate of hydrogen with applied load

Apart from the irregular geometry of the TMC, the relative orientation between adjacent plies also governs the amount of cryogen leakage through the network of TMC. A three-dimensional RVE with two plies is constructed with TMC having irregular geometries and straight channel approximations. The assumed three-dimensional profile of an irregular TMC is obtained by extruding the two-dimensional representative TMC profile. The relative orientation of the two plies is varied thus changing the junction area and therefore the amount of cryogen leakage through the composite.

The parametric study is performed for two different crack densities (being same in both plies), one corresponding to $w = l = 1909 \ \mu m$ which is the average spacing between the TMC for the 90-degree ply, and one which is assumed much smaller with $w = l = 73 \ \mu m$. For the smaller spacing, both an irregular profile and a straight channel approximation are used for the two TMC. The irregular profile is obtained by extruding the two-dimensional crack geometry at 101 MPa load from the previous paragraphs. For larger spacing (1909 $\mu m$) it is computationally prohibitive to solve a boundary value problem with irregular TMC geometry, so only straight channels are used for the two TMC.

The straight-channel approximation of the TMC in each individual ply is chosen such that the conductance of that ply is equal to the conductance when the actual TMC geometry is used. To calculate the opening of a straight channel that leads to the same ply conductance one can use a well-known analytical result for the ply conductance of a straight channel for the Haigen-Poiseuille flow problem, which leads to the openings in the lower and upper plies of the RVE respectively.

To summarize, three different types of RVE geometries were considered: straight channel approximation with average TMC spacing 1909 $\mu m$; straight channel with

average TMC spacing 73 $\mu m$; the extruded TMC profile at 101 MPa with 73 $\mu m$ average TMC spacing. The numerical computations were performed on all three cases for angles between the cracks of 30, 45, 60 and 90 degrees.

The results from the numerical simulations are summarized in Table VII. The flow rate values for the larger spacing are approximately 20% higher than those for the tight spacing. Overall, the difference in the flow rates is insignificant, provided that the ratio between the two spacing lengths is 26. Another important observation is the difference introduced by the straight channel approximation, which can be evaluated for the 73 $\mu m$ spacing. The maximum difference of approximately 26% in the volumetric flow rate is observed at 45 and 60 degrees ply orientations while the minimum is 18% at 30 degrees. The actual TMC used to form the network has different openings at the two ends, which leads to approximately 20% difference in the junction area compared to that of the straight channel one (for all angles). This alters the flow pattern near the junction area and thus the volumetric flow rate. That is, even a very good two-dimensional approximation of an actual TMC (the corresponding single ply conductance are equal) can lead to significant error when used as part of a three-dimensional analysis. Therefore the most important factor for the effective leakage estimation in a TMC-network is the correct representation of the junction geometry.

Effect of TMC and Crack Junction Opening on Hydrogen Leak Rate: A study of variation of volumetric flow rate with the TMC and crack junction openings is essential as these openings are a function of the load applied on the composite. This can be achieved by varying the TMC openings $\delta_1$ and $\delta_2$ and estimating the volumetric flow rates. Different combinations of $\delta_1$ and $\delta_2$, listed in Table VIII are considered

Table VII. Variation of hydrogen volumetric flow rate with relative orientation of adjacent plies

| Angle (degrees) | Volumetric flow rate (x$10^{-10}m^3/s$) | | |
| --- | --- | --- | --- |
| | Straight channel | | Actual TMC |
| | ($w$=1909 $\mu m$) | ($w$=73 $\mu m$) | ($w = 73$ $\mu m$) |
| 30 | 3.37 | 3.21 | 3.93 |
| 45 | 2.84 | 2.35 | 3.16 |
| 60 | 2.57 | 2.08 | 2.79 |
| 90 | 2.39 | 1.89 | 2.36 |

Table VIII. Different opening combinations considered

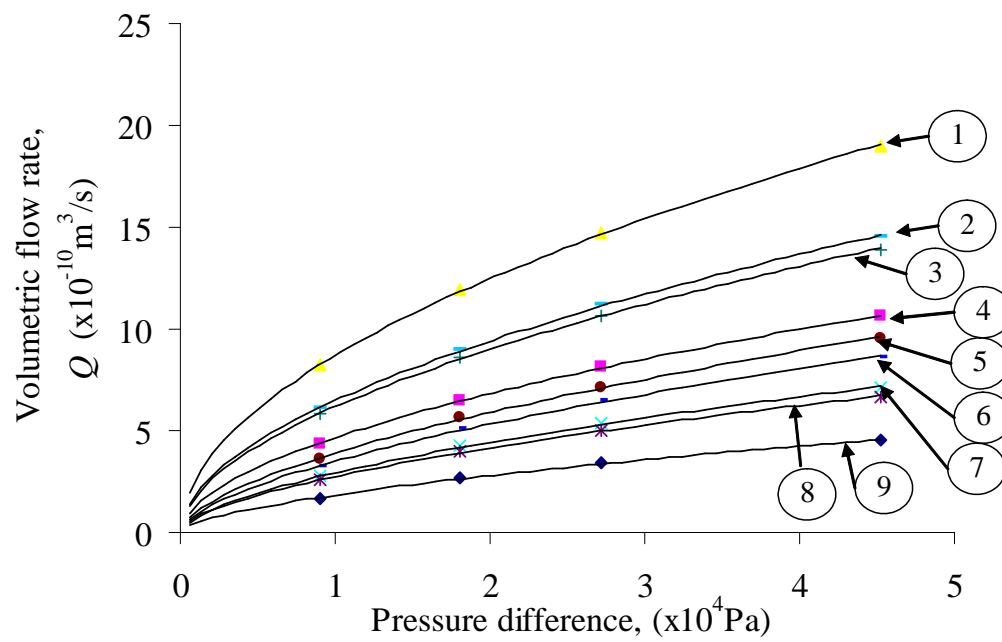| S.No | TMC openings | |
| --- | --- | --- |
| | $\delta_1$ | $\delta_2$ |
| 1 | $0.02h$ | $0.02h$ |
| 2 | $0.02h$ | $0.015h$ |
| 3 | $0.015h$ | $0.02h$ |
| 4 | $0.015h$ | $0.015h$ |
| 5 | $0.02h$ | $0.01h$ |
| 6 | $0.01h$ | $0.02h$ |
| 7 | $0.015h$ | $0.01h$ |
| 8 | $0.01h$ | $0.015h$ |
| 9 | $0.01h$ | $0.01h$ |

Fig. 38. Variation of gaseous hydrogen volumetric flow rate with applied pressure difference in the two-TMC network at different TMC opening combinations. (Refer Table VIII for opening combinations)

for the parametric study. Variation of hydrogen volumetric flow rate with the applied pressure difference for different TMC opening combinations is illustrated in Fig. 38.

The following conclusions can be made from the above results. First, the volumetric flow rate is found to increase with increase in the TMC opening, as more opening results in more leakage area for hydrogen flow through the RVE. Second, the volumetric flow rate values are close when $\delta_1$ and $\delta_2$ are interchanged. Figure 39 illustrates the variation of volumetric flow rate with the crack junction area at a pressure difference of 4.5 x $10^4$ Pa across the RVE. Since the TMC are assumed to be straight channels, the crack junction is a rectangle with dimensions $\delta_1$ x $\delta_2$. From the figure, it can be concluded that the volumetric flow rate varies linearly with the crack junction area.

### B. TMC resistance

Besides crack junctions, the overall conductance of the composite is affected by the additional TMC resistance present between offset crack junctions. A ply with single TMC and two crack junctions, as illustrated in Fig. 40 is considered to study the variation of TMC conductance with the off-set distance between the crack junctions. When the off-set distance $d = 0$, the two crack junctions are aligned *i.e,* the additional TMC resistance due to off-set is considered zero and the effective conductance of the ply is the conductance of crack junctions. Different cases are considered by increasing the offset distance between the two crack junctions and studying the corresponding variation in the effective conductance of the ply. For each case, the boundary value problem mentioned in Chapter II is solved in the domain of TMC. The four pressure differentials discussed earlier are applied across the ply, corresponding volumetric flow rates are determined and the effective conductance is estimated.
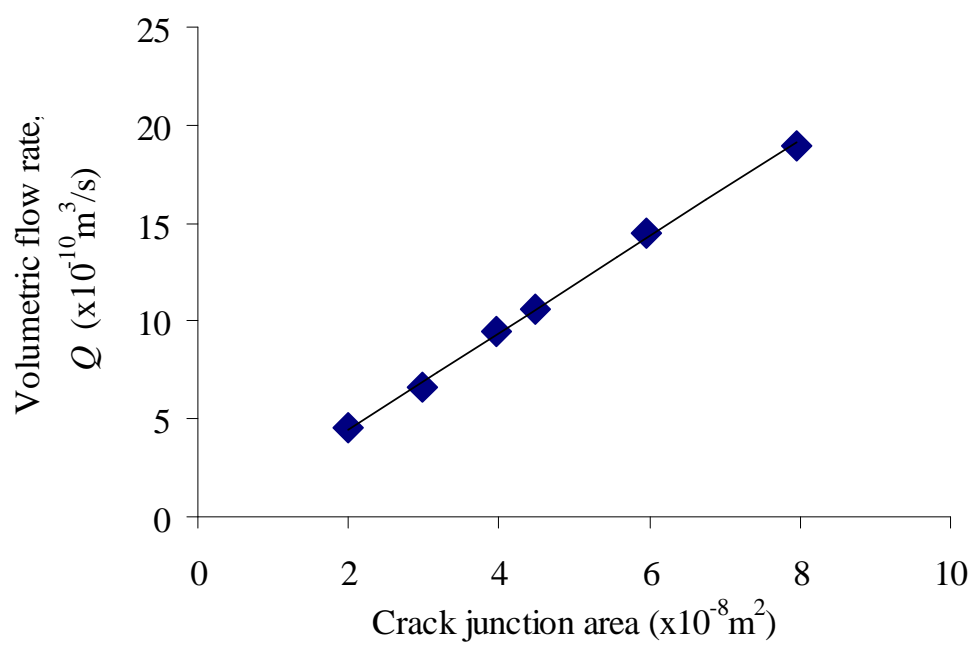
Fig. 39. Variation of gaseous hydrogen volumetric flow rate with crack junction area
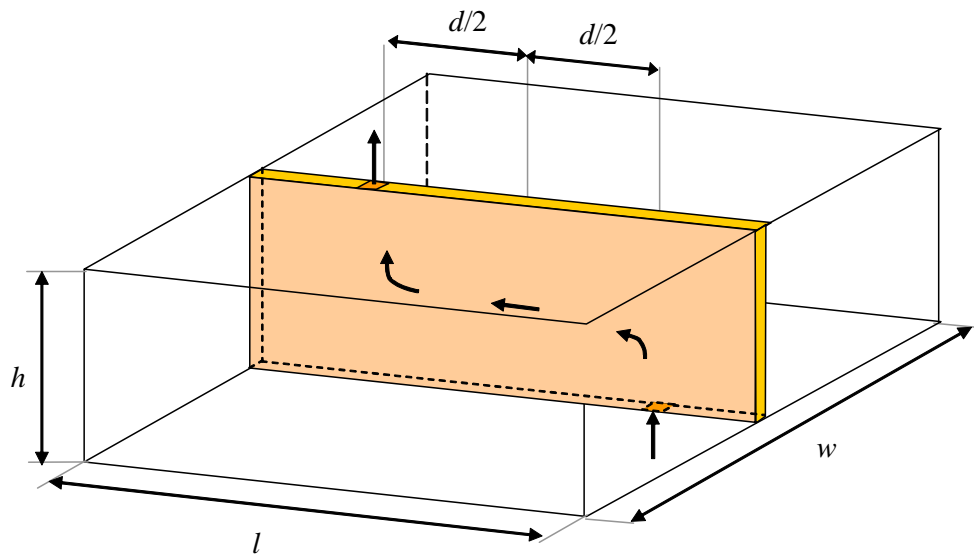
Fig. 40. Schematic of RVE of single ply with two crack junctions

The overall resistance of the ply, which is the reciprocal of the effective conductance is plotted in Figures 41 and 42 against the normalized offset distance, $d^* = (d/h)$, at the two temperatures considered in the study. As illustrated in Figures 41 and 42, the overall resistance of the ply increases linearly with increase in the normalized offset distance $d^*$. The overall resistance of the ply has two components: 1) resistance of the two crack junctions and 2) TMC resistance due to the off-set between crack junctions. An expression for overall resistance of ply can be written in terms of crack junction and TMC resistances as

$$\frac{1}{C^P(d^*)} = \frac{1}{C^J} + \frac{1}{C^T(d^*)} \tag{5.3}$$

where $1/C^P$ is the overall resistance of the ply, $1/C^J$ is the resistance of crack junctions and $1/C^T$ is the TMC resistance. Since the resistance of crack junctions is constant and does not change with change in the offset distance, the cause for linear increase in the overall resistance is increase in the TMC resistance. At cryogenic and room temperatures, the variation of the overall resistance of ply can be expressed as a function of the offset distance as

$$\frac{1}{C^P(d^*)} = C + kd^* \tag{5.4}$$

where $C$ is the y-intercept and $k$ is the slope of the straight line in Figures 41 and 42. Comparing Equations (5.3) and (5.4), the TMC resistance can be written as

$$\frac{1}{C^T} = kd^* \tag{5.5}$$

From the numerical simulation results, the value of $k$ at cryogenic and room temperatures is found to be 7.14 x $10^{10}$(s.Pa$^{0.66}/m^3$) and 2.87 x $10^{13}$(s.Pa/m$^3$) respectively.
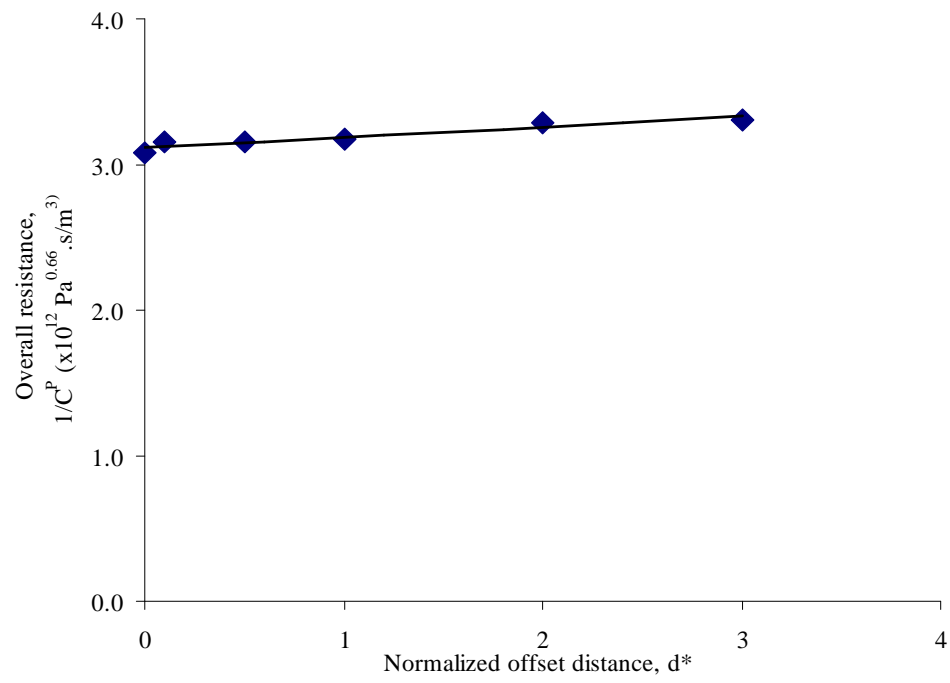
Fig. 41. Variation of effective resistance of the ply $(1/C^P)$ with normalized off-set distance (d*) at cryogenic temperature
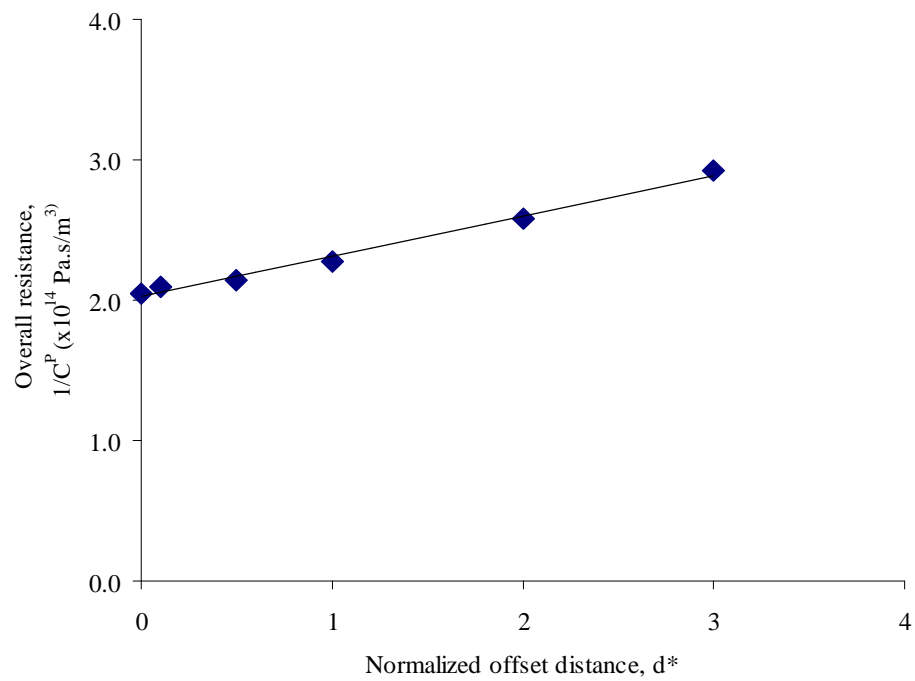
Fig. 42. Variation of effective resistance of the ply $(1/C^P)$ with normalized off-set distance (d*) at room temperature

C.  Simplified model vs. numerical simulations

The effective conductance of the five ply composite is estimated using Simplified model by substituting the crack junction conductance and TMC resistance values at the two temperatures into the expressions derived in Chapter IV. After substitution, these expressions further reduce to

1.  Normalized crack density in middle ply, $\widetilde{\alpha_3} = 1$

In this case, there is no offset between the crack junctions in adjacent ply interfaces. Hence, the TMC resistance is zero in all plies. The effective conductance of the five ply composite is the same as in Equation (4.8)

$$\left( \frac{1}{C_{eff}} \right)^{1/n} = 4 \left( \frac{1}{C^J} \right)^{1/n} \tag{5.6}$$

2.  Normalized crack density in middle ply, $\widetilde{\alpha_3} = 2$

The normalized offset distance between the crack junctions in $1^{st}$ and $2^{nd}$, $3^{rd}$ and $4^{th}$ ply-interfaces is $d_1^* = 1$. Using Equation (5.5) for TMC resistance in $2^{nd}$ and $4^{th}$ plies, the effective conductance in Equation (4.14) further reduces to

$$\left( \frac{1}{C_{eff}} \right)^{1/n} = 2 \left( \frac{1}{C^J} \right)^{1/n} + 2 \left( \frac{1}{2C^J} \right)^{1/n} + 2 \left( \frac{k}{2} \right)^{1/n} \tag{5.7}$$

3.  Normalized crack density in middle ply, $\widetilde{\alpha_3} = 3$

In this case, the normalized offset distance between the outer crack junctions in $2^{nd}$, $3^{rd}$ ply-interfaces and crack junctions in $1^{st}$ and $4^{th}$ ply-interfaces is $d_2^*=1.33$. But the offset distance between the inner crack junction and the crack junction in adjacent ply-interface is zero. From Equation (4.17), the effective conductance of the

five ply composite is written as

$$\left(\frac{1}{C_{eff}}\right)^{1/n} = 2\left(\frac{1}{C^J}\right)^{1/n} + 2\left(\frac{1}{3C^J}\right)^{1/n} \tag{5.8}$$

4. Normalized crack density in middle ply, $\widetilde{\alpha_3} = 4$

The normalized offset distance between inner crack junctions at $2^{nd}$, $3^{rd}$ ply-interfaces and crack junctions at $1^{st}$, $4^{th}$ ply-interfaces is $d_3^* = 0.5$. The normalized offset distance between outer crack junctions at $2^{nd}$, $3^{rd}$ ply-interfaces and crack junctions at $1^{st}$, $4^{th}$ ply-interfaces is $d_4^* = 1.5$. Using Equation (5.5), the TMC resistance between these offset crack junctions is written as

$$\begin{aligned} \frac{1}{C^{T_3}} &= \frac{k}{2} \\ \frac{1}{C^{T_4}} &= \frac{3k}{2} \end{aligned} \tag{5.9}$$

Incorporating above TMC resistances in Equation (4.24), the effective conductance of the five ply composite is

$$\left(\frac{1}{C_{eff}}\right)^{1/n} = 2\left(\frac{1}{C^J}\right)^{1/n} + 2\left(\frac{1}{4C^J}\right)^{1/n} + 2\left(\frac{1}{4k}\right)^{1/n} \tag{5.10}$$

The effective conductance at cryogenic and room temperatures is determined by using $C^J$ and $k$ values at cryogenic and room temperatures. Variation of the Simplified model prediction of effective conductance with the normalized crack density in middle ply at cryogenic and room temperatures is illustrated in Figures 24 and 25 respectively. In the Simplified model prediction too, at both temperatures, the effective conductance values are found to increase with increase in the normalized crack density in the middle ply. From earlier expressions for effective conductance, one can infer that the effective conductance depends on the number of crack junctions and is the harmonic sum of the overall conductance of ply-interfaces and plies.

By changing the crack density in one of the plies, the number of crack junctions are increased in certain ply-interfaces and an increase in the overall conductance of these ply-interfaces is observed. However, in remaining ply-interfaces, the number of crack junctions is constant for all four cases resulting in a constant overall conductance of these ply-interfaces. Cumulative of these two effects is a non-linear increase in the effective conductance with increase in the crack density of one of the plies.

Comparison between effective conductance values predicted by the Simplified model and Numerical simulations at cryogenic and room temperatures is shown in Figures 24 and 25 respectively. The difference in the estimated effective conductance values is found to be around 5% for all four cases considered at both temperatures studied. Hence, for the cases studied, a good comparison between predictions of the Simplified model and Numerical simulations is achieved.

## CHAPTER VI

## SUMMARY AND CONCLUSIONS

The leakage rate through the damage network was discussed based on earlier studies for the opening due to TMC and delamination, including the TMC junction area. It is assumed in the study that TMC run through the entire width of the ply and that TMC are evenly distributed in individual plies. The damage network is expressed as a function of crack density (ply by ply) and the number of TMC intersections. Cryogen leakage through composite laminates used in the manufacture of fuel tanks for reusable launch vehicles has been studied numerically. The numerical study involved analysis of gaseous hydrogen flow through leakage paths, crack junctions and TMC. From the results of the numerical simulations it was found that the TMC resistance varies linearly with the off-set distance between the crack junctions in adjacent ply interfaces. The cryogen volumetric flow rate through a crack junction was found to vary linearly with its area. Also, with increase in the relative orientation between adjacent plies, the leakage rate was found to decrease due to decrease in the crack junction area. Parametric studies were carried out to numerically estimate the conductance of a five ply composite at cryogenic and room temperatures. Due to large Reynolds number of the flow at cryogenic temperature, the leakage rate showed non-linear variation with applied pressure differential. However, at room temperature linear variation was observed due to low Reynolds number. Different cases were considered by changing the crack density in one of the plies. At both temperatures, the effective conductance was found to increase with increase in the crack density. But the increment was found to decrease with increase in the density of cracks. The conclusion was that the effective conductance is a function of crack density in all plies. The Simplified model was used to analytically estimate the effective conductance of

the five ply composite from crack junction conductance and TMC resistance. For all the cases considered, the effective conductance values predicted using the Simplified model were found to agree well with numerical estimations. From the numerical study it was also found that at constant TMC opening, the cryogen leak rate at cryogenic temperature is higher than that at the room temperature. Two-dimensional diffusion studies were carried out to investigate the effect of matrix thickness on the leakage rate between unconnected TMC in adjacent plies. The leakage rate was found to decrease gradually with increase in the thickness and beyond certain limit, the leakage rate was found constant.

Future work will include the compressibility effects of gaseous hydrogen flow through the leakage paths at cryogenic temperatures. Cryogen leakage through angle ply cryogenic composites that have been tested for gaseous hydrogen leakage will also be investigated. Variation of cryogen leak rate with loading conditions will be researched. Leak rates predicted by the Simplified model and experimental measurements will be compared.

REFERENCES

[1] James WS. Graphite-epoxy primary structures for reusable launch vehicles. AIAA, Space Programs and Technologies Conference. 1996,4268, p. 1-28.

[2] Robinson MJ, Eichinger JD, Johnson SE. Hydrogen permeability requirements and testing for reusable launch vehicle tanks. $43^{rd}$ AIAA /ASME /ASCE /AHS /ASC Structures, Structural Dynamics, and Materials Conference. 2002,1418.

[3] Morimoto T, Shimoda T, Morino Y. Pressurizing test of CFRP model tank in cryogenic temperature. $42^{nd}$ AIAA /ASME /ASCE /AHS /ASC Structures, Structural Dynamics, and Materials Conference Seattle. 2001,1882 p. 1-8.

[4] Ishikawa T, Morimoto T, Yokozeki T, Morino Y, Aoki T. Pressurization of CF/Epoxy model tank at LN2 temperature and identification of leak path formation in tank wall. $45^{th}$ AIAA /ASME /ASCE /AHS /ASC Structures, Structural Dynamics, and Materials Conference. 2004,1839, p. 1-8.

[5] Rivers HK, Sikora JG, Sankaran SN. Detection of micro-leaks through complex geometries under mechanical load and at cryogenic temperature. $42^{nd}$ AIAA /ASME /ASCE /AHS /ASC Structures, Structural Dynamics, and Materials Conference. 2001,1218, p. 1-11.

[6] Robinson MJ, Eichinger JD, Johnson SE. Trade study results for a second-generation reusable launch vehicle composite hydrogen tank. $45^{th}$ AIAA /ASME /ASCE /AHS /ASC Structures, Structural Dynamics, and Materials Conference. 2004,1932, p. 1-10.

[7] Gates TS, Grenoble RW, Whitley KS. Permeability and life-time durability of polymer matrix composites for cryogenic fuel tanks. $45^{th}$ AIAA /ASME

/ASCE /AHS /ASC Structures, Structural Dynamics, and Materials Conference. 2004,1859, p. 1-12.

[8] Bechel VT, Kim RY. Through-laminate damage in cryogenically cycled polymer composites. $45^{th}$ AIAA /ASME /ASCE /AHS /ASC Structures, Structural Dynamics, and Materials Conference. 2004,1771, p. 1-10.

[9] Evans D, Reed RP. The permeability of resin based composite materials to radiolytic gases. Cryogenics 1998;38:149-154.

[10] Disdier S, Rey JM, Pailler P, Bunsell AR. Helium permeation in composite materials for cryogenic application. Cryogenics 1998;38:135-142.

[11] Humpenoder J. Gas permeation of fiber reinforced plastics. Cryogenics 1998;38:143-147.

[12] Evans D, Morgan JT. Gas permeability through composite materials. Cryogenics 1998;28:283-284.

[13] Nishijima S, Okada T, Fujioka K, Kuraoka Y. Gas permeation and performance of a fiber reinforced plastic cryostat. Cryogenics 1998;28:285-287.

[14] Kumazawa H, Aoki T, Ishikawa T, Susuki I. Modelling of propellant leakage through matrix cracks in composite laminates. $42^{nd}$ AIAA /ASME /ASCE /AHS /ASC Structures, Structural Dynamics, and Materials Conference. 2001,1217, p. 1-8.

[15] Roy S, Utturkar A, Benjamin M. Modeling of permeation and damage in graphite/epoxy laminates at cryogenic temperatures. $45^{th}$ AIAA /ASME /ASCE /AHS /ASC Structures, Structural Dynamics, and Materials Conference. 2004,1860, p. 1-22.

[16] Mourzenko VV, Thovert JF, Adler PM. Permeability of a single fracture; validity of the Reynolds equation. Journal of Physics, II France 1995;5:465-482.

[17] Zimmerman RW, Yeo IW. Fluid flow in rock fractures: from the navier-stokes equations to the cubic law:, Dynamics of Fluids in Fractured Rock 2000, p. 213-224.

[18] Barenblatt GI, Entov VM, Ryzhik VM. Theory of fluid flows through natural rocks. Kluwer Academic Publishers; 1990.

[19] Jeppson RW. Steady flow analysis of pipe networks: an instructional manual. Department of Civil Engineering and Utah Water Research Laboratory, College of Engineering, Utah State University, Logan, Utah; 1974.

[20] Noh J, Whitcomb J, Peddiraju P, Lagoudas D. Prediction of leakage rate through damage network in cryogenic composite laminates. $45^{th}$ AIAA /ASME /ASCE /AHS /ASC Structures, Structural Dynamics, and Materials Conference. 2004,1861, p. 1-13.

[21] Loeb LB. Kinetic theory of gases. McGraw-Hill Book Company, Inc; 1927.

[22] Anderson JD. Hypersonic and high temperature gas dynamics. McGraw-Hill;1989.

[23] McCarty RD. Hydrogen technological survey-thermo physical properties. Scientific and Technical Information Office, National Aeronautics and Space Administration, Washington D.C; 1975.

[24] Wilkinson D. Mass transport in solids and fluids. Cambridge University Press; 2000.

[25] Crank, J, Park GS. Diffusion in polymers. Academic Press; 1968.

# APPENDIX A

# APPENDIX

## A.   Cryogen diffusion through matrix between unconnected TMC in a composite

When the connectivity between TMC in adjacent plies is absent, the overall cryogen leak rate is dictated by the amount of cryogen transported by diffusion through matrix. In this section, gaseous hydrogen diffusion between two unconnected representative TMC in adjacent plies of a composite is studied. Two-dimensional parametric studies are carried out to investigate the effect of matrix thickness between unconnected TMC on the volumetric flux of hydrogen transported. Also, the variation of volumetric flux of hydrogen with offset distance between two representative TMC is scrutinized. For the analysis, an IM7/5250-4 specimen with IM7 fibers and epoxy matrix is considered. The lay-up of the specimen is $[90/45/0/-45]_s$ and was tested for gaseous hydrogen leakage at MSFC. During the leak test micro cracks developed in individual plies and assisted permeation of hydrogen. When the load on the composite is not sufficient enough to create damage in all plies or provide connectivity between TMC in adjacent plies, the leakage of hydrogen through the composite depends on its transport by diffusion through matrix layer.

Micrograph comprising of TMC in adjacent plies of the IM7/5250-4 specimen is illustrated in Fig. 43. The micrograph was taken through a metallographic microscope during edge optical inspection. The optical inspection study was carried out at Air Force Research Laboratory. Due to the different orientation of the plies, it is difficult to tell if they actually intersect or not. For the following parametric
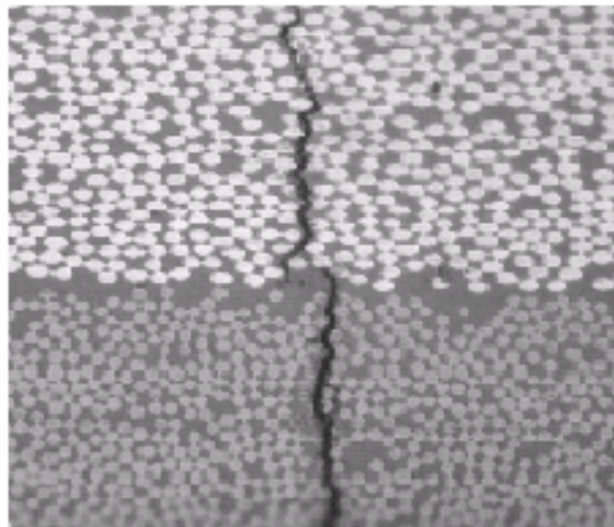
Fig. 43.  Micrograph of representative TMC in adjacent plies of IM7/5250-4 composite specimen

study, it is assumed that they do not intersect and the TMC are taken in a two-dimensional setup, that is, both of them run parallel to the depth of the specimen. This two-dimensional setting will provide an upper estimate of the cryogen volumetric flux since most of the diffusion takes place near the TMC tips. When the TMC are assumed parallel, this area runs through the depth of the specimen, while in reality it is localized to a small region. Motivated from Fig. 43, an RVE is chosen with two representative TMC in adjacent plies. Schematic of the RVE is illustrated in Fig. 44. Since diffusion takes place inside the composite and near the crack tips, it is not necessary to reproduce the TMC profile exactly. Therefore, the TMC are considered as straight channels. A pressure differential is assumed at either surfaces of the RVE and the volumetric flux of hydrogen diffusing through the matrix is estimated for several cases mentioned.

In cryogen transport by diffusion, it is assumed that the cryogen transport into TMC takes place instantaneously and hence the TMC are always saturated with cryogen; the overall cryogen transport is governed by diffusion through the matrix. As shown in Fig. 44, region $\Gamma_1$ is the top surface of RVE and the surface of the top crack; region $\Gamma_2$ is the bottom surface of RVE and the surface of the bottom crack, region $\Gamma_3$ includes the side walls of the RVE, and $\Gamma_4$ is the mid-section of RVE. The RVE is repeated periodically by consecutive reflections about the lateral surfaces $\Gamma_3$.

The diffusion process in the matrix starts by the adsorption of the cryogen onto the surface of the composite followed by Fickian diffusion through the epoxy matrix. The diffusion of cryogen through the matrix is well approximated by Ficks law [24]:

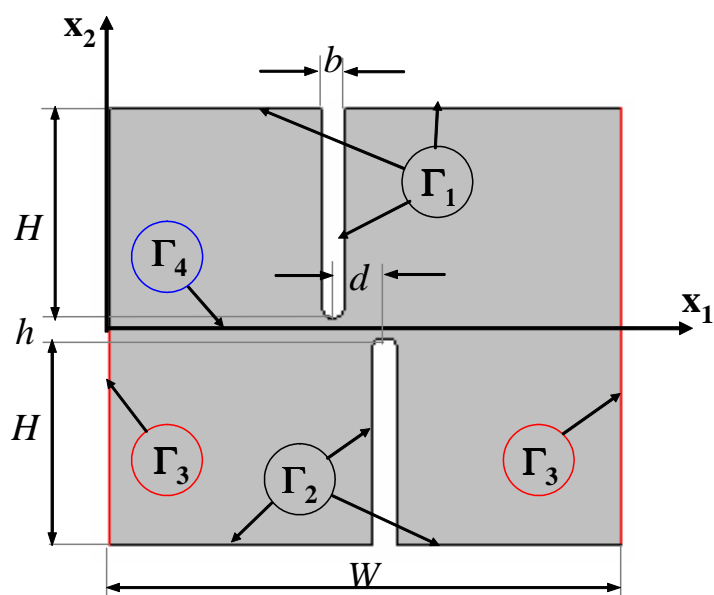$$q_i = -D_{ij}\frac{\partial c}{\partial x_j} \tag{A.1}$$

Fig. 44. Two-dimensional schematic of RVE of a two ply composite

where $q$ is the volumetric flux, $D$ is the second order diffusivity tensor component and $c$ is the concentration of cryogen in the matrix. In the present study, the diffusivity tensor is considered isotropic.

The continuity equation for the cryogen at steady state can be written as

$$\frac{\partial q_i}{\partial x_j} = 0 \tag{A.2}$$

Combining Equations (A.1) and (A.2), results in Fick's second law which is expressed as:

$$\frac{\partial}{\partial x_i}\left(D_{ij}\frac{\partial c}{\partial x_j}\right) = 0 \tag{A.3}$$

The differential equation (A.3) is solved in the RVE to obtain the spatial distribution of the cryogen concentration. In order to solve equation (A.3), concentration boundary conditions need to be specified on the top and bottom surface of the RVE (Fig. 44)

$$c = c_0 \text{ on } \Gamma_1, c = 0 \text{ on } \Gamma_1 \tag{A.4}$$

Cryogen transport is usually driven by pressure difference across the composite. Hence, the concentration $c_0$ on $\Gamma_1$ is expressed in terms of the pressure $p_0$ of cryogen on the boundary. The matrix considered for the parametric studies in this work is made of polymeric epoxy material. For diffusion of gases through polymer materials, Henry's law [25] can be used to express the concentration of gas on the boundary in terms of its solubility and pressure.

$$c_0 = kp_0 \tag{A.5}$$

where $k$ is the solubility coefficient of hydrogen in epoxy. Finally, due to the assumed periodicity of the RVE, the solution to equation (A.3) must also be periodic. Therefore

the normal component of the flux $q$ must vanish on the lateral surfaces $\Gamma_3$ , that is

$$q_i N_i = 0 \tag{A.6}$$

where $N$ is the normal vector to $\Gamma_3$. Due to the boundary conditions given by equations (A.4) and (A.6), the average volumetric flux in the $x_1$ direction, $q_1$ is zero. The quantity of interest is the averaged value $q_2$ of the $x_2$ - component of the flux, given by:

$$\langle q_2 \rangle = \frac{1}{A} \int_{\Gamma_4} q_2 \tag{A.7}$$

The numerical experiments are performed on a specimen with $h = w = 141~\mu m$. The width of the crack is $\delta = 2.82~\mu m$. The coefficient of permeability, which is the product of diffusivity and solubility for hydrogen diffusing through epoxy matrix is $kD = 7.169$ x $10^{-9}~(cm^2/s.atm)$ and is obtained based on the information in Reference [9]. Three different cases are studied for the offset distance between TMC, $d$ equal to 0, 20, 40 $\mu m$ (see Fig. 44). Different thicknesses of matrix are considered for the numerical analysis ranging from 1 $\mu m$ to 132 $\mu m$. Due to the boundary conditions described in Chapter II, the average volumetric flux in $x_1$-direction, $\langle q_1 \rangle$ is zero. The quantity of interest is the average value of the $x_2$ component of the flux, $\langle q_2 \rangle$ given by Equation (A.7).

The numerical simulations are carried out using commercial finite volume software, FLUENT and the results are illustrated in Figures 45 and 46 respectively. As can be seen from the figure, the average volumetric flux $\langle q_2 \rangle$ decreases gradually as the offset distance between the TMC is increased. For a given offset distance between the TMC, the average flux decreases as the thickness of the matrix increases. Beyond certain thickness of matrix, further increase in the matrix thickness does not affect
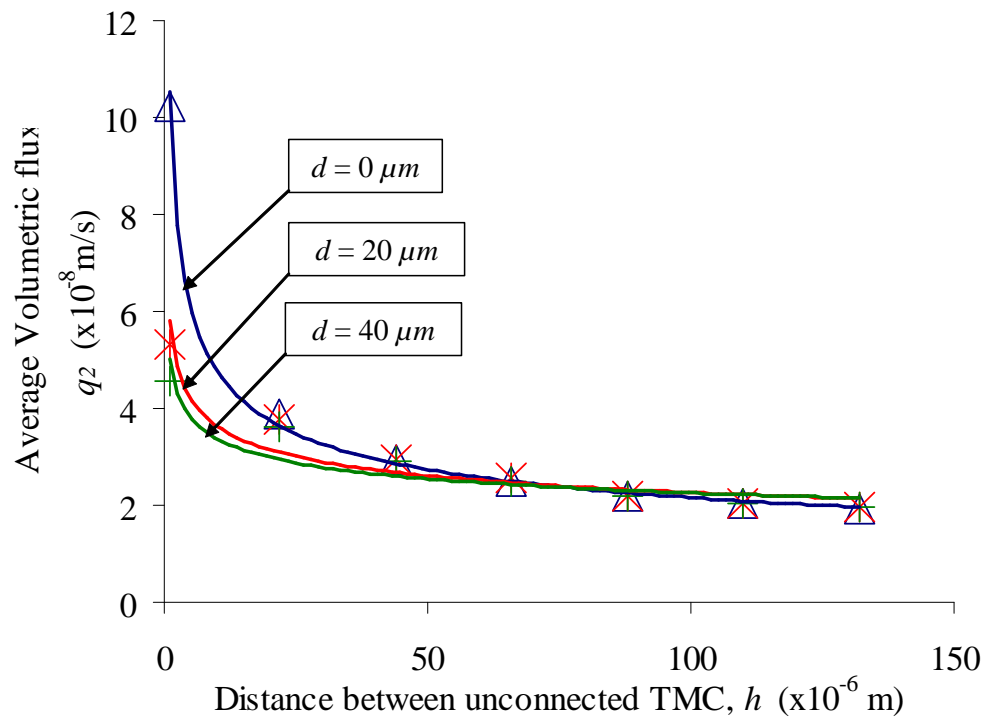
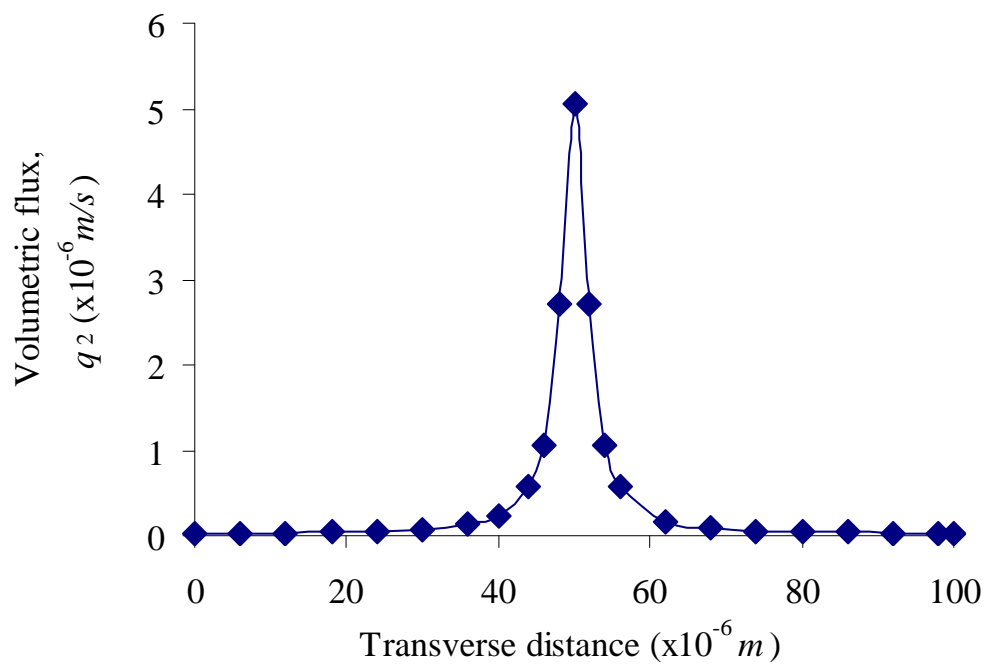Fig. 45. Average volumetric flux of hydrogen diffusing between unconnected TMC

Fig. 46. Volumetric flux of hydrogen across the mid-section of RVE for d = 0 $\mu$m

the average volumetric flux as the effect of relative orientation of cracks diminishes. The point wise values of $q_2$ along the midsection of the RVE ($\Gamma_4$) for the case $d = 0$ (the two representative TMC are aligned vertically) is plotted in Fig. 46. The flux $q_2$ is maximum near the TMC tip and decreases rapidly away from the tips and reaches negligible values (approx 100 times less than the peak value) near the two sides of the RVE.

The volumetric flux values computed in this study are compared with the allowable flux values specified for reusable launch vehicle fuel tanks of the X-33 vehicle in Reference [2]. The allowable flux value during ascent and for an inside tank pressure of 3.40 x $10^5$ $N/m^2$ is 3.58 x $10^{-6}$ $m/s$. Upon comparing the computed flux values for the different case studies, it is concluded that the average value of flux for hydrogen diffusing through epoxy layer is an order of magnitude less than the allowable value specified for X-33 fuel tank for all studied cases. Therefore, a matrix layer of thickness 1 $\mu m$ is sufficient to prevent critical leakage of hydrogen by diffusion.

B.  Validation of numerical simulations

The numerical simulations are validated with analytical results for flow through a straight channel problem. In Haigen-Poiseuille problem, a pressure differential is applied across a straight channel causing the fluid to flow through the channel as illustrated in Fig. 47. In this case, the direction of the velocity gradient and the velocity direction are perpendicular. Thus the non-linear terms in Navier-Stokes equation reduce to zero and an exact solution exists for the velocity of the fluid. The volumetric flow rate of the fluid through the channel is obtained by using Equation
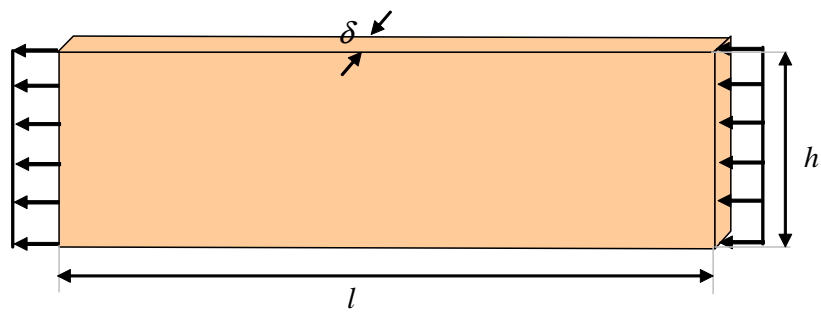
Fig. 47. Schematic of the straight channel studied for Haigen-Poiseuille flow

(2.13). The expression for volumetric flow rate is given by

$$Q = \frac{h\delta^3}{12\mu}\frac{\Delta P}{\Delta L} \qquad (A.8)$$

where $L$ is the length of the straight channel. The results of the numerical simulations and the analytical results are plotted in Fig. 48. As illustrated, the difference between the numerical simulations and the analytical predictions is less than 3%. Thus, the numerical simulation results are found to agree well with the theoretical predictions for the Haigen-Poiseuille flow problem.

C.   Convergence of numerical solution with mesh quality

The two-TMC network introduced in Chapter V is used to evaluate the convergence of solution with quality of mesh used. Schematic of the two meshes, Mesh 1 and Mesh 2 used for numerical computations are illustrated in Figures 49 and 50 respectively. Number of elements in Mesh 1 along $l$, $h$ and $\delta$ are 100, 8 and 10 respectively. In Mesh 2, the number of elements are 200, 16 and 20. BVP mentioned in Chapter II is solved in the RVE for four pressure differentials mentioned in Chapter IV. The volumetric flow rates of hydrogen through the RVE are estimated using Equation (2.13). Variation of volumetric flow rate with applied pressure differential for the two meshes considered is plotted in Fig. 51 and listed in Table IX.

As shown in the above table, the maximum difference in the volumetric flow rates between the two Meshes is 1.73%. Thus, the solution with Mesh 2 can be considered as the overkill solution and Mesh 1 produces converged solution with respect to the overkill solution.

Table IX. Comparison of volumetric flow rate of hydrogen through two-TMC network
at different pressure differentials for two qualities of meshes

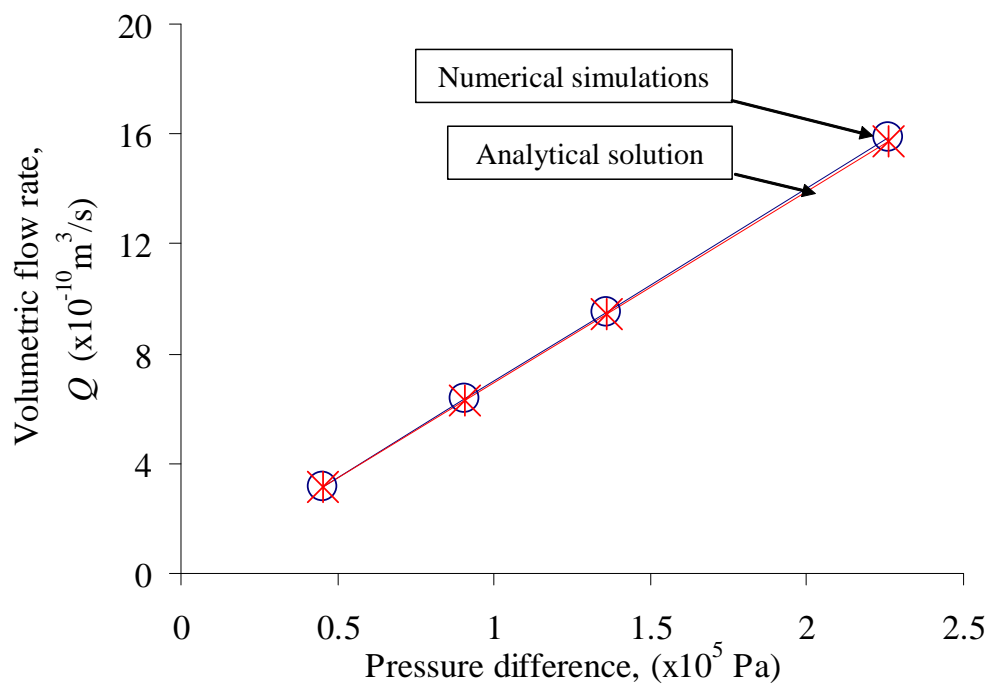| $\Delta P$ (x10$^5$ Pa) | **Volumetric flow rate** (x10$^{-10}$ m$^3$/s) | |
|:---:|:---:|:---:|
| | Mesh1 | Mesh2 |
| 0.09 | 1.67 | 1.66 |
| 0.18 | 2.61 | 2.64 |
| 0.27 | 3.34 | 3.37 |
| 0.45 | 4.44 | 4.52 |

Fig. 48. Verification of numerical simulation results with analytical solution for Haigen-Poiseuille flow through a straight channel
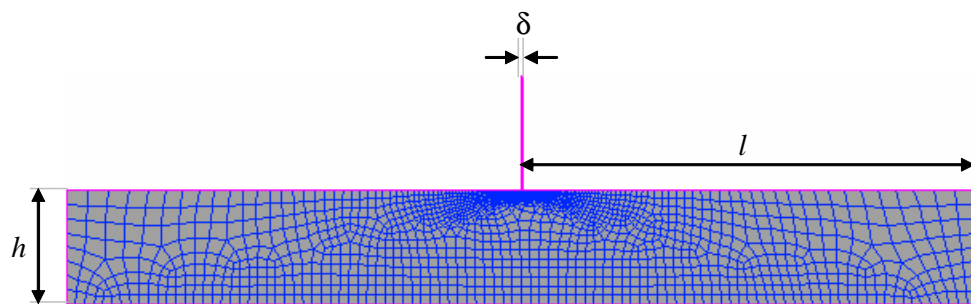
Fig. 49. Schematic of RVE of two-ply network with Mesh1 quality of mesh
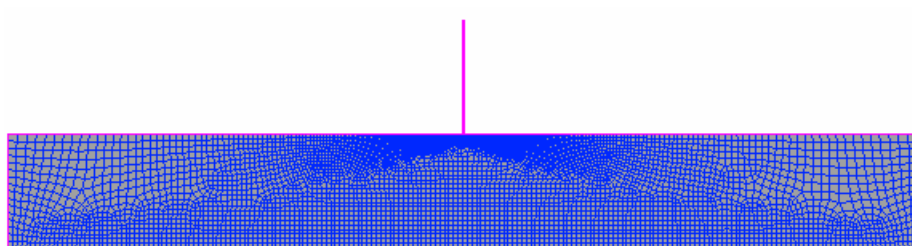
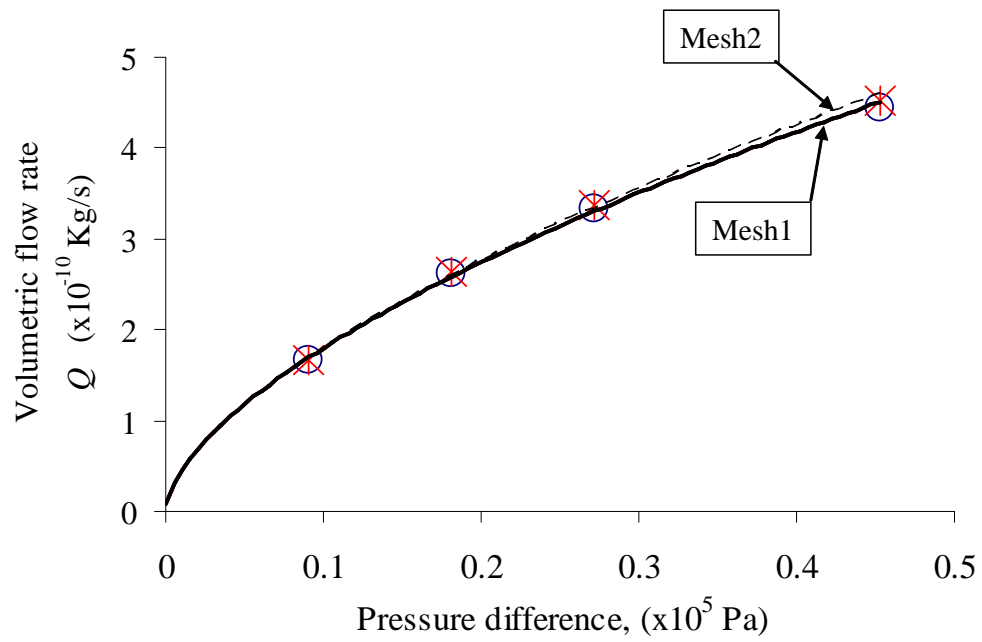Fig. 50. Schematic of RVE for crack junction with Mesh2 quality of mesh

Fig. 51. Variation of Volumetric flow rate for RVE of two-TMC network at cryogenic temperature for two different qualities of meshes

## VITA

Naga Venkata Satya Pravin Kumar Peddiraju was born in Narasaraopet, Andhra Pradesh, India, on August 20, 1978. After pursuing high school education, he received a Bachelor of Technology degree in 2001 from one of the premier engineering institutes in India, the Indian Institute of Technology-Chennai. Pravin received the Regents Fellowship Award from the Department of Aerospace Engineering at Texas A&M University, College Station, Texas during his Masters study. He is also a member of Phi Kappa Phi honor society: the top 1% graduate students at Texas A&M University. Pravin recently finished the requirements for the degree of Master of Science in Aerospace Engineering at Texas A&M University and received his degree in December 2004.

Pravin enjoys playing cricket, chess and listening to Indian classical carnatic music. He can be reached at the following address:

Flat No. 201, Annapurna Apartments, 16-10-144

Malakpet, Hyderabad, 500036

AndhraPradesh

India